1-1-2015

The B-L MSSM from Strings to the LHC

Austin Purves
University of Pennsylvania, apurves@sas.upenn.edu

Recommended Citation

Purves, Austin, "The B-L MSSM from Strings to the LHC" (2015). *Publicly Accessible Penn Dissertations*. 1120.
http://repository.upenn.edu/edissertations/1120

The B-L MSSM from Strings to the LHC

Abstract

We develop connections between a string-motivated realization of the minimal B â?? L extension of the MSSM and LHC-observable phenomenology. Using a random scan of the high-scale parameter space, together with numerical solution of the renormalization group equations, we connect the modelâ??s roots in String Theory to its phenomenological implications for the LHC. One predictive result of this approach is a limited set of possible lightest supersymmetric particles (LSPs). Motivated by this result, we study the implications of a stop or sbottom LSP at the LHC. This yields predictive connections between the neutrino sector and the LHC. We present lower bounds on the mass of stop and sbottom LSPs.

Degree Type
Dissertation

Degree Name
Doctor of Philosophy (PhD)

Graduate Group
Physics & Astronomy

First Advisor
Burt A. Ovrut

Subject Categories
Physics

THE $B - L$ MSSM FROM STRINGS TO THE LHC

Austin Purves

A DISSERTATION
in
Physics and Astronomy

Presented to the Faculties of the University of Pennsylvania in Partial Fulfillment
of the Requirements for the Degree of Doctor of Philosophy
2015

Supervisor of Dissertation

____
Burt Ovrut
Professor of Physics

Graduate Group Chairperson

____
Marija Drndic
Professor of Physics

Dissertation Committee:
Burt Ovrut, Professor of Physics
Mark Trodden, Professor of Physics
Joseph Kroll, Professor of Physics
Evelyn Thomson, Professor of Physics
Tom Lubensky, Professor of Physics

ABSTRACT

THE $B-L$ MSSM FROM STRINGS TO THE LHC
Austin Purves
Burt Ovrut

We develop connections between a string-motivated realization of the minimal $B-L$ extension of the MSSM and LHC-observable phenomenology. Using a random scan of the high-scale parameter space, together with numerical solution of the renormalization group equations, we connect the model's roots in String Theory to its phenomenological implications for the LHC. One predictive result of this approach is a limited set of possible lightest supersymmetric particles (LSPs). Motivated by this result, we study the implications of a stop or sbottom LSP at the LHC. This yields predictive connections between the neutrino sector and the LHC. We present lower bounds on the mass of stop and sbottom LSPs.

Contents

List of Tables

List of Figures

Chapter 1

Introduction

1.1 Motivation

With the beginning of a new run at the LHC, we have an exciting opportunity to probe the next energy frontier. Among the many candidates for new physics in that frontier, supersymmetry (SUSY) stands out as a rich and compelling framework. SUSY not only addresses the gauge hierarchy problem, a puzzle that has driven many model building efforts over several decades, but can also speak to other outstanding issues in the standard model (SM). This includes dark matter and a mechanism for radiative electroweak symmetry breaking. As we prepare for a new round of LHC data, it is a good time to reconsider the phenomenology of low energy supersymmetric models.

Despite their theoretically pleasing aspects, generic SUSY particle physics models potentially have a serious problem regarding proton decay. This follows from the fact that the most general MSSM superpotential allows for baryon and lepton number violating terms at tree level and, therefore, rapid proton decay. The typical, yet *ad hoc*, solution is to impose R-parity, $R_P = (-1)^{3(B-L)+2s}$ where s is the spin of the particle. This discrete symmetry forbids violation of baryon number (B) minus lepton number (L) by one unit. Accepting R-parity conservation, however, severely narrows one's view of the SUSY phenomenological landscape. This is because the lightest supersymmetric particle (LSP) in R-parity conserving theories is stable and, therefore, must be neutral to avoid a disallowed density of charged relics.

Perhaps the most appealing candidates for a deeper origin for R-parity, models with gauged $U(1)_{B-L}$, are based on the observation that R-parity is a discrete subgroup of $U(1)_{B-L}$. In such models, R-parity is a good symmetry as long as $U(1)_{B-L}$ is. However, once $U(1)_{B-L}$ is broken, the $B-L$ number of the field that breaks $U(1)_{B-L}$ determines the fate of R-parity: an even $B-L$ field leads to automatic R-parity conservation (RPC) [6, 7, 8] (for more recent studies see [9, 10, 11, 12, 13]) , while an odd $B-L$ field triggers spontaneous R-parity violation (RPV) [14, 15, 16, 17][1]. Typically, spontaneous R-parity violation is safe in the sense that only lepton number violation is generated at tree level, leaving the proton as stable as it would be with RPC.

As one might expect, the approach in these early $B-L$ studies was to introduce a new "Higgs" sector (that is, superfields with a $B-L$ charge) with which to spontaneously break the $B-L$ symmetry. However, the $B-L$ anomaly cancellation conditions provide a subtle, and more minimal, alternative to this approach. Note that the three generations of right-handed neutrino superfields required to cancel these anomalies contain right-handed sneutrinos. Remarkably, the right-handed sneutrinos have the correct quantum numbers to spontaneously break $B-L$ in a phenomenologically acceptable way. Specifically, they are neutral under the SM, carry no baryon number and, of course, have a $B-L$ charge of one. Therefore, anomaly cancellation defines the most minimal $B-L$ extension of the MSSM. This model has exactly the MSSM particle content plus three generations of right-handed neutrino supermultiplets, and it does *not* require a new Higgs sector. This minimal $B-L$ theory was proposed in [20, 21, 22, 23], arguing for its appeal from a "bottom up" point of view.[2] The same theory was found from a "top down" approach within the context of a class of vacua of heterotic M-theory [24, 25, 26, 27, 28, 29]. Due to the odd $B-L$ charge of the sneutrino, the minimal $B-L$ model must always spontaneously break R-parity. However, because the right-handed sneutrino has no baryon number, its vacuum expectation value (VEV) does not introduce proton decay at tree level. In addition, this model has several potentially testable and interesting predictions:

- R-parity violation is manifest though lepton number violating operators, which could lead to lepton number violating signatures at the LHC, *e.g.* [30, 31].

- The existence of two neutral light fermions (sterile neutrinos), in addition

---

[1] See also recent studies of explicit R-parity violation assuming minimal flavor violation [18, 19].

[2] Such a minimal model was outlined as a possible low energy manifestation of E_6 GUT models in [16].

to the usual three neutrinos [16, 32, 33]. These may play a role in cosmology [32, 34, 31].

- A $B - L$ neutral gauge boson, Z', whose mass is proportional to the soft mass of the right-handed sneutrino. This gauge boson must be at the TeV scale and, therefore, detectable at the LHC.
- The right-handed sneutrino VEV directly links the neutrino sector to lepton number violation by one unit. This generates tree-level Majorana contributions to the neutrino masses.

This last statement is significant, since it specifies the size of the RPV. It follows from the upper bound placed on this contribution by the neutrino masses that the RPV is only relevant for the decay of the LSP, which would otherwise be stable under RPC. All other SUSY processes will effectively be R-parity conserving. The last bullet point is also crucial because it relates neutrino masses to collider physics through R-parity violation, an exciting synergy. It suggests that one may be able to infer information about the neutrino sector from LSP decays. Finally, it is worthwhile to note that despite RPV, a gravitino LSP, while unstable, may live long enough to be the dark matter of the universe [35, 36, 37].

This model of spontaneous RPV is, therefore, a well-motivated alternative to RPC. As with all SUSY models, its phenomenology will be highly dependent on the identity of the LSP[3] and other details of the spectrum. In this thesis, we address this by searching the parameter space using a random scan. We combine this random scan with sophisticated numerical methods to solve the renormalization group equations, resulting in a new way to connect the string-theory-motivated construction of the model to observable physics. R-parity violation plays an important role in the LHC phenomenology because it allows the LSP to decay. This liberates the LSP to be any superpartner, including those that have color and charge. One example, of this type, is a charged slepton LSP. However, this will decay like a charged Higgs, an element that already exists in the MSSM. Squark LSP's, on the other hand, offer an opportunity for a whole new set of signals since they act as leptoquarks; that is, scalar particles that are pair produced and decay into a quark and a lepton. Among the squarks, the third generation is perhaps the most interesting LSP candidate since these are generally expected to have the lowest masses due to renormalization group effects, *e.g.* [38]. Furthermore, since

---

[3] While the complete model would include a gravitino LSP as the dark matter of the universe, throughout this thesis we shall use LSP to refer to the lightest supersymmetric particle *relevant for collider physics*.

the lower generations must be fairly degenerate due to the SUSY flavor problem, they would be produced more readily and, therefore, have stronger bounds. Finally, stops are the most engaging of all the squarks because of their substantial radiative contribution to the Higgs mass and the role they play as a measure of fine-tuning in SUSY. For these reasons, we study in some detail the implications of a third-generation squark LSP at the LHC.

1.2 The TeV Scale Model

Motivated by both phenomenological considerations and string theory, we analyze the minimal anomaly free extension of the MSSM with gauge group

$$SU(3)_C \otimes SU(2)_L \otimes U(1)_{3R} \otimes U(1)_{B-L} \ . \tag{1.1}$$

As discussed in Section 2.3 and [1], we prefer to work with the Abelian factors $U(1)_{3R} \otimes U(1)_{B-L}$ rather than $U(1)_Y \otimes U(1)_{B-L}$– although they are physically equivalent. This is motivated by the fact that the former is the unique choice that does not introduce kinetic mixing between the associated field strengths at any scale in their renormalization group equation (RGE) evolution. The gauge covariant derivative can be written as

$$D = \partial - iT_{3R} g_R W_R - i\frac{B-L}{2} g_{BL} B' \ , \tag{1.2}$$

where T_{3R} is the $U(1)_{3R}$ charge and the factor of $\frac{1}{2}$ is introduced in the last term by a redefinition of the gauge coupling g_{BL}– thus simplifying many equations. As discussed in [1] and throughout this thesis, a radiatively induced vacuum expectation value (VEV) for a right-handed sneutrino will spontaneously break the Abelian factors $U(1)_{3R} \otimes U(1)_{B-L}$ to $U(1)_Y$, in analogy with the way that the Higgs fields break $SU(2)_L \otimes U(1)_Y$ to $U(1)_{EM}$ in the SM. For simplicity, we will refer to this as "$B-L$" symmetry breaking–even though it is technically the breaking of a linear combination of the $U(1)_{3R}$ and $U(1)_{B-L}$ generators, leaving the hypercharge group generated by

$$Y = T_{3R} + \frac{B-L}{2} \tag{1.3}$$

invariant. The particle content of the minimal model is simply that of the MSSM plus three right-handed neutrino chiral multiplets. That is, three generations of matter superfields

$$\begin{array}{lll} Q=\left(\begin{array}{c} u \\ d \end{array}\right) \sim (\mathbf{3},\mathbf{2},0,\frac{1}{3}) & \begin{array}{l} u^c \sim \\ d^c \sim \end{array} \begin{array}{l} (\bar{\mathbf{3}},\mathbf{1},-1/2,-\frac{1}{3}) \\ (\bar{\mathbf{3}},\mathbf{1},1/2,-\frac{1}{3}) \end{array} & , \\ L=\left(\begin{array}{c} \nu \\ e \end{array}\right) \sim (\mathbf{1},\mathbf{2},0,-1) & \begin{array}{l} \nu^c \sim \\ e^c \sim \end{array} \begin{array}{l} (\mathbf{1},\mathbf{1},-1/2,1) \\ (\mathbf{1},\mathbf{1},1/2,1) \end{array} & , \end{array} \tag{1.4}$$

along with two Higgs supermultiplets

$$\begin{aligned} H_u &= \left(\begin{array}{c} H_u^+ \\ H_u^0 \end{array}\right) \sim (\mathbf{1},\mathbf{2},1/2,0)\ , \\ H_d &= \left(\begin{array}{c} H_d^0 \\ H_d^- \end{array}\right) \sim (\mathbf{1},\mathbf{2},-1/2,0)\ . \end{aligned} \tag{1.5}$$

We refer to this model throughout the remainder of this thesis as the $B-L$ MSSM.

The superpotential of the $B-L$ MSSM is given by

$$W = Y_u Q H_u u^c - Y_d Q H_d d^c - Y_e L H_d e^c + Y_\nu L H_u \nu^c + \mu H_u H_d\ , \tag{1.6}$$

where flavor and gauge indices have been suppressed and the Yukawa couplings are three-by-three matrices in flavor space. In principle, the Yukawa matrices are arbitrary complex matrices. However, the observed smallness of the three CKM mixing angles and the CP-violating phase dictate that the quark Yukawa matrices be taken to be nearly diagonal and real. The lepton Yukawa coupling matrix can also be chosen to be diagonal and real. This is accomplished by moving the rotation angles and phases into the neutrino Yukawa couplings which, henceforth, must be complex matrices. Furthermore, the smallness of the first and second family fermion masses implies that all components of the up, down, and lepton Yukawa couplings–with the exception of the (3,3) components–can be neglected for the purposes of the renormalization group (RG) running. Similarly, the very light neutrino masses imply that the neutrino Yukawa couplings are sufficiently small so as to be neglected for the purposes of RG running. The μ-parameter can be chosen to be real, but not necessarily positive, without loss of generality. The soft supersymmetry breaking Lagrangian is then given by

$$
\begin{aligned}
-\mathcal{L}_{\text{soft}} = \Big(&\frac{1}{2}M_3\tilde{g}^2 + \frac{1}{2}M_2\tilde{W}^2 + \frac{1}{2}M_R\tilde{W}_R^2 + \frac{1}{2}M_{BL}\tilde{B'}^2 \\
&+ a_u\tilde{Q}H_u\tilde{u}^c - a_d\tilde{Q}H_d\tilde{d}^c - a_e\tilde{L}H_d\tilde{e}^c + a_\nu\tilde{L}H_u\tilde{\nu}^c + bH_uH_d + h.c.\Big) \\
&+ m^2_{\tilde{Q}}|\tilde{Q}|^2 + m^2_{\tilde{u}^c}|\tilde{u}^c|^2 + m^2_{\tilde{d}^c}|\tilde{d}^c|^2 + m^2_{\tilde{L}}|\tilde{L}|^2 + m^2_{\tilde{\nu}^c}|\tilde{\nu}^c|^2 + m^2_{\tilde{e}^c}|\tilde{e}^c|^2 \\
&+ m^2_{H_u}|H_u|^2 + m^2_{H_d}|H_d|^2 \ .
\end{aligned}
\tag{1.7}
$$

The b parameter can be chosen to be real and positive without loss of generality. The gaugino soft masses can, in principle, be complex. This, however, could lead to CP-violating effects that are not observed. Therefore, we proceed by assuming they all are real. The a-parameters and scalar soft mass can, in general, be Hermitian matrices in family space. Again, however, this could lead to unobserved flavor and CP violation. Therefore, we will assume they all are diagonal and real. Furthermore, we assume that only the (3,3) components of the up, down, and lepton a-parameters are significant and that the neutrino a parameters are negligible for the purposes of RG running. For more explanation of these assumptions, see Section 3.2.2.

Spontaneous breaking of $B-L$ symmetry results from a right-handed sneutrino developing a non-vanishing VEV, since it carries the appropriate T_{3R} and $B-L$ charges. However, since sneutrinos are singlets under the $SU(3)_C \otimes SU(2)_L \otimes U(1)_Y$ gauge group, it does not break any of the SM symmetries. To acquire a VEV, a right-handed sneutrino must develop a tachyonic mass[4]. As discussed in [16, 32, 33], a VEV can only be generated in one linear combination of the right-handed sneutrinos. Furthermore, beyond the fact that its VEV breaks $B-L$ symmetry, in which combination it occurs has no further observable effect. This is because there is no right-handed charged current to link the right-handed neutrinos to a corresponding right-handed charged lepton. Therefore, without loss of generality, one can assume that it is the third generation right-handed sneutrino that acquires a VEV. At a lower mass scale, electroweak symmetry is spontaneously broken by the neutral components of both the up and down Higgs multiplets acquiring non-zero VEV's. In combination with the right-

---

[4] Here and throughout this thesis we use the term "tachyon" to describe a scalar particle whose m^2 parameter is negative. Although all m^2 parameters at high scale will be chosen positive, one or more can be driven negative at lower energy by radiative corrections. This signals dynamical instability at the origin–although a stable VEV may, or may not, develop.

handed sneutrino VEV, this also induces a VEV in each of the three generations of left-handed sneutrinos. The notation for the relevant VEVs is

$$\langle \tilde{\nu}_3^c \rangle \equiv \frac{1}{\sqrt{2}} v_R, \;\; \langle \tilde{\nu}_i \rangle \equiv \frac{1}{\sqrt{2}} v_{Li}, \;\; \left\langle H_u^0 \right\rangle \equiv \frac{1}{\sqrt{2}} v_u, \;\; \left\langle H_d^0 \right\rangle \equiv \frac{1}{\sqrt{2}} v_d, \tag{1.8}$$

where $i = 1, 2, 3$ is the generation index.

The neutral gauge boson that becomes massive due to $B - L$ symmetry breaking, Z_R, has a mass at leading order, in the relevant limit that $v_R \gg v$, of

$$M_{Z_R}^2 = \frac{1}{4} \left(g_R^2 + g_{BL}^2 \right) v_R^2 \left(1 + \frac{g_R^4}{g_R^2 + g_{BL}^2} \frac{v^2}{v_R^2} \right) \;, \tag{1.9}$$

where

$$v^2 \equiv v_d^2 + v_u^2 \;. \tag{1.10}$$

The second term in the parenthesis is a small effect due to mixing in the neutral gauge boson sector. The hypercharge gauge coupling is given by

$$g_Y = g_R \sin\theta_R = g_{BL} \cos\theta_R \;, \tag{1.11}$$

where

$$\cos\theta_R = \frac{g_R}{\sqrt{g_R^2 + g_{BL}^2}} \;. \tag{1.12}$$

Since the neutrino masses, discussed in Appendix 6.4, are roughly proportional to the $Y_{\nu ij}$ and v_{Li} parameters, it follows that $Y_{\nu ij} \ll 1$ and $v_{Li} \ll v_{u,d}, v_R$. In this phenomenologically relevant limit, the minimization conditions of the potential are simple and worthwhile to note. They are

$$v_R^2 = \frac{-8 m_{\tilde{\nu}_3^c}^2 + g_R^2 \left(v_u^2 - v_d^2 \right)}{g_R^2 + g_{BL}^2} \;, \tag{1.13}$$

$$v_{Li} = \frac{\frac{v_R}{\sqrt{2}} (Y_{\nu i3}^* \mu v_d - a_{\nu i3}^* v_u)}{m_{\tilde{L}_i}^2 - \frac{g_2^2}{8} (v_u^2 - v_d^2) - \frac{g_{BL}^2}{8} v_R^2} \;, \tag{1.14}$$

$$\frac{1}{2} M_Z^2 = -\mu^2 + \frac{m_{H_u}^2 \tan^2\beta - m_{H_d}^2}{1 - \tan^2\beta} \;, \tag{1.15}$$

$$\frac{2b}{\sin 2\beta} = 2\mu^2 + m_{H_u}^2 + m_{H_d}^2 \;. \tag{1.16}$$

Here, the first two equations correspond to the sneutrino VEVs. The third and fourth equations are of the same form as in the MSSM, but new $B - L$ scale contributions to m_{H_u} and m_{H_d} shift their values significantly compared to the MSSM. Eq. (1.13) can be used to re-express the Z_R mass as

$$M_{Z_R}^2 = -2m_{\tilde{\nu}_3^c}^2 \left(1 + \frac{g_R^4}{g_R^2 + g_{BL}^2} \frac{v^2}{v_R^2}\right) \ . \tag{1.17}$$

This makes it clear that, to leading order, the Z_R mass is determined by the soft SUSY breaking mass of the third family right-handed sneutrino. The term proportional to v^2/v_R^2 is insignificant in comparison and, henceforth, neglected in our calculations.

A direct consequence of generating a VEV for the third family sneutrino is the spontaneous breaking of R-parity. The induced operators in the superpotential are

$$W \supset \epsilon_i \, L_i \, H_u - \frac{1}{\sqrt{2}} Y_{ei} \, v_{Li} \, H_d^- \, e_i^c \ , \tag{1.18}$$

where

$$\epsilon_i \equiv \frac{1}{\sqrt{2}} Y_{\nu i3} v_R \ . \tag{1.19}$$

This general pattern of R-parity violation is referred to as bilinear R-parity breaking and has been discussed in many different contexts, especially in reference to neutrino masses– see references [39, 40, 41, 42] for early works. In addition, the Lagrangian contains additional bilinear terms generated by v_{Li} and v_R from the super-covariant derivative. These are

$$\begin{aligned} \mathcal{L} \supset & -\frac{1}{2} v_{Li}^* \left[g_2 \left(\sqrt{2} \, e_i \tilde{W}^+ + \nu_i \tilde{W}^0 \right) - g_{BL} \nu_i \tilde{B}' \right] \\ & -\frac{1}{2} v_R \left[-g_R \nu_3^c \tilde{W}_R + g_{BL} \nu_3^c \tilde{B}' \right] + \text{h.c.} \end{aligned} \tag{1.20}$$

The consequences of spontaneous R-parity violation are quite interesting, and have been discussed in a variety of papers. For LHC studies, see [30, 31]. Predictions for the neutrino sector were discussed in [16, 32, 33]. It was shown that the lightest left-handed, or active, neutrino is massless and that the model contains two right-handed neutrinos, referred to as sterile neutrinos, that are lighter than the remaining two active neutrinos. Sterile neutrinos can influence the cosmological evolution of the universe due to their role as dark radiation. This effect was studied in [31].

In this section, we have focussed on the TeV scale manifestation of the $B - L$ MSSM. The remainder of this thesis will explore this model at a variety of scales, seeking to connect the model's origins in $E_8 \otimes E_8$ heterotic string theory with its phenomenological manifestations in the LHC.

Chapter 2

Through the Desert

2.1 Scales

The goal of this chapter is to address the physics associated with the string construction of the $B - L$ MSSM. This takes us from the unification scale through the particle physics "desert" to the electroweak scale. The results developed here are used throughout the thesis in connecting the string-motivated considerations at high scale to observable physics at the LHC.

After compactification to four-dimensions, the theory takes the form of an $SO(10)$ grand unified theory. This is then further broken to the $B - L$ MSSM gauge group by the turning on of two Abelian Wilson lines, denoted by χ_{3R} and χ_{B-L} respectively. The energy scales associated with these Wilson lines need not be the same. In fact, exact gauge coupling unification at one-loop, which we will assume throughout this thesis, requires that the scales be different– implying there is a two-step symmetry breaking process from $SO(10)$ to the gauge group of the $B - L$ MSSM. This leads to an intermediate regime between the two scales associated with the Wilson lines. The particle content and gauge group in this regime depends on which Wilson line turns on first. Defining the mass scales of χ_{3R} and χ_{B-L} as $M_{\chi_{3R}}$ and $M_{\chi_{B-L}}$ respectively, we have the following two initial symmetry breaking patterns.

- $M_{\chi_{B-L}} > M_{\chi_{3R}}$: $SO(10) \to SU(3)_C \otimes SU(2)_L \otimes SU(2)_R \otimes U(1)_{B-L}$, the "left-right" model
- $M_{\chi_{3R}} > M_{\chi_{B-L}}$: $SO(10) \to SU(4)_C \otimes SU(2)_L \otimes U(1)_{3R}$, a modified version of the "Pati-Salam" model

In each case, the turning on of the second Wilson line breaks the intermediate model to the $B - L$ MSSM.

To fully understand the evolution of this model from unification to the electroweak scale, it should be noted that there are five relevant mass scales of interest, two of which were mentioned briefly above. All five are described in the following:

- M_{U}: The unification mass and the scale of the first Wilson line. We assume that all gauge couplings unify at this scale to a single value g_{U}.
- M_{I}: The intermediate scale associated with the second Wilson line and the symmetry breaking.
- M_{B-L}: The $B - L$ scale is the mass at which the right-handed sneutrino VEV triggers $U(1)_{3R} \otimes U(1)_{B-L} \to U(1)_Y$. Physically, this corresponds to the mass of the neutral gauge boson Z_R of the broken symmetry and, therefore, the scale of Z_R decoupling. Specifically

  $$M_{Z_R} = M_{B-L}, \tag{2.1}$$

  where M_{Z_R} depends on parameters evaluated at M_{B-L}–see Eq. (1.9). Substituting Eq. (1.9) into this relation yields a transcendental equation that must be solved using iterative numerical methods to obtain the correct value for M_{B-L}.

  At this scale, we also evaluate the hypercharge gauge coupling using its relationship to the gauge parameters of $B - L$ and the third component of right-handed isospin. This is given by

  $$g_1 = \sqrt{\frac{5}{3}} g_R \sin\theta_R = \sqrt{\frac{5}{2}} g'_{BL} \cos\theta_R \ , \tag{2.2}$$

  where

  $$\cos\theta_R = \frac{g_R}{\sqrt{g_R^2 + \frac{3}{2} g'^2_{BL}}} \ . \tag{2.3}$$

  Note that Eq. (2.2) is just a restatement of Eq. (1.11) with gauge couplings properly normalized for unification, including a rescaled hypercharge gauge coupling g_1 defined by

  $$g_1 = \sqrt{\frac{5}{3}} g_Y \ . \tag{2.4}$$

- M_{SUSY}: The soft SUSY breaking scale. This is the scale at which all sparticles are integrated out with the exception of the right-handed sneutrinos. The right-handed sneutrinos are associated with $B-L$ breaking and, therefore, are integrated out at the $B-L$ scale. While there is obviously no single scale associated with the masses of all the SUSY partners, we use the scale of stop decoupling given by

  $$M_{\text{SUSY}} = \sqrt{m_{\tilde{t}_1}\, m_{\tilde{t}_2}}. \tag{2.5}$$

  This scale is useful because when the stops decouple, the parameter that controls electroweak symmetry breaking, that is, the soft H_u mass parameter, effectively stops running– see [43] for more details. Like the $B-L$ scale, the SUSY scale must be determined using iterative numerical methods because the physical stop masses in Eq. (2.5) depend implicitly on the SUSY scale.

- M_{EW}: The electroweak scale. This is the well-known scale associated with the Z and W gauge bosons of the SM. We will make the identification

  $$M_{\text{EW}} = M_Z. \tag{2.6}$$

  For correct electroweak breaking, one must satisfy the conditions

  $$2b < 2\mu^2 + m_{H_u}^2 + m_{H_d}^2\ , \tag{2.7}$$
  $$b^2 > (\mu^2 + M_{H_d}^2)(\mu^2 + M_{H_u}^2)\ . \tag{2.8}$$

  The first constraint guarantees that the Higgs potential is bounded from below while the second indicates that the trivial vacuum is not stable.

2.2 Matter Content

With the relevant mass scales appropriately defined, we can now discuss the physical regimes that exist in between them. To begin with, we will be interested in the evolution of the gauge couplings–since our assumption that they unify will help relate these disparate scales to each other. Note that while $M_{\text{U}} > M_{\text{I}} \gg M_{B-L}, M_{\text{SUSY}}$, the hierarchy between the SUSY and $B-L$ scales depends on the point chosen in the initial parameter space. Each of the two possibilities will be addressed below. We present below, for each regime, the slope factors b_a appearing in the gauge RGE's

$$\frac{d}{dt}\alpha_a^{-1} = -\frac{b_a}{2\pi} \ , \tag{2.9}$$

where a indexes the associated gauge groups.

The scaling regime from $M_{\rm U}$ to $M_{\rm I}$ is populated by either the left-right model or the Pati-Salam model discussed above. The two cases will be treated separately.

In the case of the left-right intermediate regime, the particle content consists of nine copies of the matter family

$$Q \sim (\mathbf{3}, \mathbf{2}, \mathbf{1}, \frac{1}{3}), \qquad Q^c = \left(\begin{array}{c} d^c \\ u^c \end{array}\right) \sim (\bar{\mathbf{3}}, \mathbf{1}, \mathbf{2}, -\tfrac{1}{3}) \tag{2.10}$$

$$L \sim (\mathbf{1}, \mathbf{2}, \mathbf{1}, -1), \qquad L^c = \left(\begin{array}{c} e^c \\ \nu^c \end{array}\right) \sim (\mathbf{1}, \mathbf{1}, \mathbf{2}, 1), \tag{2.11}$$

two copies of a Higgs bi-doublet, which contains the MSSM Higgs fields,

$$\mathcal{H}_1, \ \mathcal{H}_2 \sim (\mathbf{1}, \mathbf{2}, \mathbf{2}, 0) \ , \tag{2.12}$$

and a pair of color triplets

$$H_C \sim (\mathbf{3}, \mathbf{1}, \mathbf{1}, 2), \quad \bar{H}_C \sim (\bar{\mathbf{3}}, \mathbf{1}, \mathbf{1}, -2) \ . \tag{2.13}$$

In this interval, the b_a factors are

$$b_3 = 10, \ b_2 = 14, \ b_R = 14, \ b_{B-L} = 19 \ . \tag{2.14}$$

We will refer to this scaling interval as the "left-right regime". Once the second Wilson line turns on, the extra particle content is integrated out and we are left with exactly the spectrum of the $B-L$ MSSM.

In the case of Pati-Salam type intermediate regime the particle content consists of nine copies of the matter family

$$\left(\begin{array}{c} Q \\ L \end{array}\right) \sim (\mathbf{4}, \mathbf{2}, 0) \tag{2.15}$$

$$\left(\begin{array}{c} u \\ \nu \end{array}\right) \sim (\bar{\mathbf{4}}, \mathbf{1}, -1/2) \tag{2.16}$$

$$\left(\begin{array}{c} Q \\ L \end{array}\right) \sim (\bar{\mathbf{4}}, \mathbf{1}, 1/2) \ , \tag{2.17}$$

and the $B-L$ MSSM higgs fields,

$$H_u \sim (\mathbf{1}, \mathbf{2}, 1/2) \tag{2.18}$$

$$H_d \sim (\mathbf{1}, \mathbf{2}, -1/2) \ . \tag{2.19}$$

In this interval, the b_a factors are

$$b_4 = 6,\ b_2 = 14,\ b_{3R} = 20 \ . \tag{2.20}$$

We will refer to this scaling interval as the "Pati-Salam regime". Once the second Wilson line turns on, the extra particle content is integrated out and we are left with exactly the spectrum of the $B-L$ MSSM.

Both sequential breaking patterns, specifying the gauge groups and the associated zero-mode spectra, are shown schematically in Figure 2.1.

The scaling regime from M_{I} to $\max(M_{\text{SUSY}}, M_{B-L})$ is populated by the $B-L$ MSSM model with the matter content discussed in Section 1.2. The b_a factors in this case are

$$b_3 = -3,\ b_2 = 1,\ b_R = 7,\ b_{B-L} = 6 \ . \tag{2.21}$$

We will refer to this scaling interval as the "B-L MSSM regime".

The remaining two regimes depend on which of the following two cases occurs: $M_{B-L} > M_{\text{SUSY}}$–the "right-side-up" hierarchy–and $M_{\text{SUSY}} > M_{B-L}$–the "upside-down" hierarchy.

right-side-up hierarchy:

- $M_{B-L} - M_{\text{SUSY}}$: In this case $B-L$ has been broken but SUSY is still a good symmetry, thereby giving an MSSM-like theory–that is, the MSSM plus two light right-handed neutrino chiral multiplets. Another possible deviation might occur in the composition of the bino, which is discussed in Section 2.4. In general, however, this is the MSSM. Specifically, the gauge couplings in this regime evolve like the well-known MSSM gauge couplings with b_a coefficients

  $$b_3 = -3,\ b_2 = 1,\ b_1 = \frac{33}{5} \ . \tag{2.22}$$

  We refer to this interval as the "MSSM regime".

- $M_{\text{SUSY}} - M_{\text{EW}}$: In this regime, one simply has the SM with two sterile neutrinos. It has the well-known slope factors

  $$b_3 = -7,\ b_2 = -\frac{19}{6},\ b_1 = \frac{41}{10} \ . \tag{2.23}$$

  We refer to this as the "SM regime".

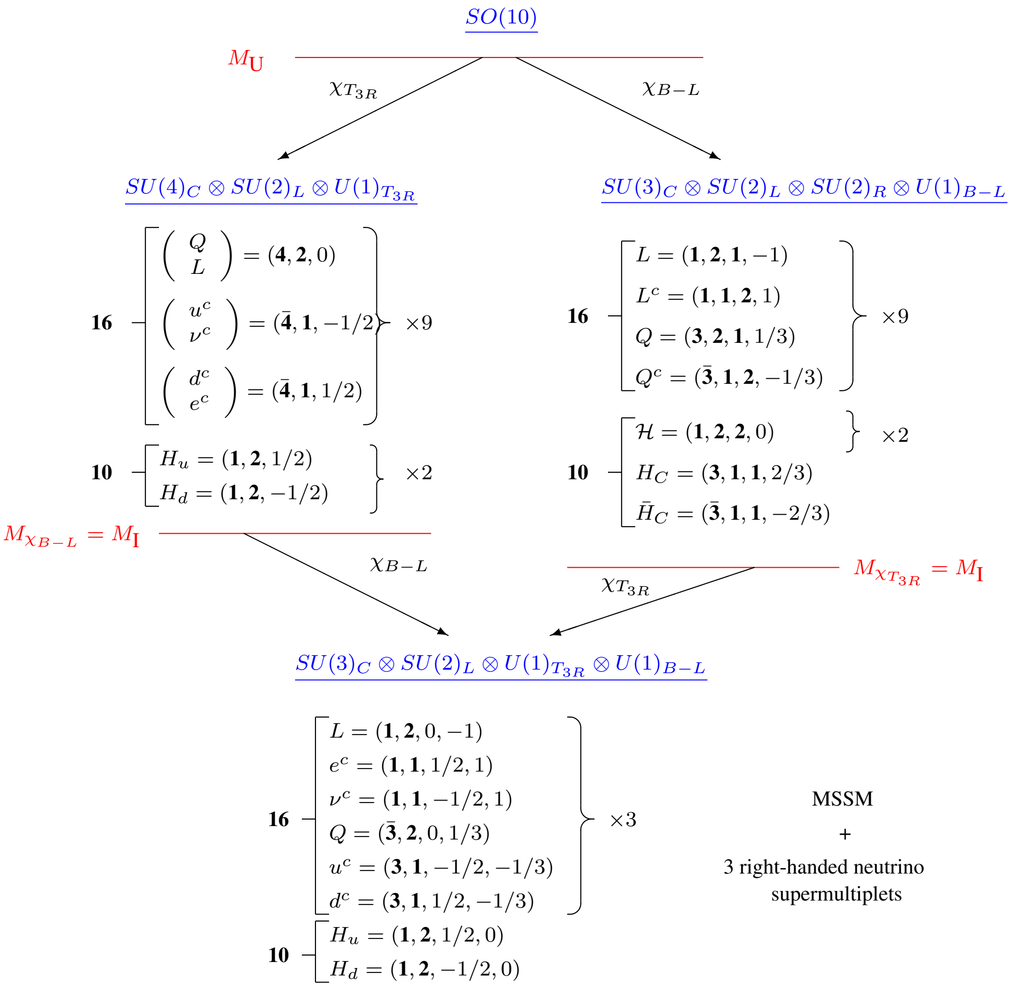

Figure 2.1: The particle spectra in the associated scaling regimes of the two sequential Wilson line breaking patterns of $SO(10)$.

upside-down hierarchy:

- $M_{\rm SUSY} - M_{B-L}$: Now $B-L$ remains a good symmetry below the average stop mass, where we effectively integrated out the SUSY partners. The resulting theory is simply a non-SUSY $SU(3)_C \otimes SU(2)_L \otimes U(1)_{3R} \otimes U(1)_{B-L}$ model, which also includes three generations of right-handed sneutrinos–

the third of which acts as the $B-L$ Higgs. The slope factors are

$$b_3=-7,\ b_2=\frac{19}{6},\ b_R=\frac{53}{12},\ b_{BL}=\frac{33}{8}. \tag{2.24}$$

- $M_{B-L}-M_{\text{EW}}$: Here, again, we have the SM with two sterile neutrinos and the slope factors given in Eq. (2.23).

2.3 Gauge Unification

The discussion of gauge unification requires a brief digression on kinetic mixing. For general $U(1)\otimes U(1)$, the two Abelian field strengths can exhibit kinetic mixing; that is,

$$\mathcal{L}_{kinetic}=-\frac{1}{4}((F^1_{\mu\nu})^2+2\alpha F^1_{\mu\nu}F^{2\mu\nu}+(F^2_{\mu\nu})^2+\dots) \tag{2.25}$$

for some real parameter α. Note that the mixing parameter must satisfy $|\alpha|<1$ so that the diagonalized kinetic energy will be ghost free. Note that $U(1)_{3R}\otimes U(1)_{B-L}$ are orthogonal subgroups of $SO(10)$, that is

$$\text{Tr}_{\,\text{representation}}(T_{3R}(B-L))=0\ , \tag{2.26}$$

where the trace is over a complete representation of $SO(10)$. It follows that the value of α at the unification scale, M_{U}, must vanish. This is an important property of the $U(1)_{3R}\otimes U(1)_{B-L}$ Abelian gauge symmetries.

• *Since the generators of the $U(1)$ charges are orthogonal in $SO(10)$, the value of the kinetic field strength mixing parameter α must vanish at the unification scale. That is, $\alpha(M_U)=0$.*

Once the $SO(10)$ symmetry is broken by both Wilson lines, either by turning them on at the same scale or sequentially, as discussed below, one expects the mixing parameter α to regrow due to radiative corrections. In this case, the Abelian field strengths develop a non-vanishing mixing term which greatly complicates the renormalization group analysis of the low energy effective theory. Since this kinetic mixing is purely due to radiative corrections, it always satisfies the constraint $|\alpha|<1$, thus ensuring that the diagonalized kinetic energy remains ghost free. Radiative kinetic mixing has been discussed by a number of authors, see, for example, [44, 45, 46, 47, 48, 49]. Let us briefly review the analysis. Consider a theory with unspecified $U(1) \otimes U(1)$ gauge factors. Then, in general, at an arbitrary momentum scale, equation (2.25) holds. The associated gauge covariant derivative is given by

$$D = \partial - iT^1 g_1 A^1 - iT^2 g_2 A^2 \ , \tag{2.27}$$

where we denote the coupling parameters and gauge fields associated with T^1 and T^2 by g_1, A^1 and g_2, A^2 respectively. Defining new gauge fields by $\vec{A} = \mathcal{O}\vec{A}'$ where

$$\mathcal{O} = \frac{1}{\sqrt{2}} \begin{pmatrix} 1 & 1 \\ -1 & 1 \end{pmatrix} \tag{2.28}$$

diagonalizes the kinetic energy terms to

$$\mathcal{L}_{kinetic} = -\frac{1}{4}((1-\alpha)(F'^1_{\mu\nu})^2 + (1+\alpha)(F'^2_{\mu\nu})^2 + \ldots) \ . \tag{2.29}$$

Further rescaling of the gauge fields by $\vec{A}' = \mathcal{D}^{-\frac{1}{2}}\vec{A}''$ with

$$\mathcal{D}^{-\frac{1}{2}} = \begin{pmatrix} \frac{1}{\sqrt{1-\alpha}} & 0 \\ 0 & \frac{1}{\sqrt{1+\alpha}} \end{pmatrix} \tag{2.30}$$

leads to a canonically normalized kinetic term

$$\mathcal{L}_{kinetic} = -\frac{1}{4}((F''^1_{\mu\nu})^2 + (F''^2_{\mu\nu})^2 + \ldots) \ . \tag{2.31}$$

However, the covariant derivative now has off-diagonal gauge couplings

$$D = \partial - i(T^1, T^2) \begin{pmatrix} \frac{g_1}{\sqrt{1-\alpha}} & \frac{g_1}{\sqrt{1+\alpha}} \\ \frac{-g_2}{\sqrt{1-\alpha}} & \frac{g_2}{\sqrt{1+\alpha}} \end{pmatrix} \begin{pmatrix} A''^1 \\ A''^2 \end{pmatrix} \ . \tag{2.32}$$

Note that the four gauge couplings are not independent, being functions of the three parameters α, g_1 and g_2 in the original Lagrangian. It is not surprising, therefore, that a further field redefinition will eliminate one of them. The transformation should be orthogonal so as to leave the field strength kinetic term diagonal and canonically normalized. This can be achieved by setting $\vec{A}'' = \mathcal{P}\vec{\mathcal{A}}$ where

$$\mathcal{P} = \frac{1}{\sqrt{2}} \begin{pmatrix} \sqrt{1-\alpha} & -\sqrt{1+\alpha} \\ \sqrt{1+\alpha} & \sqrt{1-\alpha} \end{pmatrix} \ . \tag{2.33}$$

We find that the covariant derivative now becomes

$$D = \partial - i(T^1, T^2) \begin{pmatrix} \mathcal{G}_1 & \mathcal{G}_M \\ 0 & \mathcal{G}_2 \end{pmatrix} \begin{pmatrix} \mathcal{A}^1 \\ \mathcal{A}^2 \end{pmatrix} , \tag{2.34}$$

with

$$\mathcal{G}_1 = g_1, \quad \mathcal{G}_2 = \frac{g_2}{\sqrt{1-\alpha^2}}, \quad \mathcal{G}_M = \frac{-g_1 \alpha}{\sqrt{1-\alpha^2}} . \tag{2.35}$$

Note that in the limit that $\alpha \to 0$, $\mathcal{G}_2 = g_2$ and $\mathcal{G}_M = 0$.

The renormalization group equations for the gauge couplings in this "upper triangular" realization were given in [44]. Here, however, it suffices to present the RGE for the off-diagonal coupling $\mathcal{G}_M$. It is found to be

$$\frac{d\mathcal{G}_M}{dt} = \frac{1}{16\pi^2} \beta_M \tag{2.36}$$

where

$$\beta_M = \mathcal{G}_2^2 \mathcal{G}_M B_{22} + \mathcal{G}_M^3 B_{11} + 2\mathcal{G}_1^2 \mathcal{G}_M B_{11} + 2\mathcal{G}_2 \mathcal{G}_M^2 B_{12} + \mathcal{G}_1^2 \mathcal{G}_2 B_{12} \tag{2.37}$$

and

$$B_{ij} = Tr(T^i T^j) . \tag{2.38}$$

The trace in (2.38) is over the entire matter and Higgs spectrum of the theory (not just a complete representation of the unifying gauge group). Note that all of the terms in the β function (2.37), with the exception the last term, contain at least one power of $\mathcal{G}_M$. If the mixing parameter α and, hence, the off-diagonal coupling $\mathcal{G}_M$ vanish at some initial scale, as they will for our canonical basis, then the terms containing $\mathcal{G}_M$ will not, by themselves, generate a non-zero mixing parameter at any lower scale. However, a non-vanishing $\mathcal{G}_M$ will be generated by the last term. The only exception to this is if the charges T^1 and T^2 are such that

$$B_{12} = Tr(T^1 T^2) = 0 . \tag{2.39}$$

Generically, this will not be the case for arbitrary charges of $U(1) \otimes U(1)$. However, for the matter content and gauge group of the $B - L$ MSSM it is the case that

$$\mathrm{Tr}_{\,\mathrm{matter}}(T_{3R}(B-L)) = 0 , \tag{2.40}$$

this trace vanishes.[1] Therefore, for the canonical basis if the initial value of α and, hence, $\mathcal{G}_M$ vanish, then both will remain zero at any lower scale. This is a second

---

[1] Note that this is not redundent to Eq. (2.26) because the trace in over the complete matter content of the $B - L$ MSSM, rather than a complete representation of $SO(10)$.

important property possessed by the $U(1)$ charges of the $B-L$ MSSM.

- *The generators of the $U(1)\otimes U(1)$ gauge groups are such that Tr*$_{\text{matter}}(T_{3R}(B-L))=0$*, where the trace is performed over the matter and Higgs spectrum of the $B-L$ MSSM. This guarantees that if the original kinetic mixing parameter vanishes, then α and, hence, $\mathcal{G}_M$ will remain zero under the RG at any scale. This property of not having kinetic mixing greatly simplifies the renormalization group analysis of the $SU(3)_C\otimes SU(2)_L\otimes U(1)_{T_{3R}}\otimes U(1)_{B-L}$ low energy theory.*

At this point, it is important to make a quick note on notation for the $B-L$ gauge coupling. Thus far, we have discussed the gauge parameter g_{BL}, which couples to $\frac{1}{2}(B-L)$ charge. As is well known, this gauge coupling has to be properly normalized so as to unify with the other gauge parameters. We use g'_{BL} defined by

$$g'_{BL}=\sqrt{\frac{2}{3}}g_{BL} \tag{2.41}$$

to denote the properly unifying coupling. The parameter g'_{BL} couples to $\sqrt{\frac{3}{8}}(B-L)$ charge and will appear in the RGEs. For quantities of physical interest, such as physical masses, g_{BL} will be used.

We begin our analysis of gauge unification assuming the left-right intermediate regime. Hence, the intermediate regime contains the left-right model. We then make the identifications

$$M_{\mathrm{U}}\equiv M_{\chi_{B-L}},\quad \text{the scale of gauge coupling unification} \tag{2.42}$$

$$M_{\mathrm{I}}\equiv M_{\chi_{3R}},\quad \text{the intermediate scale} \tag{2.43}$$

Given the above information, and the demand that all gauge couplings unify, we can solve for a given mass scale in terms of the others. First consider the unification mass–corresponding to the scale at which the four gauge couplings become equal to each other. Practically, it is derived as the energy-momenta at which $g_3=g_2$. As is well-known, this will not be influenced by any scale that acts as a threshold for complete multiplets of a minimal group that unifies $SU(3)$ and $SU(2)$–for example, $SU(5)$. The $B-L$ and intermediate scales are both such thresholds. The $B-L$ scale is a threshold for singlets of $SU(5)$, that is, the right-handed neutrinos, while M_{I} is a threshold for six new matter generations, a pair of Higgs doublets and their $SU(5)$ color partners. All of these particles fit into the **1**, **5**, $\bar{\mathbf{5}}$ and **10** of $SU(5)$– see Eqs. (2.10)-(2.13). Working through the algebra of setting $g_3(M_{\mathrm{U}}) = g_2(M_{\mathrm{U}})$ yields

$$M_{\mathrm{U}} = \left[e^{\frac{2\pi(\alpha_3-\alpha_2)}{\alpha_2\alpha_3}} M_Z^{\left(b_2^{\mathrm{SM}}-b_3^{\mathrm{SM}}\right)} M_{\mathrm{SUSY}}^{\left(b_2^{\mathrm{MSSM}}-b_2^{\mathrm{SM}}+b_3^{\mathrm{SM}}-b_3^{\mathrm{MSSM}}\right)} \right]^{\frac{1}{b_2^{\mathrm{LR}}-b_3^{\mathrm{LR}}}} , \tag{2.44}$$

where the superscripts on the slope factors indicate their regime of relevance and the α_i take their experimental values at M_Z [50]:

$$\alpha_3(M_Z) = 0.118,\ \alpha_2(M_Z) = 0.0337,\ \alpha_1(M_Z) = 0.0170\ . \tag{2.45}$$

Inserting all the coefficients, the unification scale becomes

$$M_{\mathrm{U}} \simeq 2.186 \times 10^{16} \left(\frac{M_{\mathrm{SUSY}}}{1\ \mathrm{GeV}}\right)^{0.0417} (\mathrm{GeV})\ . \tag{2.46}$$

Similarly, the intermediate scale can be solved for by setting $g_R(M_{\mathrm{U}}) = g'_{BL}(M_{\mathrm{U}}) = g_3(M_{\mathrm{U}})$ and using the relationship between the gauge couplings of hypercharge , $B - L$ and the third component of right-handed isospin given in Eq. (2.2). The intermediate scale is found to be

$$M_{\mathrm{I}} = \left[e^{\frac{10\pi(\alpha_1-\alpha_2)}{\alpha_1\alpha_2}} M_Z^{5\left(b_2^{\mathrm{SM}}-b_1^{\mathrm{SM}}\right)} M_{\mathrm{SUSY}}^{5\left(b_2^{\mathrm{MSSM}}-b_2^{\mathrm{SM}}+b_1^{\mathrm{SM}}-b_1^{\mathrm{MSSM}}\right)} M_{\mathrm{U}}^{\left(3b_R^{\mathrm{LR}}+2b_{BL}^{\mathrm{LR}}-5b_2^{\mathrm{LR}}\right)} \right]^{\frac{1}{5\left(b_2^{\mathrm{BL}}-b_2^{\mathrm{LR}}\right)+2\left(b_{BL}^{\mathrm{LR}}-b_{BL}^{\mathrm{BL}}\right)+3\left(b_R^{\mathrm{LR}}-b_R^{\mathrm{BL}}\right)}} . \tag{2.47}$$

Substituting for M_{U} using Eq. (4.17) gives

$$M_{\mathrm{I}} \simeq 1.835 \times 10^{17} \left(\frac{M_{\mathrm{SUSY}}}{1\ \mathrm{GeV}}\right)^{-0.486} (\mathrm{GeV}). \tag{2.48}$$

The associated running coupling parameters are plotted in Figure 2.2 for representative choices of $M_{\mathrm{SUSY}} = 1$ TeV and $M_{B-L} = 10$ TeV.

We continue our analysis of gauge unification assuming the left-right intermediate regime. Hence, the intermediate regime contains the left-right model. We then make the identifications

$$M_{\mathrm{U}} \equiv M_{\chi_{3R}},\ \text{ the scale of gauge coupling unification} \tag{2.49}$$

$$M_{\mathrm{I}} \equiv M_{\chi_{B-L}},\ \text{ the intermediate scale.} \tag{2.50}$$

The algebra in this case is a bit more complicated because the intermediate scale is not a threshold for complete multiplets of a group that unifies $SU(3)$ and

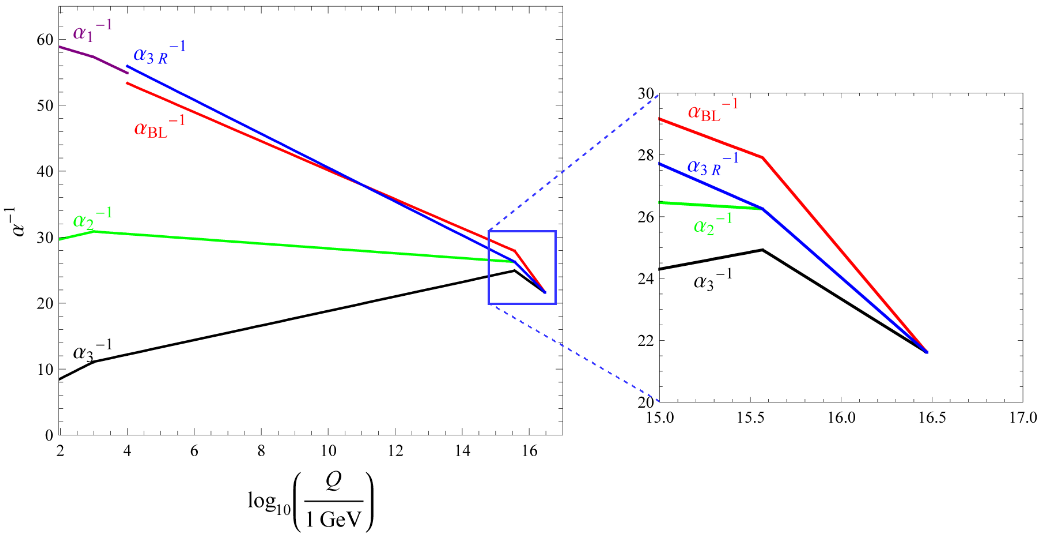

Figure 2.2: One-loop RGE running of the inverse gauge couplings, α_i^{-1} in the case of the left-right model with $M_{B-L} = 10$ TeV with an enlarged image of the intermediate region.

$SU(2)$. Therefore the solution for the unification scale can not be separated from the solution for the interemdiate scale. Setting $g_3(M_{\text{I}}) = g'_{BL}(M_{\text{I}})$ and $g_4(M_{\text{U}}) = g_2(M_{\text{U}}) = g_R(M_{\text{U}})$ yields a system of four equations that can be solved for the scales M_{U} and M_{I}.

The associated running coupling parameters are plotted in Figure 2.3 for representative choices of $M_{\text{SUSY}} = 1$ TeV and $M_{B-L} = 10$ TeV.

2.3.1 Gauge Unification with Simultaneous Wilson Lines

When both Wilson lines turn on simultaneously, so that $M_{\text{I}} = M_{\text{U}}$, the intermediate region is absent and $SO(10)$ is immediately broken to $SU(3)_C \otimes SU(2)_L \otimes U(1)_{T_{3R}} \otimes U(1)_{B-L}$ with the MSSM particle content supplemented by three families of right-handed neutrino chiral mulitplets.

Naively, one might try to impose the boundary condition

$$\alpha_3(M_{\text{U}}) = \alpha_2(M_{\text{U}}) = \alpha_{3R}(M_{\text{U}}) = \alpha_{BL}(M_{\text{U}}) \ . \tag{2.51}$$

However, as we will see below, unlike in the left-right and Pati-Salam cases, this unification condition is inconsistent with the experimental values of α_3, α_2 and α_1

at M_Z within the assumptions we have made about the mass thresholds. Hence, we will not input this condition. Rather, we will scale up to M_{U} from the experimental input at M_Z and examine to what extent unification is violated. Of course, the boundary condition

$$\alpha_1(M_{B-L}) = \frac{5}{3\alpha_{3R}^{-1}(M_{B-L}) + 2\alpha_{BL}^{-1}(M_{B-L})}, \tag{2.52}$$

at M_{B-L} continues to hold. Since the theory is identical to the left-right and Pati-Salam cases below M_{I}, the beta functions in all subsequent scaling regimes are given in (2.21), (2.22), (2.23) and (2.24).

In the previous two sections, the final step of the RG procedure was to solve for M_{I}. In both cases, there was a unique solution for M_{I} that satisfied the boundary conditions–including gauge coupling unification at M_{U}. In the simultaneous Wilson lines case, however, we are fixing $M_{\text{I}} = M_{\text{U}}$ in advance. Hence, if we continue to use the full set of boundary conditions mandated in the previous sections, the system will be overdetermined. Specifically, we find that one cannot simultaneously impose (2.51) and (2.52) while also matching the low energy experimental input (2.45). To proceed, some boundary condition must be relaxed. Constraint (2.51) has the greatest uncertainty due to string threshold effects. Hence, we will no longer impose it. There is no flexibility in the running of α_3 and α_2, their running and unification being completely determined by the experimental input. However, the low energy value of α_Y along with (2.52) can be used to write a relationship between α_{3R} and α_{BL} at M_{B-L}, but not fix them. Most choices for these two couplings will lead to neither of them unifying with α_3, α_2 at M_{U}. However, it is possible to choose one of them so that it indeed unifies with α_3 and α_2 at M_{U}. In this case, however, the other coupling, calculated from the first using (2.52), will not unify. And vice, versa.

Let us first demand that α_{BL} unify with α_3, α_2 at M_{U}. Using (2.52) to solve for α_{3R} at M_{B-L}, we find that $\alpha_{3R}(M_{\text{U}})$ will miss unification by $\sim 8\%$. To be precise,

$$\left| \frac{\alpha_{BL}(M_{\text{U}}) - \alpha_{3R}(M_{\text{U}})}{\alpha_{3R}(M_{\text{U}})} \right| \approx 8\%. \tag{2.53}$$

Another, potentially instructive, way to think of this procedure is to start with the left-right model of Subsection 2.3 and move M_{I} continuously up to M_{U}, without changing any of the RG running below M_{I}. Recall that the unification scale of α_3 and α_2 is independent of M_{I}, since the additional particle content in the intermediate region fits into complete multiplets of $SO(10)$. Note that α_{BL} is affected in the same way, which means that all three of these couplings will continue to unify at the same scale as we move $M_{\rm I}$ up toward $M_{\rm U}$. However, α_{3R} will be affected differently because, at the intermediate scale, it changes from a $U(1)_{T_{3R}}$ coupling to an $SU(2)_R$ coupling. Hence, it will not continue to unify with the others as $M_{\rm I}$ approaches $M_{\rm U}$.

If we demand that α_{3R} unify with α_3, α_2, and use (2.52) to solve for α_{BL} at M_{B-L}, we find that $\alpha_{3R}(M_{\rm U})$ will miss unification by $\sim 13\%$. The RG running of the gauge coupling in each of these scenarios is shown in Figure 2.4.

It is interesting to note that exact unification (of gauge couplings) with simultaneous Wilson lines *can* be achieved by taking into account the fact that not all superpartners will have precisely the same mass, and, therefore, will not all decouple at the same scale, $M_{\rm SUSY}$. We now explore two possibilities in this regard. First, group all of the non-colored sparticles together at mass scale $M_{{\rm SUSY}_n}$. Similarly, we will put all colored sparticles at mass $M_{{\rm SUSY}_c}$, where $M_{{\rm SUSY}_c} > M_{{\rm SUSY}_n}$. The beta functions below $M_{{\rm SUSY}_n}$ and above $M_{{\rm SUSY}_c}$ are unchanged. In between these two scales, the theory is the MSSM without the colored superpartners. The beta function coefficients in the regime $M_{{\rm SUSY}_c} \to M_{{\rm SUSY}_n}$ are calculated to be

$$b_3 = -7, \quad b_2 = -\frac{1}{2}, \quad b_1 = \frac{11}{2}. \tag{2.54}$$

Choosing $M_{{\rm SUSY}_n}$ and M_{B-L} and demanding unification of gauge couplings specifies the value of $M_{{\rm SUSY}_c}$. A specific example is shown in Figure 2.5, where

$$M_{{\rm SUSY}_n} = 500 \text{ GeV}, \quad M_{B-L} = 10 \text{ TeV} \tag{2.55}$$

is chosen. This yields

$$\begin{gathered} M_{\rm U} = 8.3 \times 10^{15} \text{ GeV}, \quad M_{{\rm SUSY}_c} = 3.7 \text{ TeV} \\ \alpha_u = 0.038, \quad \alpha_{3R}(M_{B-L}) = 0.0176, \quad \alpha_{BL}(M_{B-L}) = 0.0191 \,. \end{gathered} \tag{2.56}$$

Let us explore a second possibility. Group all non-colored sparticles, as well as all left-handed squarks, at $M_{{\rm SUSY}_{n+}}$. Now let

$$(M_{{\rm SUSY}_{n+}} \sim M_2) : M_3 = 2 : 5 \,. \tag{2.57}$$

Finally, let all right-handed squarks have mass $M_{{\rm SUSY}_{c-}} > M_3$. To summarize, $M_{\rm SUSY}$ has been split into three thresholds: $M_{{\rm SUSY}_{n+}}$, M_3, and $M_{{\rm SUSY}_{c-}}$.

$$M_{EW} < \overbrace{M_{{\rm SUSY}_{n+}} < M_3 < M_{{\rm SUSY}_{c-}}}^{M_{\rm SUSY}} < M_{B-L} \,. \tag{2.58}$$

The beta functions below $M_{\text{SUSY}_{n+}}$ and above $M_{\text{SUSY}_{c-}}$ are unchanged. The beta function coefficients in the regime $M_{\text{SUSY}_{n+}} \to M_3$ are found to be

$$b_3 = -6, \quad b_2 = 1, \quad b_1 = \frac{28}{5}, \tag{2.59}$$

and these coefficients in the regime $M_3 \to M_{\text{SUSY}_{c-}}$ are found to be

$$b_3 = -4, \quad b_2 = 1, \quad b_1 = \frac{28}{5}. \tag{2.60}$$

Choosing $M_{\text{SUSY}_{n+}}$ and M_{B-L} and demanding unification of gauge couplings specifies the value of $M_{\text{SUSY}_{c-}}$. A specific example is shown in Figure 2.6, where

$$M_{\text{SUSY}_{n+}} = 500 \text{ GeV}, \quad M_{B-L} = 10 \text{ TeV} \tag{2.61}$$

is chosen. This yields

$$\begin{gathered} M_{\text{U}} = 1.2 \times 10^{16} \text{ GeV}, \quad M_{\text{SUSY}_{c-}} = 2.3 \text{ TeV} \qquad (2.62) \\ \alpha_u = 0.039, \quad \alpha_{3R}(M_{B-L}) = 0.0177, \quad \alpha_{BL}(M_{B-L}) = 0.0192 \ . \end{gathered}$$

These two scenarios indicate that gauge unification is indeed possible for an appropriate arrangement of sparticle masses.

2.4 The Framework

The approach to the RG evolution of the parameters is similar to other such work, with several deviations that will be highlighted below. The RGEs of interest are calculated using reference [51] and are presented in Appendix 6.1. Gauge couplings and gaugino masses are evolved up to the unification scale. The remaining parameters, Yukawa couplings, sfermion mass parameters and a-terms, are only evaluated in the scaling regimes below the intermediate scale. This is because in the string construction considered here, the scaling regime between the unification scale and M_{I} contains six additional copies of matter fields as well as an additional copy of Higgs fields.We note that each component field of a given generation of matter originates from a different **16** of $SO(10)$. This is important and will be discussed later. Since these new Yukawa couplings are unknown, RG running them through this regime would not contribute to the predictability of this study. In practice, we implement these calculations piecewise starting with the analytically tractable equations first. These are the gauge couplings, gaugino mass parameters and the first and second generation sfermion mass parameters, as well as all sneutrino mass parameters. We then numerically calculate the evolution of the remaining parameters.

As is traditional, we begin by inputting the experimentally determined parameters–that is, the gauge couplings and Yukawa couplings derived from fermion masses–at the electroweak scale. The initial values of the gauge couplings were given above in Eq. (2.45). For the purposes of RG running, the SM Yukawa couplings, which are three-by-three matrices in flavor space, can all be approximated to be zero except for the three-three elements which give mass to the third generation SM fermions. We use the initial conditions

$$y_t = 0.955, \quad y_b = 0.0174, \quad y_\tau = 0.0102. \tag{2.63}$$

For details on relating fermion masses to Yukawa couplings, see [52]. Here the lower case y represents Yukawa couplings in the non-SUSY regime. These can be evolved to the SUSY scale, both in the right-side-up hierarchy, Eqs. (6.5) - (6.7), and up-side-down hierarchy, Eqs. (6.8) - (6.10). At the SUSY scale, one has the non-trivial boundary conditions

$$\begin{aligned} y_t(M_{\text{SUSY}}) &= Y_t(M_{\text{SUSY}}) \sin\beta \\ y_{b,\tau}(M_{\text{SUSY}}) &= Y_{b,\tau}(M_{\text{SUSY}}) \cos\beta. \end{aligned} \tag{2.64}$$

The boundary condition at the $B - L$ scale is trivial. Above the $B - L$ and SUSY scales, the Yukawa couplings are only evolved up to the intermediate scale utilizing the RGEs in Eqs. (6.14) - (6.16).

The gauge couplings in the various regimes were discussed in previous sections. With those solutions in hand, the RGE evolution of the gauginos can be easily derived. Gaugino masses are inputted at the unification scale and evolved down. Naively, one might expect gaugino mass unification. However, this is not always the case–as has been discussed in a number of contexts, see for example [53, 54]. Therefore, and to be as general as possible, we impose no relationship between the different gaugino masses at the unification scale. The general RGE for a gaugino mass parameter is

$$\frac{d}{dt} M_a = \frac{b_a \alpha_a M_a}{2\pi}, \tag{2.65}$$

where a indexes the gauge groups. These equations can be solved analytically. For the gauginos associated with $SU(3)_C$, $SU(2)_L$, $U(1)_{3R}$ and $U(1)_{B-L}$ the solution is

$$M_a(t) = \frac{M_a(M_{\rm U})}{\alpha_a(M_{\rm U})}\alpha_a(t). \tag{2.66}$$

The bino, however, is a treated somewhat differently for each of the two possible hierarchies between the $B-L$ and SUSY scales. For the right-side-up hierarchy, at the M_{B-L} scale, we have three neutral fermions that mix: the third generation right-handed neutrino ν_3^c, the $B-L$ gaugino (blino) and the T_{3R} gaugino (rino). This is a direct consequence of R-parity violation in the $B-L$ MSSM. As we will see, it is possible for a neutralino LSP mass eigenstate to have a significant ν_3^c component. The mixing between the third-family right-handed neutrino and the $U(1)$ gauginos is described in the $(\nu_3^c, \tilde{W}_R, \tilde{B}')$ basis by the mass matrix[2]

$$\begin{pmatrix} 0 & -\cos\theta_R M_{Z_R} & \sin\theta_R M_{Z_R} \\ -\cos\theta_R M_{Z_R} & M_R & 0 \\ \sin\theta_R M_{Z_R} & 0 & M_{BL} \end{pmatrix} . \tag{2.67}$$

Due to the RGEs monotonically pushing the values of M_R and M_{BL} down, they will typically be significantly lighter than M_{Z_R}. It is, therefore, instructive to perturbatively diagonalize this mass matrix in the limit $M_R, M_{BL} \ll M_{Z_R}$. At zeroth order, the mass eigenstates are

$$\tilde{B} = \tilde{W}_R \sin\theta_R + \tilde{B}'\cos\theta_R \tag{2.68}$$

$$\nu_{3a}^c = \frac{1}{\sqrt{2}}(\nu_3^c - \tilde{W}_R\cos\theta_R + \tilde{B}'\sin\theta_R) \tag{2.69}$$

$$\nu_{3b}^c = \frac{1}{\sqrt{2}}(\nu_3^c + \tilde{W}_R\cos\theta_R - \tilde{B}'\sin\theta_R), \tag{2.70}$$

with masses

$$M_1 = 0, \quad m_{\nu_{3a}^c} = M_{Z_R}, \quad m_{\nu_{3b}^c} = M_{Z_R} \; . \tag{2.71}$$

At first order, the effect of adding M_R and M_{BL} back into the mass matrix is to give the bino a mass of

$$M_1 = \sin^2\theta_R M_R + \cos^2\theta_R M_{BL}. \tag{2.72}$$

This shows that, in the right-side-up hierarchy, between the scales M_{B-L} and $M_{\rm SUSY}$ we have the gauge group and particle content of the MSSM plus two right-handed neutrino supermultiplets–that is, the two sneutrino generations that do not

---

[2] This mass matrix neglects mixing with the Higgsinos through the electroweak breaking Higgs VEV. This is a safe approximation since the lower bound on the Z_R mass implies that the electroweak Higgs VEV will be negligible compared to the third-family right-handed sneutrino VEV.

acquire a VEV.[3] Below the $B-L$ scale, the bino mass is

$$M_1(t) = \frac{M_1(M_{B-L})}{\alpha_1(M_{B-L})}\alpha_1(t). \tag{2.73}$$

In the upside-down case, all neutralinos are diagonalized at the SUSY mass scale.

The running of the tri-linear a-terms is straightforward. Their initial values are inputted at the intermediate scale, M_{I}. The a-term RGEs in the $B-L$ MSSM regime are given in Eqs. (6.17) - (6.19), while those for the MSSM are in Eqs. (6.20) - (6.22). All relevant threshold conditions are trivial.

The RGEs for the square of the soft sfermion mass parameters can be broken into two categories: 1) those with simple analytic solutions–given in Eqs. (6.29) - (6.34) and Eqs. (6.35) - (6.40) for the $B-L$ MSSM and MSSM regimes respectively–and 2) those requiring numerical solutions–given in Eqs. (6.42) - (6.48) and Eqs. (6.49) - (6.55) for the $B-L$ MSSM and MSSM regimes. Initial values for these parameters are all inputted at the intermediate scale. The third generation right-handed sneutrino soft masses are then evolved to the $B-L$ scale–while all other sfermion soft mass parameters are RG evolved to the SUSY scale. The third generation right-handed sneutrino mass squared plays an important role here since, when it runs negative, it triggers $B-L$ breaking as was discussed in detail in [29, 55]. The right-handed sneutrino mass RGE is

$$16\pi^2\frac{d}{dt}m^2_{\tilde{\nu}^c_3} = -3g^2_{BL}M^2_{BL} - 2g^2_R M^2_R + \frac{3}{4}g^2_{BL}S_{BL} - g^2_R S_R\ , \tag{2.74}$$

where

$$\begin{aligned} S_{BL} &= \mathrm{Tr}\,(2m^2_{\tilde{Q}} - m^2_{\tilde{u}^c} - m^2_{\tilde{d}^c} - 2m^2_{\tilde{L}} + m^2_{\tilde{\nu}^c} + m^2_{\tilde{e}^c})\ , && (2.75)\\ S_R &= m^2_{H_u} - m^2_{H_d} + \mathrm{Tr}\left(-\frac{3}{2}m^2_{\tilde{u}^c} + \frac{3}{2}m^2_{\tilde{d}^c} - \frac{1}{2}m^2_{\tilde{\nu}^c} + \frac{1}{2}m^2_{\tilde{e}^c}\right). && (2.76)\end{aligned}$$

Despite the lack of a large Yukawa coupling, the right-handed sneutrino mass can still be driven tachyonic by appropriate signs and magnitudes of the S-terms defined in Eqns (2.75, 2.76). To emphasize this, the analytic solution to the sneu-

---

[3] At some points in parameter space, it is possible that the required limit will not be satisfied and there will not be a mass eigenstate that can clearly be identified as the bino. However, since the scaling regime between M_{B-L} and M_{SUSY} is always small, the errors introduced by assuming the existence of a bino are insignificant.

trino mass RGE is presented here. It is

$$\begin{aligned}
m^2_{\nu_3}(M_{B-L}) = m^2_{\nu_3}(M_{\rm I})& \\
+\frac{1}{14}\frac{g_R^4(M_{\rm I})-g_R^4(M_{B-L})}{g_{\rm U}^4}M_R(M_{\rm U})^2&+\frac{1}{8}\frac{g_{BL}^4(M_{\rm I})-g_{BL}^4(M_{B-L})}{g_{\rm U}^4}M_{BL}(M_{\rm U})^2 \\
+\frac{1}{14}\frac{g_R^2(M_{\rm I})-g_R^2(M_{B-L})}{g_R^2(M_{\rm I})}S_R(M_{\rm I})&-\frac{1}{16}\frac{g_{BL}^2(M_{\rm I})-g_{BL}^2(M_{B-L})}{g_{BL}^2(M_{\rm I})}S_{BL}(M_{\rm I})\ .
\end{aligned} \tag{2.77}$$

Recall that the value of any Abelian gauge couplings grows larger at higher scale. Therefore, we see that a tachyonic sneutrino is only possible when $S_R(M_{\rm I})$ is negative and/or $S_{BL}(M_{\rm I})$ is positive. This demonstrates the central role played by the S-terms in the breaking of $B-L$ symmetry. Note that in typical unification scenarios all soft masses are "universal" and, hence, both S-terms vanish. However, it was mentioned earlier that, in this string construction, different elements of a given generation arise from different **16** representations of $SO(10)$. Therefore, the soft masses of a given generation are generically non-degenerate. Hence, the S-terms can be non-zero.

As mentioned above, $M_{Z_R} \simeq \sqrt{2}|m_{\tilde{\nu}_3^c}|$ and the relationship

$$M_{Z_R}(M_{B-L}) = M_{B-L} \tag{2.78}$$

is used to iteratively solve for the $B-L$ scale. The SUSY mass scale must also be solved for iteratively using the equation

$$\sqrt{m_{\tilde{t}_1}(M_{\rm SUSY})m_{\tilde{t}_2}(M_{\rm SUSY})} = M_{\rm SUSY}\ , \tag{2.79}$$

where $m_{\tilde{t}_1} < m_{\tilde{t}_2}$ are the physical stop masses. The relationships between the soft mass parameters and the physical masses are given in Appendix 6.2.1. The soft mass squared parameter for the up-type Higgs is driven tachyonic, as usual, by the large top Yukawa coupling. Furthermore, the decoupled values of the soft Higgs mass squared parameters are used to calculate the μ- and b-terms using Eqs. (1.15) and (1.16).

The soft mass parameters have non-trivial boundary conditions at the $B-L$ scale due to the effects of the $B-L$ and T_{3R} D-terms:

$$\begin{aligned}
m^2_\phi(M^-_{B-L}) - m^2_\phi(M^+_{B-L}) &= -\frac{1}{4}\left(g_R^2+g_{BL}^2\right)v_R^2\left(T_{3R}-Y\sin^2\theta_R\right) \\
&\simeq -M^2_{Z_R}\left(T_{3R}-Y\sin^2\theta_R\right)\ ,
\end{aligned} \tag{2.80}$$

where M_{B-L}^{-} and M_{B-L}^{+} indicate a scale slightly below and slightly above the $B-L$ scale respectively, and T_{3R} and Y are the third component of right-handed isospin and hypercharge of a generic scalar ϕ.

Having discussed the relevant scales, boundary conditions, and renormalization group equations for relating parameters at different scales, we are left with a glaring problem. Like the MSSM, the $B-L$ MSSM contains ~ 100 unknown parameters. A combination of phenomenological considerations, string considerations, and the use of a random scan will enable us to exatract predictions, even from such a vast unknown parameter space.

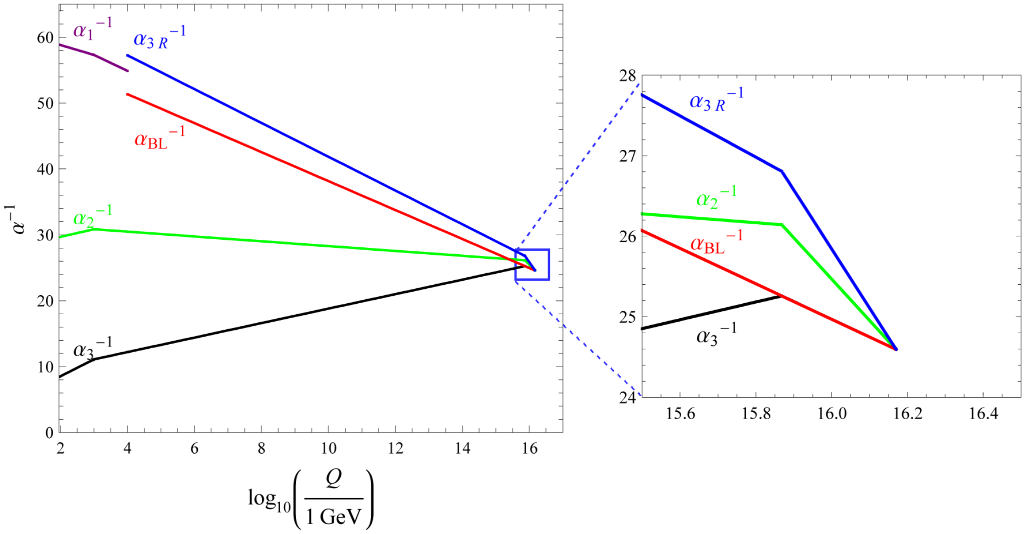

Figure 2.3: One-loop RGE running of the inverse gauge couplings, α_i^{-1} in the case of the Pati-Salam type model with $M_{B-L} = 10$ TeV with an enlarged image of the intermediate region.

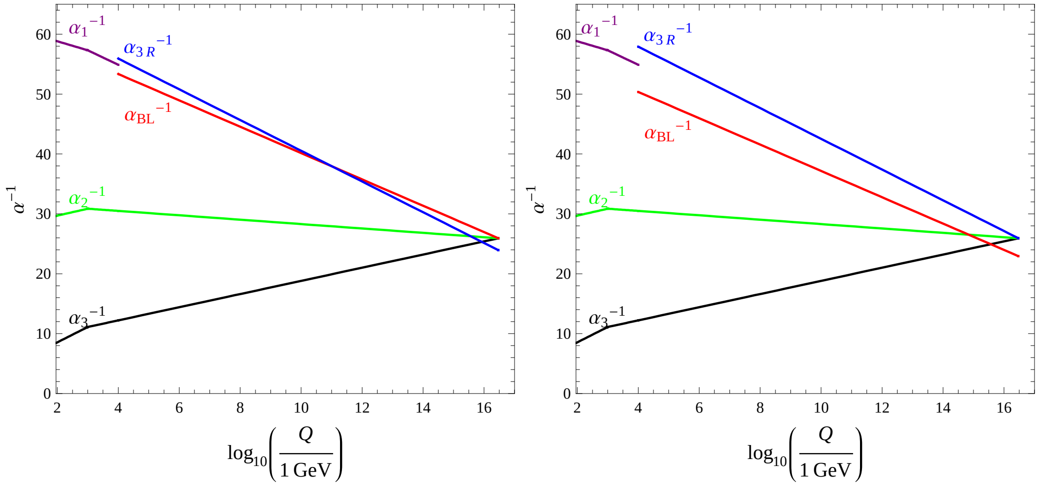

Figure 2.4: The gauge couplings do not unify exactly if the two Wilson lines turn on simultaneously. In (a), α_{BL} is chosen to unify exactly. In (b) α_{3R} is chosen to unify exactly. $M_{B-L} = 10$ TeV in both plots.

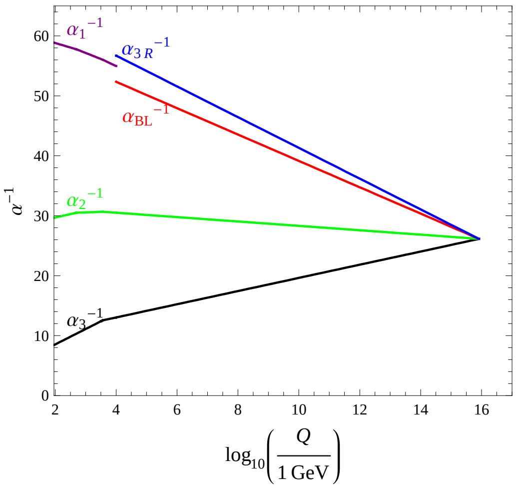

Figure 2.5: Exact unification for simultaneous Wilson lines, requiring a splitting between all colored and all non-colored superpartners. This scenario is not consistent with the 2:5 ratio of wino and gluino masses required by unification of gauge groups.

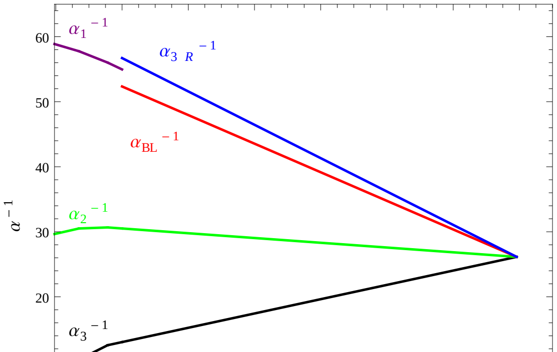

Figure 2.6: Exact unification for simultaneous Wilson lines, requiring a splitting between the mass thresholds of the right handed squarks and all other superpartners, while also remaining compatible with the gaugino mass relations derived in Subsection 3.6.

Chapter 3

The Parameter Problem

3.1 Approach

In this chapter, we address the techniques used to extract predictions from a theory with many free parameters. Schematically, this starts with using phenomenological considerations to greately shrink the parameter space. String considerations further limit the parameter space and suggest a probability distribution for randomly sampling the parameter space. The techniques discussed in the previous chapter connect parameters to LHC scales where we can apply experimental constraints to select a relatively small set of "valid points" in the parameter space. Finally, the predictions of the valid points are discussed.

Once the parameters have been properly evolved to their appropriate scales, the physical masses can be evaluated. For much of the spectrum, this has been discussed in the literature, see for example [38], and has been included in Appendix 6.2.1. The new element here is the mass of the scalar associated with the third generation right-handed sneutrino–the $B - L$ Higgs. It's mass is degenerate with the Z_R mass. In addition, the calculation for the SM-like Higgs mass is crucial since the experimentally measured value of $\sim$125 GeV requires substantial radiative corrections from the stop sector. In this thesis we follow the approach of references [56, 57, 58]–taking into account the decoupling scale of the stops, matching the quartic Higgs coupling at that scale and RG evolving the quartic coupling to the electroweak scale to calculate the Higgs mass. Full details are given in Appendix 6.2.2.

Once a given physical mass is calculated, it is compared to current lower bounds or, in the case of the SM Higgs, the experimentally measured value. If a given point in parameter space predicts a physical mass that is inconsistent with current bounds, it is rejected as being an invalid point. Points that satisfy current bounds are referred to as “valid points”.

3.2 Experimental Constraints

3.2.1 Collider Constraints

The bounds placed by collider data on SUSY masses are, in general, model dependent. That is, they depend on the spectrum and decay modes. Despite the much larger energy of the LHC, LEP 2 still has competitive bounds on colorless particles that couple to the Z and/or the photon–including sleptons in scenarios with both R-parity conservation [59, 60] and violation [61], bounds on charginos [62, 63] and bounds on sneutrinos in the case of R-parity violation [61]. As one may expect, due to the relatively clean environment at LEP, these bounds are close to one half the center of mass energy of LEP 2. Therefore, for simplicity, we proceed with the bound that all colorless fields that couple to the photon must be heavier than 100 GeV. That is,

$$m_{\tilde{\ell}}, m_{\tilde{\chi}_1^\pm} > 100 \text{ GeV}, \tag{3.1}$$

where $\tilde{\ell}$ is any charged slepton. Colorless states that couple to the Z, *the left-handed sneutrino*, must be heavier than half the Z mass:

$$m_{\tilde{\nu}_L} > 45.6 \text{ GeV}, \tag{3.2}$$

Colorless states that do not couple to the Z, such as right-handed sneutrinos/neutrinos and the bino, have such small collider production cross-sections that they do not have collider-based lower bounds. Wino and Higgsino neutralinos are degenerate with their chargino partner, thereby effectively putting a lower bound of 100 GeV on those states as well.

The bounds from the LHC are much more dependent on the parameters. For example, if one investigated the bound on degenerate squarks in this model with a neutralino LSP, those bounds could be significantly different than in the case of a sneutrino, or some other, LSP. Allowing the squark masses to split would further alter the lower bounds. A full treatment would involve calculating the signatures of a given point in parameter space, comparing the number of events to the most recent LHC bounds on such events, and determining if the parameter point is valid. We do not expect the details of these lower bounds to heavily affect our results. We will, therefore, simply use the naive bounds

$$m_{\tilde{q}} > 1000 \text{ GeV}, \quad m_{\tilde{g}} > 1300 \text{ GeV}\ , \tag{3.3}$$

which are based on recent CMS [64] and ATLAS [65] studies of the R-parity conserving MSSM. In these studies, the colored states decay into jets and missing energy–possible final states in our model whenever the LSP decays into neutrinos. In this thesis, we impose these bounds except in the case of a stop or sbottom LSP. These two cases are thoroughly discussed in Chatper 4 and yield the following lower bounds:

$$\text{admixture (right-handed) stop LSP: } m_{\tilde{t}_1} > 450\ (400) \text{ GeV}, \quad m_{\tilde{b}_1} > 500 \text{ GeV}, \tag{3.4}$$

where $\tilde{t}_1$ ($\tilde{b}_1$) denotes the lightest stop (sbottom). Here, right-handed refers to a stop that is almost completely right-handed–that is, a stop mixing angle, $\theta_{\tilde{t}} > 85^\circ$ or, equivalently, a state composed of 99% right-handed stop–while admixture stop refers to all other stops. This distinction is based on the phenomenology of the stops; right-handed stops have significant decays into a top quark and neutrinos while admixture stops decay almost exclusively to a bottom quark and a charged lepton.

The lower bound on the Z_R mass from LHC searches is 2.5 TeV [66, 67]. Finally, we require that the Higgs mass be within the 2σ allowed range from the value measured at the ATLAS experiment at the LHC. We naively obtain the two sigma range by adding in quadrature the systematic and statistical uncertainties from [68], and multiplying the result by two:

$$m_{h^0} = 125.36 \pm 0.82 \text{ GeV}. \tag{3.5}$$

See [69] for comparable data from CMS. A summary of the collider bounds mentioned above is given in Table 3.1.

3.2.2 Constraints from Flavor and CP-Violation

A large number of low-energy experiments exist which place constraints on the SUSY parameter space. Some of the oldest and most well-known are the constraints placed on flavor changing neutral currents from the analyses in references [70, 71, 72]–for example, those arising from $K - \bar{K}$ oscillation–and on

Particle(s)	Lower Bound
Left-handed sneutrinos	45.6 GeV
Charginos, sleptons	100 GeV
Squarks, except for stop or sbottom LSP's	1000 GeV
Stop LSP (admixture)	450 GeV
Stop LSP (right-handed)	400 GeV
Sbottom LSP	500 GeV
Gluino	1300 GeV
Z_R	2500 GeV

Table 3.1: The different types of SUSY particles and the lower bounds implemented in this thesis.

CP violation [73, 74, 75, 76, 77]–for example, from electric dipole moment measurements. The implication of these constraints are, approximately, as follows:

- Soft sfermion mass matrices are diagonal.
- The first two generations of squarks are degenerate in mass.
- The trilinear a-terms are diagonal.
- The gaugino masses and trilinear a-terms are real.

In addition, it is typically assumed that the soft trilinear a-terms are proportional to the Yukawa couplings, that is, generically $a = YA$ for each fermions species. Each A is a dimensionful real number on the order of a TeV, while each Y factor is a dimensionless matrix in flavor space. This condition effectively makes all non-third generation trilinear terms insignificant. Note that this assumption does not immediately follow from the above experimental constraints. However, significant radiative corrections to fermion masses, proportional to the a-term, can arise in SUSY, as first discussed for fermions in references [78, 79, 80]. For example, a down quark mass is modified by gluino exchange, through the diagram in Fig. 3.1, as follows:

$$\Delta M_d = M_d M_{\tilde{g}} \frac{2\alpha_3}{3\pi} \left(\frac{a_d}{Y_d} + \mu \tan\beta \right) I\left(m^2_{\tilde{b}_L}, m^2_{\tilde{b}_R}, M^2_{\tilde{g}} \right), \tag{3.6}$$

where

$$I(x, y, z) = \frac{xy \ln \frac{x}{y} + yz \ln \frac{y}{z} + xz \ln \frac{z}{x}}{(x - y)(y - z)(x - z)}, \tag{3.7}$$

and $M_{\tilde{g}}$ is the gluino mass. If a_d is on the order of a TeV, this radiative correction can be quite large, possibly larger than the down quark mass. If this were the case, the radiative correction would have to be fine-tuned against the tree-level contribution to reproduce the correct down quark mass. This motivates allowing only the third generation a-terms to be significant. Therefore, we assume that

$$a(M_{\rm I}) = Y(M_{\rm I})A(M_{\rm I}) \ . \tag{3.8}$$

This makes all a-parameters, except for those associated with t, b and τ, negligible for the purposes of RG running.

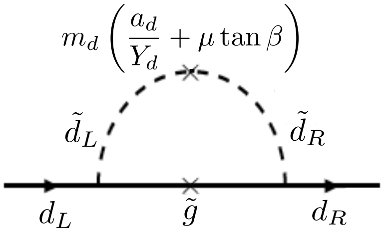

Figure 3.1: Radiative contribution of the gluino to the down quark mass. Similar contributions exist for the other fermions.

Summarizing the above, we employ the following constraints motivated by low-energy physics:

$$\begin{aligned}
m^2_{\tilde{q}} &= \text{diag}\left(m^2_{\tilde{q}_1}, m^2_{\tilde{q}_1}, m^2_{\tilde{q}_3}\right) \quad , \quad \tilde{q} = \tilde{Q},\, \tilde{U},\, \tilde{D} \ , \\
m^2_{\tilde{\ell}} &= \text{diag}\left(m^2_{\tilde{\ell}_1}, m^2_{\tilde{\ell}_2}, m^2_{\tilde{\ell}_3}\right) \quad , \quad \tilde{\ell} = \tilde{L},\, \tilde{E}\ , \tilde{\nu}^c \ , \\
a_f(M_{\rm I}) &= Y_f(M_{\rm I})A_f(M_{\rm I}) \quad , \quad f = t,\, b,\, \tau \ .
\end{aligned} \tag{3.9}$$

Note that the first two constraints can be implemented at the high scale, since RG evolution to the SUSY scale will not spoil these relations. Furthermore, we do not assume here that the first and second generation slepton masses are degenerate– unlike the squark masses– since this is not required by low energy experiments. The degeneracy or non-degeneracy of these states would not, however, greatly effect the results in this thesis.

3.3 The Parameter Space and Scan

The previous chapter reviewed the framework used in this thesis for connecting the high scale to LHC accessible physics. It remains at this point to discuss the input values for the SUSY breaking parameters. In this section, we introduce a novel way to analyze the initial parameter space of a SUSY model. While there have been many studies of specific, fixed boundary conditions at the high scale, and some recent interesting discussions of random parameter scans at the TeV scale [81, 82], a study that combines both has not–until now– been undertaken. Specifically, our approach in this thesis is to make a statistical scan of input parameters at the high scale–followed by a RG evolution of those parameters to the TeV scale and an analysis of which of these high scale initial conditions lead to realistic physics. While the soft SUSY breaking sector contains over 100 dimensionful parameters, the constraints of low energy experiments discussed in Section 3.2.2 only allow collider significant values for about a fifth of these– 24 to be specific. These, along with $\tan\beta$ and a discussion of the sign of certain parameters, are presented in Table 3.2.

The high scale initial values of the 24 relevant SUSY breaking parameters are determined as follows. To conduct our scan, we make the assumption that there is only one overall scale associated with SUSY breaking. This assumption does not require that the soft mass parameters be equal to each other, or even have similar values. It does, however, require that these parameters be at least within an order of magnitude, or so, of each other. To quantify this, we demand that any dimension one soft SUSY breaking parameter be chosen at random within the range

$$(\frac{M}{f}, Mf)\ , \tag{3.10}$$

where M is the mass setting the scale of SUSY breaking and f is a dimensionless number satisfying $1 \leq f \lesssim 10$. We will further insist that any such parameter be evenly scattered around M; that is, that M be the average of the randomly generated values. This will not be the case if parameters are chosen from a uniform probability distribution in the range $(\frac{M}{f}, Mf)$–referred to as a "flat prior". Instead, a "log prior" is adopted. This means that the natural logarithm of a given soft SUSY breaking parameter is chosen from a uniform distribution in the range

$$(\ln\left(\frac{M}{1\ \text{GeV}}\frac{1}{f}\right), \ln\left(\frac{M}{1\ \text{GeV}}f\right))\ . \tag{3.11}$$

With a log prior distribution, M is the geometric mean of the randomly generated parameters. In addition to the dimensionful soft masses, we also scan $\tan\beta$ as a flat prior in the range (1.2, 65), thus selected so that all Yukawa couplings remain perturbative through the entire range. Furthermore, we randomly generate the signs of μ, the three tri-scalar couplings $a_{t,b,\tau}$, and the four gaugino masses $M_{3,2,R,BL}$.

In this thesis, we are interested in the low energy spectra being accessible at the LHC or a next generation collider. Therefore, in addition to the experimental constraints mentioned in the previous section, we further demand that all sparticle masses be lighter than 10 TeV. We call any point that satisfies this, as well as all previous criteria, a "valid accessible" point. The parameters M and f are chosen in such a way as to maximize the number of such points. To determine the values of M and f which yield the greatest number of valid accessible points, we begin by making a ten by ten grid in the $M - f$ plane. At each of these hundred points, we randomly generate one hundred thousand initial points in the 24-dimensional parameter space discussed above, RG scale them to low energy, and count the subset that satisfies the experimental checks discussed above. We then plot curves corresponding to a constant number of valid accessible points in Fig. 3.2. The plot shows a broad peak or plateau, the center of which maximizes the number of such points. This maximum occurs approximately for

$$M = 2700\,\text{GeV},\ f = 3.3\ . \tag{3.12}$$

These values will be used to generate the results in the remainder of this thesis. Note that for these values, the smallest soft parameter is maximally about an order of magnitude away from the largest soft parameter. For M and f in Eq. (3.12), the ranges for the random scan of each parameter are given in Table 3.2.

The existence of a peak in Fig. 3.2 around moderate values of f is a consequence of combining the various experimental checks we apply to each of the randomly generated points. For a fixed value of M, some individual checks favor higher values of f, while others favor lower values. This is analyzed in terms of the "survival rate". The survival rate for a given check is defined as the number of points in the 24-dimensional initial parameter space surviving that check as a percentage of the number of points that survived all previous checks. This will be discussed in detail in the next section for the fixed values of M and f given in Eq. (3.12). Here, for $M = 2700$ GeV, we analyze the impact of f on the various survival rates. The peak around moderate values of f shown Fig. 3.2 can be understood by observing how the survival rates for different checks depend on f. This is shown in Fig. 3.3. The $B - L$ symmetry breaking check and the Z_R

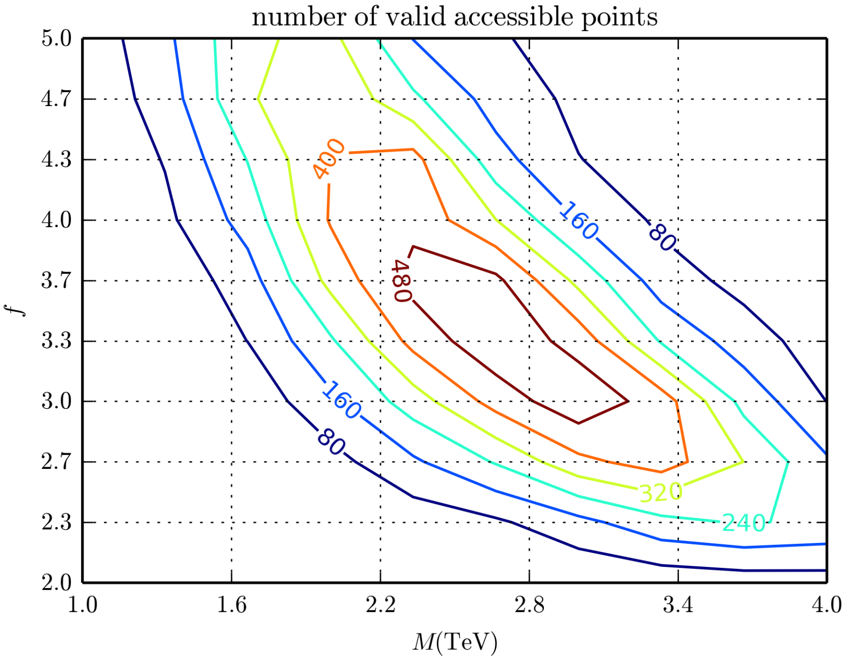

Figure 3.2: A contour plot in the M - f plane of the number of valid accessible points; that is, points that meet all experimental constraints given in the previous section and for which all sparticles are below 10 TeV. A broad peak or plateau is evident around $M = 2700$ GeV and $f = 3.3$.

Parameter	Range	Prior
$m_{\tilde{q}_1} = m_{\tilde{q}_2},\ m_{\tilde{q}_3}: \quad \tilde{q} = \tilde{Q}, \tilde{u}^c, \tilde{d}^c$	(820, 8900) GeV	log
$m_{\tilde{\ell}_1}, m_{\tilde{\ell}_2},\ m_{\tilde{\ell}_3}: \quad \tilde{\ell} = \tilde{L}, \tilde{e}^c, \tilde{\nu}^c$	(820, 8900) GeV	log
m_{H_u}, m_{H_d}	(820, 8900) GeV	log
$\lvert A_f \rvert: \quad f = t, b, \tau$	(820, 8900) GeV	log
$\lvert M_a \rvert: \quad a = R, BL, 2, 3$	(820, 8900) GeV	log
$\tan\beta$	(1.2, 65)	flat
Sign of $\mu, a_f, M_a: \quad f = t, b, \tau \quad a = R, BL, 2, 3$	[-,+]	flat

Table 3.2: The parameters and their ranges scanned in this study, as well as the type of prior. The ranges for the soft SUSY breaking parameters are optimized to produce the greatest number of valid points with all masses below 10 TeV.

lower bound check both favor higher values of f. This is because higher values of f favor larger S-terms and thereby promote $B-L$ symmetry breaking. The EW symmetry breaking check favors lower values of f. Intuitively, this is not surprising since universal boundary conditions (which correspond to $f = 1$) in the MSSM allow electroweak symmetry breaking. The sparticle lower bounds check favors low f. This is because larger f leads to larger S-terms which, in turn, can drive some sparticles masses to be light through the RGE's. The Higgs mass check also favors low f because larger S-terms may drive the stop masses away from the $\sim$ TeV value favored by the Higgs mass. With some checks favoring large f and others small f, it is not surprising that all checks taken together favor a moderate values of f.

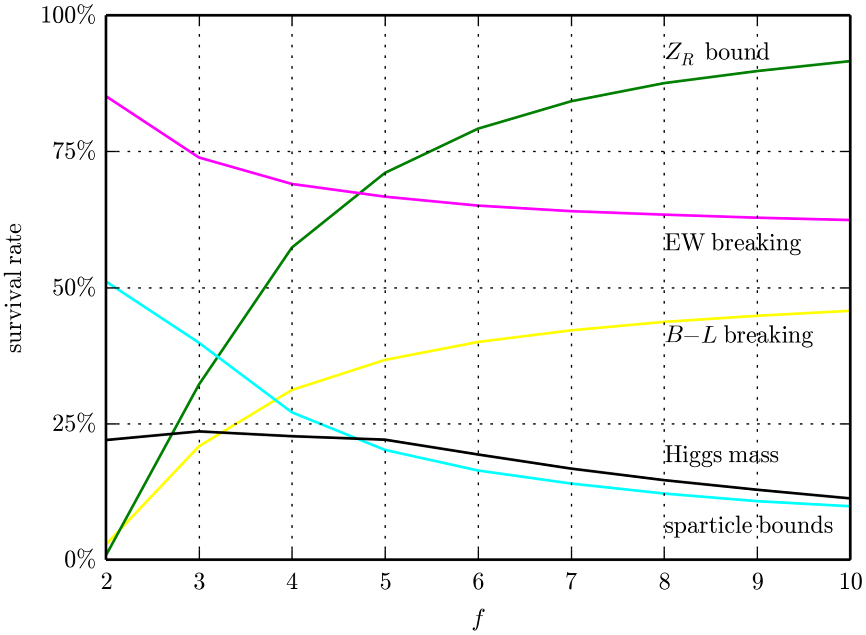

Figure 3.3: Survival rates of the various checks as a function of f for $M = 2700$ GeV. The $B - L$ breaking and Z_R lower bound checks favor larger f while the others favor small f. All of the checks taken together favor a moderate value of $f \sim 3.3$.

3.4 Results

All of the following results arise from a scan consisting of ten million randomly generated points with $M = 2700$ GeV and $f = 3.3$. We will refer to this as the "main scan". Recall that in the previous section, in addition to the experimental constraints, we imposed an extra condition that all masses be lighter than 10 TeV. Technically, this was done to ensure the maximum number of valid accessible points–that is, valid points with masses accessible to the LHC or a next generation collider. Having done this, we, henceforth, remove this additional condition. That is, the only constraints in the main scan are the experimental ones given in Section 2.4. All valid points must satisfy these constraints as well as some other checks, which are reviewed here briefly.

In order to be valid, a point must break $B-L$ symmetry, the Z_R mass must be above the lower bound, electroweak symmetry must be broken and since the stops play a crucial role in electroweak breaking, we designate a check that the stops are not tachyonic. Since our numerical analysis uses an iterative process to solve for the SUSY and $B-L$ scales, it is possible that a point may pass a check on the first iteration but fail it on the final iteration, although this is very uncommon. Therefore, we include a "spill" check of the Z_R bound, electroweak breaking check and non-tachyonic stop checks. Points that pass these spill checks did so on the final iteration of solving for the $B-L$ and SUSY scales. Furthermore, a valid point must have $B-L$ and SUSY scales that converge to a value in the iterative solution process. We also check that–in addition to the stops–all other SUSY sparticles are not tachyonic and satisfy the imposed mass bounds. Finally, we check that the Higgs mass matches its experimental value.

All of these conditions are listed in the first column of Table 3.3. The second column lists the number of points in the main scan that passed that check, out of ten million. The third column is the same information listed as a percent of the number of points in the main scan. The fourth column is the same information listed as a percent of the number of points that passed the previous checks. We refer to this quantity as the rate of survival for each check. This is an interesting quantity because it quantifies how easy or hard it is for a randomly generated point to pass that specific check.

A striking feature of Table 3.3 is that $B-L$ breaking happens robustly. This was one of the central questions that this thesis sought to answer. Our analysis demonstrates that, for $M = 2700$ GeV and $f = 3.3$, no special tuning or choice of parameters is required at the M_{I} scale to achieve $B-L$ symmetry breakdown. Further analysis–for other values of M and f–shows that the percentage of points

check	number surviving	percent surviving	rate of survival
$B - L$ breaking	2,225,704	22.3 %	22.3 %
Z_R bound	919,117	9.19 %	41.3 %
EW breaking	722,750	7.23 %	78.6 %
non-tachyonic stops	619,668	6.2 %	85.7 %
Z_R bound spill	597,988	5.98 %	96.5 %
EW breaking spill	565,272	5.65 %	94.5 %
non-tachyonic stops spill	553,592	5.54 %	97.9 %
convergence	553,150	5.53 %	99.9 %
sparticle bounds	276,676	2.77 %	50 %
Higgs mass	58,096	0.581 %	21 %

Table 3.3: This table shows all of the checks applied to the randomly generated points. It specifies the number of such points passing each check, as well as their percent of survival. The fourth column is the most informative because it provides insight into how likely it is that an individual check is satisfied by a randomly generated point. Because the SUSY and $B - L$ scales are solved for iteratively, it is possible to pass a check in the first iteration and fail it later. A passed “spill” check indicates that that check was passed in the final iteration.

that break $B-L$ is, in general, independent of M. This is because $B-L$ breaking is not a question of generating a specific scale. Rather, it involves having soft masses aligned in such a way as to allow the S-terms to drive the third family right-handed sneutrino tachyonic, see Eq. (2.74). $B-L$ breaking is dependent on the choice of f. In the limit $f \to 1$, $S_{BL,R} \to 0$ and $B-L$ breaking becomes impossible–while increasing f will favor $B-L$ breaking. A second feature of Table 3.3 is that, for $M = 2700$ GeV and $f = 3.3$, the Z_R mass exceeding the experimental lower bound, although less prevalent, is still rather robust. In contrast to $B-L$ breaking, since $M_{Z_R} \simeq \sqrt{2}|m_{\tilde{\nu}^c}|$, passing the Z_R mass bound check is sensitive to the choice of M–with the survival rate increasing with M.

A third important conclusion drawn from Table 3.3 is that, for the main scan, a large percentage of the initial points that have $B-L$ breaking consistent with the Z_R mass lower bound, also lead to the radiative breakdown of electroweak symmetry. Note that the Z mass can always be adjusted–albeit by fine-tuning–to its experimental value of 91.2 GeV. Further analysis–for other values of M and f–shows that electroweak breaking, like $B-L$ breaking, is roughly independent of M. However, unlike $B-L$ breaking, small f favors electroweak symmetry breaking. As is well known from the literature [83, 84, 85], electroweak breaking occurs for universal boundary conditions–that is, for $f = 1$. On the other hand, as f increases, the randomly generated parameter $m^2_{H_u}(M_{\mathrm{I}})$ can be considerably larger than the square of the initial stop masses. In this case, the RGE evolution to the SUSY scale may be insufficient to render $m^2_{H_u}(M_{\mathrm{SUSY}})$ tachyonic. Since the initial soft masses are randomly generated, the electroweak breaking survival rate will decrease with increasing f, but it will not go to zero.

Whether or not stop masses remain non-tachyonic at low scale depends on the randomly chosen values of several of the initial parameters. As can be seen from Table 3.3, for the values of M and f chosen for the main scan, non-tachyonic stops are very common. To remind the reader, the checks labeled spill are repeats of earlier checks that are conducted after the final iteration of solving for the SUSY scale. Since this iterative process usually only affects the relevant checks logarithmically, the spill bins are expected to have high survival rates. The survival rate for convergence of the iterative process of finding values of M_{B-L} and M_{SUSY} is almost 100%–since the soft masses have a logarithmic dependence on the scale. The survival rate for the SUSY particle mass bounds check is, for $M = 2700$ GeV and $f = 3.3$, comparable to that of the Z_R mass bound. Further analysis shows that this rate is also controlled by the choice of M–a higher value for M resulting in a higher survival rate for this check. The Higgs mass survival rate for the main scan is, perhaps, surprisingly high–given that we are checking that the

Higgs mass for a randomly generated point matches an experimentally measured value within an error of less than one percent. The reason this rate is so high is that the measured value of the Higgs mass is within the range expected for TeV scale supersymmetry breaking.

Since the initial soft SUSY breaking parameter space is 24-dimensional, graphically displaying the subspaces associated with each survival check in Table 3.3 is very difficult. However, as can be seen from the RGEs and has been discussed in the text, much of the scaling behavior of the parameters is controlled by the two S-terms, S_R and S_{BL}, defined in Eqs. (6.24) and (6.23). It follows that the results in Table 3.3 can be reasonably displayed in the two-dimensional $S_{BL}(M_{\mathrm{I}})$ - $S_R(M_{\mathrm{I}})$ plane. We begin by presenting in Fig. 3.4 the initial points in the $S_{BL}(M_{\mathrm{I}})$ - $S_R(M_{\mathrm{I}})$ plane that satisfy, sequentially, the first two fundamental checks in Table 3.3; that is, $B-L$ breaking and the experimental Z_R mass lower bound. Points that do not break $B-L$ are shown in red, points that satisfy $B-L$ breaking but not the Z_R mass bound are in yellow, and points that break $B-L$ symmetry and satisfy the Z_R mass bound are shown in green. This plot reaffirms the conclusion drawn from Table 3.3 that $B-L$ breaking consistent with present experiments is a robust phenomena. Furthermore, it shows the strong dependence of $B-L$ breaking and the Z_R mass on the values of the S-terms. There is a line in the S_{BL} - S_R plane–between the yellow and red regions–below which $B-L$ breaking is not possible. Note that this includes the origin, which corresponds to vanishing S-terms and, hence, universal soft masses. This shows that at least a small splitting from sfermion universality is required for $B-L$ breaking. Another line exists–between the green and yellow regions–below which Z_R is always lighter than its lower bound.

Proceeding sequentially, we present in Fig. 3.5 the initial points in the $S_{BL}(M_{\mathrm{I}})$ - $S_R(M_{\mathrm{I}})$ plane that, in addition to breaking $B-L$ with a Z_R mass above the experimental bound, also break EW symmetry. The entire colored region encompasses the green points shown in Fig. 3.4. Those points that also break EW symmetry are displayed in purple. This plot reaffirms the conclusion drawn from Table 3.3 that most of the points that break $B-L$ with a Z_R mass above the experimental bound, also break EW symmetry. Note that some green points that do not break EW symmetry are obscured by the purple points.

In Fig. 3.6, we reproduce Fig. 3.5 but now, in addition, sequentially indicate the points that are consistent with the remaining checks–that is, non-tachyonic stops/spill checks/convergence/all lower bounds on sparticles masses satisfied and, finally, that they reproduce the Higgs mass within the experimental uncertainty. Points that appropriately break $B-L$ symmetry but do not satisfy electroweak

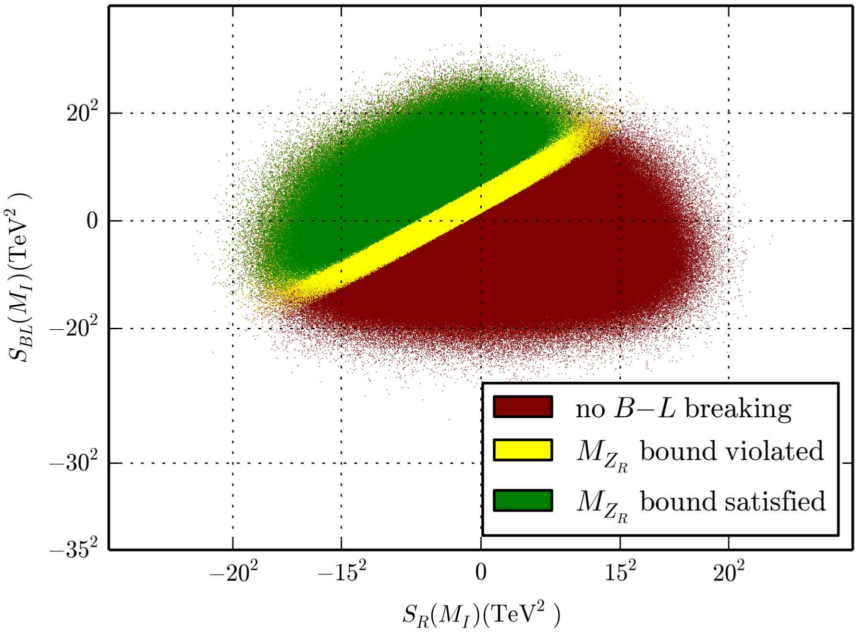

Figure 3.4: Points from the main scan in the $S_{BL}(M_\mathrm{I})$ - $S_R(M_\mathrm{I})$ plane. Red indicates no $B-L$ breaking, in the yellow region $B-L$ is broken but the Z_R mass is not above its 2.5 TeV lower bound, while green points have M_{Z_R} above this bound. The figure expresses the fact that, despite there being 24 parameters at the UV scale scanned in our work, $B-L$ physics is essentially dependent on only two combinations of them–the two S-terms. Note that the green points obscure some of the yellow and red points behind them. Similarly the yellow points obscure some red points.

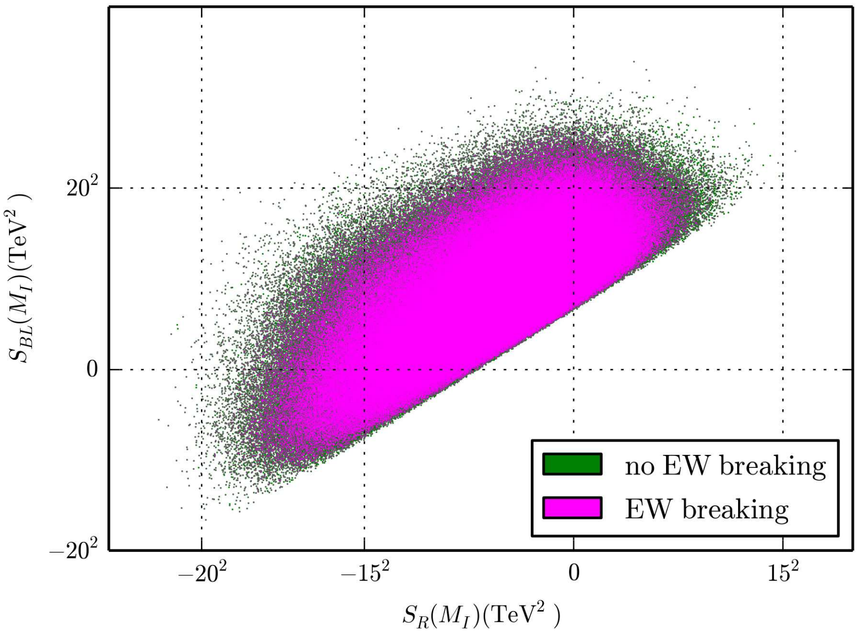

Figure 3.5: A plot encompassing the green region in Fig 3.4. The green points in this plot correspond to those which appropriately break $B - L$ symmetry, but which do not break electroweak symmetry. However, the purple points, in addition to breaking $B - L$ symmetry with an appropriate Z_R mass, also break EW symmetry. Note that some green points that do not break EW symmetry are obscured by the purple points.

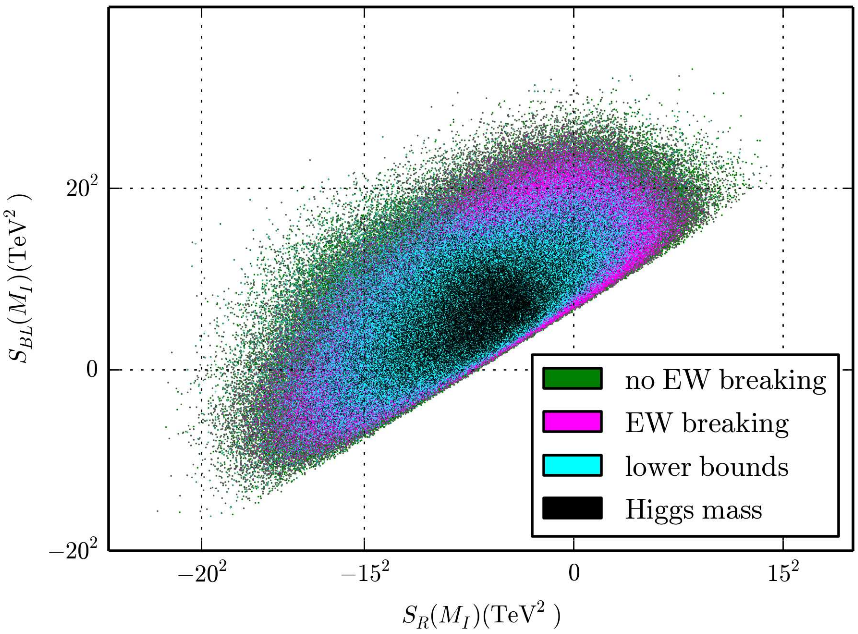

Figure 3.6: A plot of the valid points in our main scan. The green and purple points correspond to the green and purple points in Fig 3.5. The cyan points additionally have non-tachyonic stops, pass all spill checks and convergence, and satisfy all sparticle mass lower bounds. The black points are fully valid. That means that, in addition to satisfying all previous checks, they reproduce the correct Higgs mass within the stated tolerance. The distribution of points indicates that while $B - L$ breaking prefers large S-terms, sfermion mass constraints prefer them to be not too large. Again, the purple, cyan, and black points obscure a some other points not satisfying their constraint.

symmetry breaking are still shown in green. Points that, additionally, do break electroweak symmetry are again shown in purple. Such points that also have non-tachyonic stops, pass all spill checks and convergence, and which satisfy all lower bounds on sparticles masses, but do not match the known Higgs mass, are now indicated in cyan. Finally, points that satisfy all checks, including the correct Higgs mass, are shown in black. These are the valid points. The density of black points indicates, as observed above, that there is a surprisingly high number of initial parameters that satisfy all present low energy experimental constraints. The distribution of black points can be explained from the fact that, while $B - L$ breaking favors non-zero S-terms, very large S-terms can effect the RGE evolution of sfermion masses adversely. Since the effect of the S-terms depends on the charge of the sfermion in question, some sfermions will become quite heavy while others light or tachyonic. Therefore, in general, the valid points in our scan are a compromise between large S-terms, needed for a Z_R mass above its lower bound, and small S-terms needed to keep the sfermion RGEs under control.

The most important property of the inital SUSY parameter space in determining low-energy phenomenology is the identity of the LSP. Recall that when R-parity is violated, no restrictions exist on the identity of the LSP; for example, it can carry color or electric charge. Our main scan provides an excellent opportunity to examine the possible LSP's and the probability of their occurence. To this end, a histogram of possible LSP's is presented in Fig. 3.7–with the possible LSP's indicated along the horizontal axis, and $\log_{10}$ of the number of valid points with a given LSP on the vertical axis. The notation here is a bit condensed, but is specified in more detail in Table 3.4. The notation is devised to highlight the phenomenology of the different LSP's, specifically their decays, which are also presented in Table 3.4.

The most common LSP in our main scan is the lightest neutralino, $\tilde{\chi}_1^0$. However, not all $\tilde{\chi}_1^0$ states are created equal. LHC production modes for the lightest neutralino depend significantly on the composition of the neutralino–a bino LSP cannot be directly produced at the LHC, but the other neutralino LSP's can. This is the basis we use for the division of these states. The state $\tilde{\chi}_{\tilde{B}}^0$ designates a mostly rino or mostly blino neutralino, $\tilde{\chi}_{\tilde{W}}^0$ a mostly wino neutralino and $\tilde{\chi}_{\tilde{H}}^0$ a mostly Higgsino neutralino. Here, the word mostly indicates the greatest contribution to that state. As an unrealistic example, if $\tilde{\chi}_1^0$ is 34% wino, 33% bino and 33% Higgsino, it is still labeled $\tilde{\chi}_{\tilde{W}}^0$. The chargino LSP's are similarly separated into wino-like and higgsino like charginos. The notation for the stop LSP's is based on the discussion in Section 3.2.1. Note that this notation for the stops, $\tilde{t}_{ad}$ and $\tilde{t}_r$, are only used to describe stop LSP's. For non-LSP stops, we use the conventional

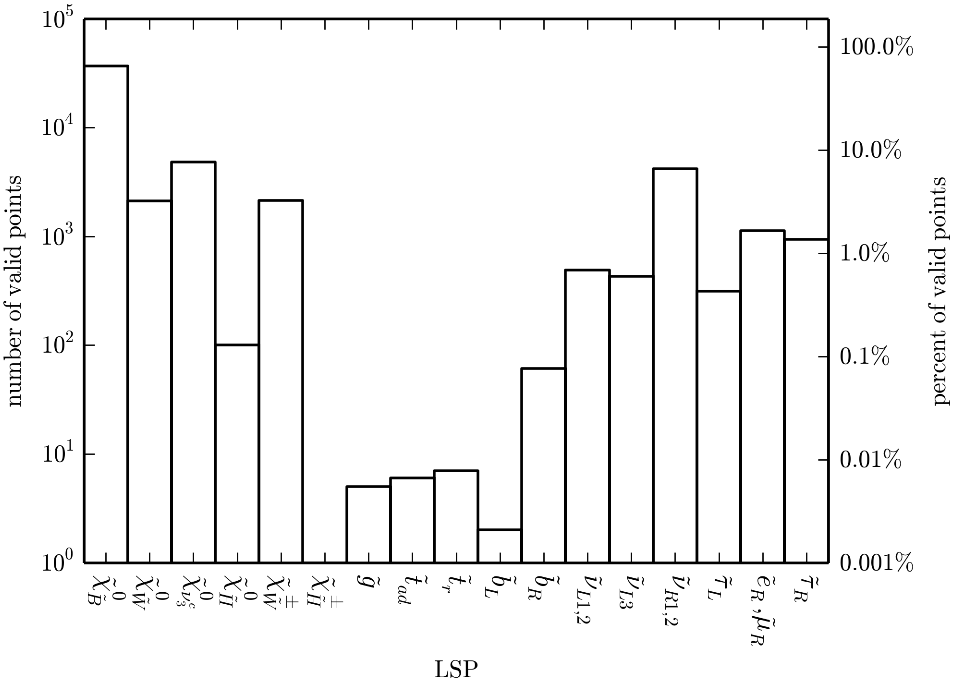

Figure 3.7: A histogram of the LSP's in the main scan showing the percentage of valid points with a given LSP. Sparticles which did not appear as LSP's are omitted. The y-axis has a log scale. The dominant contribution comes from the lightest neutralino, as one might expect. The notation for the various states, as well as their most likely decay products, are given in Table 3.4. Note that we have combined left-handed first and second generation sneutrinos into one bin, and that each generation makes up about 50% of the LSP's. The same is true for the first and second generation right-handed sleptons and sneutrinos.

Symbol	Description	Decay
$\tilde{\chi}^0_{\tilde{B}}$ $\tilde{\chi}^0_{\tilde{W}}$ $\tilde{\chi}_{\nu^c}$ $\tilde{\chi}^0_{\tilde{H}}$	A bino-like neutralino. Mostly wino neutralino. Mostly third generation right-handed neutrino. Mostly Higgsino neutralino.	$\ell^\pm W^\mp$, νZ, νh
$\tilde{\chi}^\pm_{\tilde{W}}$ $\tilde{\chi}^\pm_{\tilde{H}}$	Mostly wino charginos. Mostly Higgsino charginos.	$\nu W^\pm$, $\ell^\pm Z$, $\ell^\pm h$
$\tilde{g}$	Gluino.	$t\bar{t}\nu$, $t\bar{b}\ell^-$
$\tilde{t}_{ad}$	Left- and right-handed stop admixture.	$\ell^+ b$
$\tilde{t}_r$	Mostly right-handed stop (over 99%).	$t\nu$, $\tau^+ b$
$\tilde{q}_R$	Right-handed 1st and 2nd generation squarks.	$\ell^+ j$, νj
$\tilde{b}_L$	Mostly left-handed sbottom.	$b\nu$
$\tilde{b}_R$	Mostly right-handed sbottom.	$b\nu$, $\ell^- t$
$\tilde{\nu}_{L_{1,2}}$ $\tilde{\nu}_{L_3}$	1st and 2nd generation left-handed sneutrinos. LSP's evenly split among two generations. Third generation left-handed sneutrino.	$b\bar{b}$, W^+W^-, ZZ, $t\bar{t}$, $\ell'^+\ell^-$, hh, $\nu\nu$
$\tilde{\nu}_{R_{1,2}}$	1st and 2nd generation right-handed sneutrinos.	$\nu\nu$
$\tilde{\tau}_L$	Third generation left-handed stau.	$t\bar{b}$, $W^- h$, $e\nu$, $\mu\nu$, $\tau\nu$
$\tilde{e}_R, \mu_R$	1st and 2nd generation right-handed sleptons. LSP's evenly split among two generations.	$e\nu$, $\mu\nu$
$\tilde{\tau}_R$	Third generation right-handed stau.	$t\bar{b}$, $e\nu$, $\mu\nu$, $\tau\nu$

Table 3.4: The notation used for the states in Fig. 3.7 and their probable decays. More decays are possible in certain situations depending on what is kinematically possible and the parameter space. Gluino decays are especially dependent on the NLSP, here assumed to be a neutralino. Here, the word "mostly" means it is the greatest contribution to the state. The symbol ℓ represents any generation of charged leptons. The left-handed sneutrino decay into $\ell'^+\ell^-$ indicates a lepton flavor violating decay–that is, ℓ'^+ and ℓ^- do not have the same flavor. Note that j is a jet–indicating a light quark.

notation $\tilde{t}_1$ and $\tilde{t}_2$.

To make Fig. 3.7 more readable, we have made an effort to combine bins that have similar characteristics. The first and second generation left-handed sneutrinos are combined into one bin, where about 50% of the LSP's are first generation sneutrinos. The same holds true for the first and second generation right-handed sleptons, while the first generation right-handed sneutrino is always chosen to be lighter than the second generation right-handed sneutrino. This similarity between the first and second generation sleptons is expected, since their corresponding Yukawa couplings are not large enough to distinguish them through the RG evolution. For both sleptons and squarks, more LSP's exist for the third generation–as expected from the effects of the third generation Yukawa couplings, which tend to decrease sfermion masses in RGE evolution.

The myriad of possible LSP's leads to a rich collider phenomenology. With the exception of the stop and sbottom LSP's, discussed in Chapter 4, this phenomenology is not the main focus of this thesis, but it is worthwhile to briefly review it here. In models where R-parity is parameterized by bilinear R-parity, such as the $B-L$ MSSM, SUSY particles are still pair produced and cascade decay to the LSP. At this point, the bilinear R-parity violating terms allow the LSP to decay. While only a few studies have been done on the phenomenology of the minimal $B-L$ MSSM [30, 31, 2, 3], there have been several works on the phenomenology of explicit bilinear R-parity violation, which has some similarities to this model. References to such papers are mentioned below. See [86, 87, 88, 89] for general discussions. Table 3.4 provides some basic information on the most probable decay modes of each of the possible LSP's. Note that ℓ signifies a charged lepton of any generation and j a jet–implying a light quark. Interesting aspects of Table 3.4 are the following.

LSP Phenomenology

- **Neutralinos**: Only neutralinos with significant non-bino-like components can be significantly produced at the LHC. Note that in addition to the usual possibilities, a mostly right-handed third generation neutrino is also a possible lightest neutralino component here, because of R-parity violation. This can be pair produced through the Z_R resonance. Due to the Majorana nature of the neutralinos, they can lead to same-sign dilepton signals–a clear sign of lepton number violation. This is true whether they are directly produced or occur at the end of a cascade decay. The generation of ℓ depends on the neutrino mass hierarchy, as discussed in [2, 3]. In the normal hierarchy, muons and taus are most likely, while in the inverted hierarchy all charged leptons are possible.

- **Gluino**: Most of the LSP decay products mentioned in Table 3.4 mimic well-known hypothetical states–for example, neutralinos decay like TeV scale right-handed neutrinos and squarks decay like leptoquarks. The same can not be said of the gluino, making it an interesting candidate for further study. However, its decays depend strongly on the identity of the next to lightest supersymmetric particle (NLSP). Also, bounds on the gluino are the strongest because of its large production cross section. Therefore, when the gluino is the LSP, it is likely that it is the only LHC-accessible SUSY particle. As with the neutralinos, the gluino's Majorana nature allows same-sign dilepton final states–indicating lepton number violation.

- **Squarks**: All squark LSP's act like leptoquarks in this model, meaning they are pair-produced and decay into a lepton and a quark. Stop and sbottom LSP's in this model are discussed in Chapter 4. For both a down- and an up-type non-third generation squark LSP, there will be two highly degenerate LSP states–either a degenerate down and strange squark pair or a degenerate up and charm squark pair–as required by phenomenological considerations discussed in Section 3.2.2. In the inverted hierarchy, these can decay into an electron and jet or a neutrino and a jet, making them tempting explanations for the recent CMS excess, see [90], in the $eejj$ and $e\nu jj$ channels [91]. However, the branching ratios seem to be inconsistent with the cross section [92, 93]. See reference [94] for a study of stops in trilinear R-parity violation.

- **Left-handed sneutrinos**: Left-handed sneutrinos decay like heavier neutral Higgs bosons, that is, H^0 and A^0, due to their R-parity violating mixing with the Higgs sector. In general, decays into heavier Higgses are also possible, depending on kinematics. The final state $\ell'^+\ell^-$ represent a lepton flavor violating final state, such as μ^+e^-. Sneutrinos LSP decays were studied in the case of explicit bilinear R-parity violation, which has some similarities to the $B-L$ MSSM, in reference [95, 96].

- **Right-handed sneutrinos**: These states decay into missing energy and, therefore, cannot be easily distinguished from the R-parity conserving MSSM. However, since the sneutrino is spin 0, as opposed to spin half neutralinos, a detailed collider study might reveal some differences. It is also interesting to note that it may be possible to pair produce right-handed sneutrinos through a Z_R resonance.

- **Sleptons**: Both left-handed and right-handed charged sleptons decay like charged Higgs bosons, with which the sleptons mix due to R-parity violation. The left-handed sleptons have more channels open to them because of their isospin charge. Each left-handed slepton comes in an $SU(2)$ doublet with the associated left-handed sneutrino. Splitting of this doublet is mainly due to electroweak D-term contributions to the mass, which push the associated left-handed sneutrino to lighter mass values, making it the LSP. In the case of the left-handed stau, however, mixing effects through the Yukawa and tri-scalar couplings (see Appendix 6.2.1) have the potential to make its mass lighter than the third-family left-handed sneutrino. Therefore, the left-handed stau is the only left-handed charged slepton capable of being the LSP. Slepton LSP's with explicit R-parity violation were discussed in reference [97].

To get a sense of the non-LSP spectrum, we produce histograms of the masses of the sparticles from the main scan. In the following histograms, there will be quite a few pairs of fields that will be highly degenerate; these will be represented by only one curve. This includes $SU(2)_L$ sfermion partners, which are only split by small electroweak terms. First generation squarks are also degenerate with second generation squarks with the same isospin, due to phenomenological constraints. A consequence of this is that all first and second generation left-handed squarks are highly degenerate. In viewing these histograms, it is helpful to remember that aside from the usual RGE effects of the MSSM, there are two additional effects involved. The first of these is the boundary conditions at the $B-L$ scale, corresponding to the $B-L$ and T_{3R} D-terms which are given in Eq. (2.80). The second is the new RGE effects of the S_R and S_{BL} terms. Although the signs of these terms are not fixed, Fig. 3.4 shows that S_{BL} is typically positive while S_R is typically negative. This indicates that S_R will tend to increase (decrease) sfermion masses for sfermions with a positive (negative) T_{3R} charge, while S_{BL} tends to increase (decrease) sfermion masses for sfermions with negative (positive) $B-L$.

Figure 3.8 shows histograms of the squark masses. Because they come in $SU(2)$ doublets and the first- and second-family squarks must be degenerate, all four of the first- and second-family left-handed squarks have nearly identical mass and the histograms coincide. The degeneracy of first- and second-family squarks is also evident in the right-handed squark masses. The first and second family right-handed down squarks are generally lighter than their up counterparts because of the effect of the $U(1)_{3R}$ charge in the RGEs.

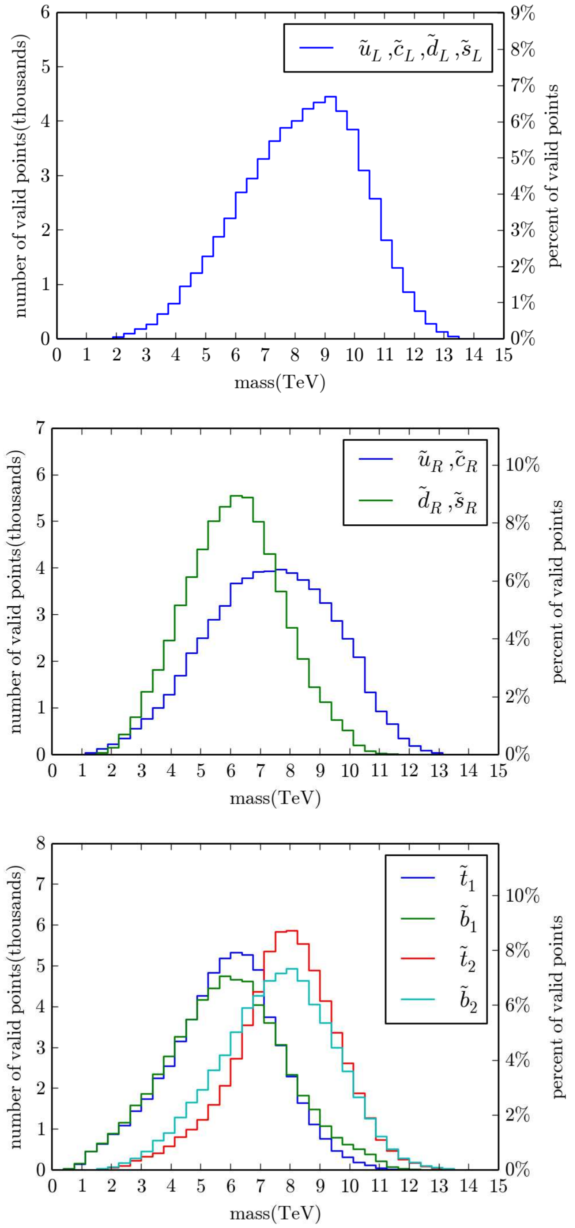

Figure 3.8: Histograms of the squark masses from the main scan. The first- and second-family left-handed squarks are shown in the first panel. The first- and second-family right-handed squarks are shown in the second panel. The right-handed down squarks are generally lighter than their up counterparts because of the effect of the $U(1)_{3R}$ charge in the RGEs. The third family squarks are shown in the third panel.

Figure 3.9 shows histograms of the masses of the sneutrinos and sleptons. The third-family sleptons and left-handed sneutrinos tend to be the lighter because of the influence of the tau Yukawa couplings. The right-handed sneutrinos are labeled such that $\tilde{\nu}_{R_1}$ is always lighter than $\tilde{\nu}_{R_2}$.

Figures 3.10 and 3.11 present histograms of the CP-even component of the third generation right-handed sneutrino, the heavy Higgses, the neutralinos, the charginos, and the gluino. The CP-even component of the third generation right-handed sneutrino is degenerate with Z_R. It is always heavier than 2.5 TeV because we have imposed the collider bound on Z_R. The neutralinos and charginos are labeled from lightest to heaviest as is canonical in SUSY models. The $\tilde{\chi}_5^0$ and $\tilde{\chi}_6^0$ are typically Higgsinos.

We emphasize that all of the above histograms are calculated using our main scan; that is, for the choice of $M = 2700$ GeV and $f = 3.3$. We remind the reader that these values were chosen so as to maximize the number of valid accessible points. However, the mass scale of these histograms is heavily dependent on the choice of M. Smaller values for M will move the above distributions distinctly toward lighter sparticle masses.

Plots of the physical particle spectra for four valid points are presented in Figs. 3.12 and 3.13. These four points are automatically selected from the pool of valid points from the main scan based on simple criteria. The first is the spectrum with an admixture stop LSP with the largest gap between stop LSP and the next lightest sparticle. The second is similar; now, however, with a right-handed sbottom LSP. The third and fourth are the valid points with the largest right-side-up and upside-down hierarchy respectively; that is, the largest splittings between the $B - L$ and SUSY scales in the two possible hierarchies.

Plots of the high-scale boundary values for four sample valid points from our main scan are presented in Figs. 3.14 and 3.15. While these look like Figs. 3.12 and 3.13, they do not correspond to physical masses but, rather, mass parameters at M_{I}. These four valid points are automatically selected from the pool of valid points from the main scan based on simple criteria. The first two are those with the lightest and heaviest initial value of the third-family right-handed sneutrino mass. These show that it is not necessary to artificially choose a very light initial mass for the third-family right-handed sneutrino to effect the destabilizing of its potential and $B - L$ symmetry breaking. Note when reading these plots that the lightest right-handed sneutrino is always, without loss of generality, defined to be the third-family. The next two plots show the valid points with the largest and smallest amount of splitting in the initial values of the scalar soft mass parameters. The amount of splitting is defined as the standard deviation of the initial values of

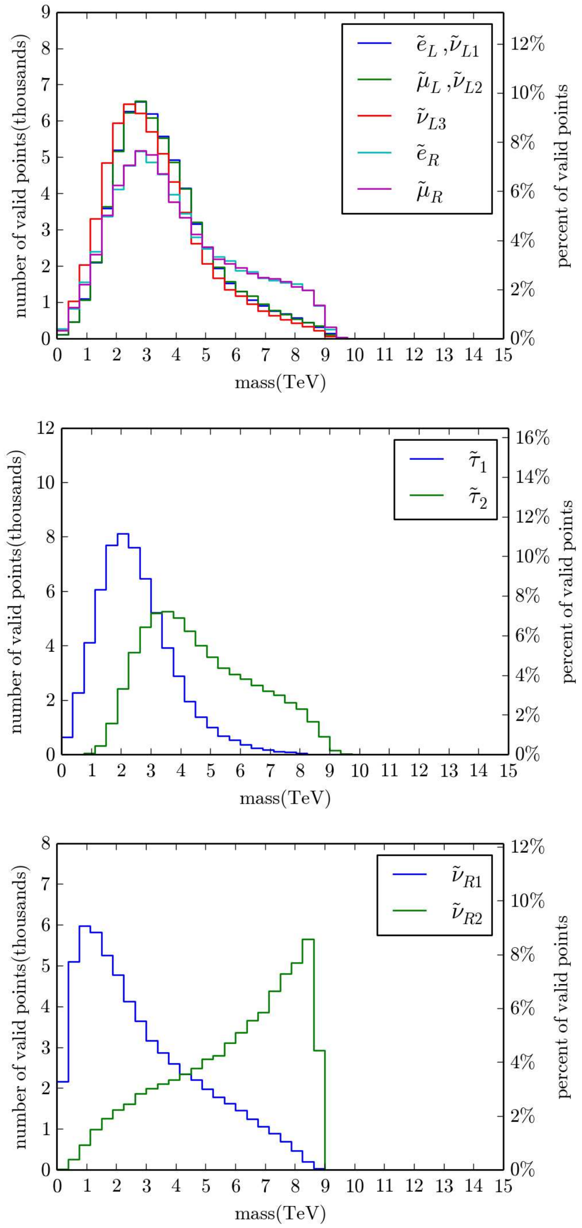

Figure 3.9: Histograms of the sneutrino and slepton masses in the the main scan. First- and second-family entries are in the first panel, along with the third family left-handed sneutrino. Staus are in the second panel with mass-ordered labeling. In the third panel, the first- and second-family right-handed sneutrinos are labeled such that $\tilde{\nu}_{R1}$ is always lighter than $\tilde{\nu}_{R2}$.

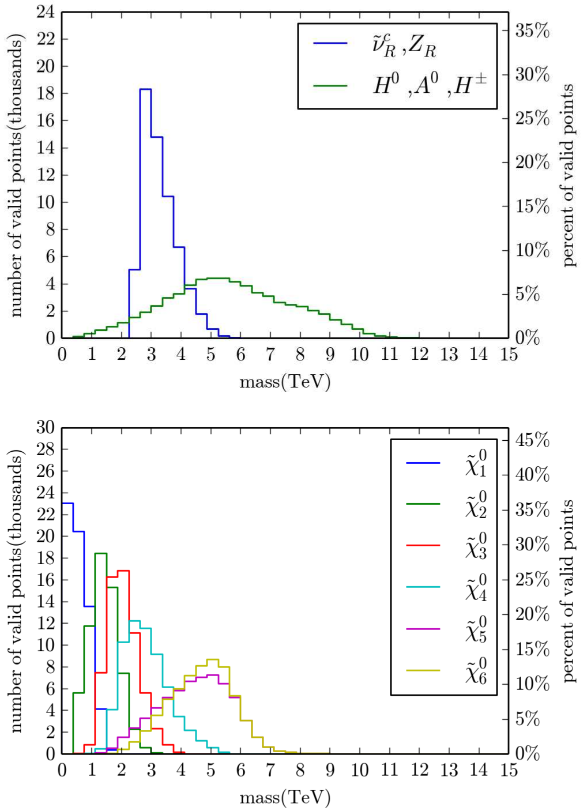

Figure 3.10: The CP-even component of the third-family right-handed sneutrino, heavy Higgses, and neutralinos in the valid points from our main scan. The CP-even component of the third generation right-handed sneutrino is degenerate with Z_R. The $\tilde{\chi}_5^0$ and $\tilde{\chi}_5^0$ are typically Higgsinos.

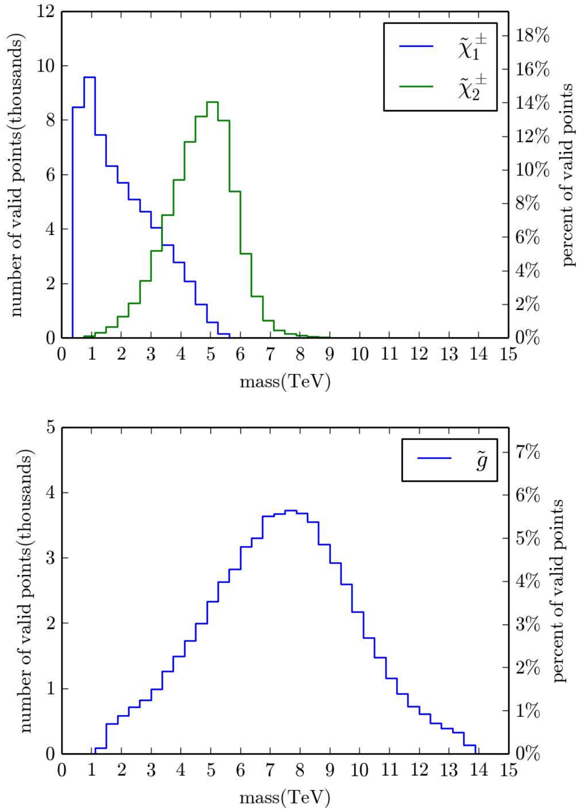

Figure 3.11: The CP-even component of the charginos and the gluino in the valid points from our main scan.

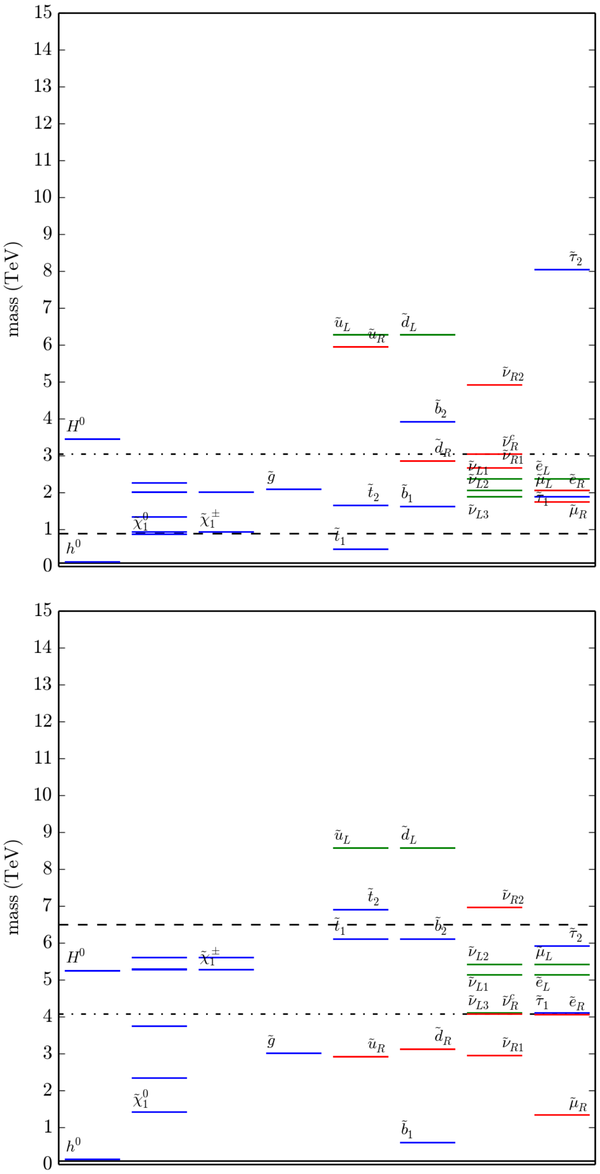

Figure 3.12: Two sample physical spectra with an admixture stop LSP and right-handed sbottom LSP. The $B-L$ scale is represented by a black dot-dash-dot line. The SUSY scale is represented by a black dashed line. The electroweak scale is represented by a solid black line. The label $\tilde{u}_L$ is actually labeling the nearly degenerate $\tilde{u}_L$ and $\tilde{c}_L$ masses. The labels $\tilde{u}_R$, $\tilde{d}_L$ and $\tilde{d}_R$ are similarly labeling the nearly degenerate first- and second- family masses.

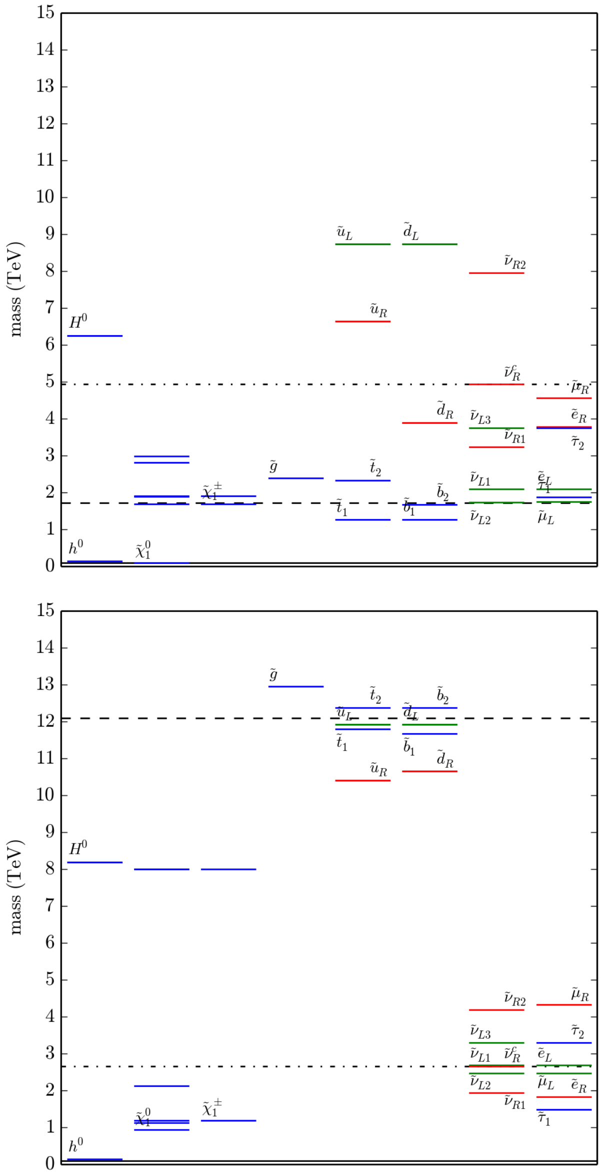

Figure 3.13: Two sample physical spectra with a right-side-up hierarchy and upside-down hierarchy. The $B - L$ scale is represented by a black dot-dash-dot line. The SUSY scale is represented by a black dashed line. The electroweak scale is represented by a solid black line. The label $\tilde{u}_L$ is actually labeling the nearly degenerate $\tilde{u}_L$ and $\tilde{c}_L$ masses. The labels $\tilde{u}_R$, $\tilde{d}_L$ and $\tilde{d}_R$ are similarly labeling the nearly degenerate first- and second- family masses.

the 20 scalar soft mass parameters.

3.5 Fine-Tuning

Fine-tuning in supersymmetric models arises from Eq. (1.15),

$$\frac{1}{2}M_Z^2 = \frac{m_{H_u}^2 \tan^2\beta - m_{H_d}^2}{1-\tan^2\beta} - \mu^2. \tag{3.13}$$

In both the MSSM and the minimal $B-L$ extension of the MSSM, the soft masses $m_{H_u}^2$ and $m_{H_d}^2$ receive contributions from other soft masses. Most important are the contributions from stop and gluino soft masses that appear in the RGEs for $m_{H_u}^2$–see Eq. (6.42). They must be TeV-scale to satisfy sparticle mass lower bounds and the measured Higgs mass. These large TeV-scale contributions must be almost exactly cancelled to yield the relatively small value of M_Z^2 on the left side of Eq. (3.13). This cancellation can come either from other soft masses or the μ^2 term. The delicate cancellation between the parameters on the right side to yield the smaller term on the left side is "fine-tuning". The necessity of such fine-tuning in supersymmetric models has been referred to as the "little hierarchy problem".

Here we explain the little hierarchy problem within the context of the $B-L$ MSSM, using a rough analytic argument along the lines of that presented in [98]. Although we discuss it using the language and notation of the minimal $B-L$ extension of the MSSM, the same argument holds in the MSSM. The largest contributions to $m_{H_u}^2$ come through its RGE in the $B-L$ MSSM scaling regime, Eq. (6.42). Focusing on just the stop and gluino soft mass contributions, we can write a solution to this equation to first-order in $\ln(M_{\mathrm{I}}/M_{\mathrm{SUSY}})$. Such a solution is quantitatively innacurate because it neglects higher powers of the large logarithm $\ln(M_{\mathrm{I}}/M_{\mathrm{SUSY}})$. Be that as it may, it can still provide insight into how various scales enter the problem. The solution is

$$m_{H_u}^2 = -\frac{6}{16\pi^2}Y_t^2(m_{Q_3}^2 + m_{t^c}^2)\ln\left(\frac{M_{\mathrm{I}}}{M_{\mathrm{SUSY}}}\right) + \cdots\ , \tag{3.14}$$

where the ellipsis represents neglected higher order terms and terms due to other contributions in Eq. (6.42). Additionally, there are corrections due to the boundary condition Eq. (2.80). The $m_{Q_3}^2$ and $m_{t^c}^2$ themselves receive large contributions through their RGEs, Eqs. (6.44) and (6.46). Focusing on the contributions from

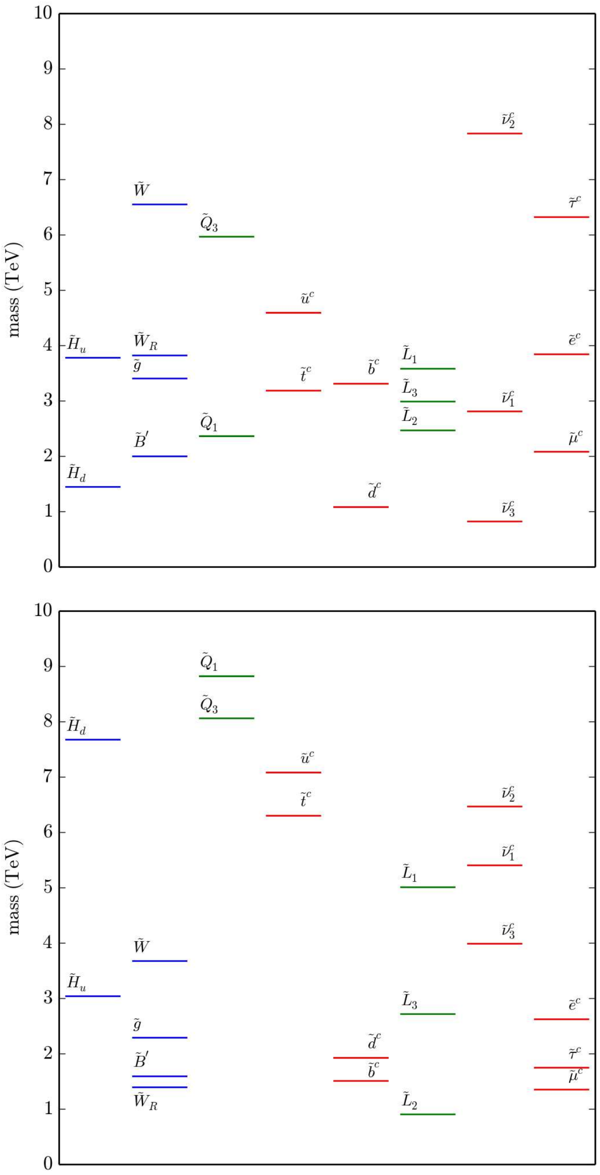

Figure 3.14: Example high-scale boundary conditions for the two valid points with the lightest and heaviest initial value of the third-family right-handed sneutrino soft mass. The label $\tilde{Q}_1$ is actually labeling the nearly degenerate $\tilde{Q}_1$ and $\tilde{Q}_2$ soft masses. The labels $\tilde{u}^c$ and $\tilde{d}^c$ are similarly labeling the nearly degenerate first and second family masses.

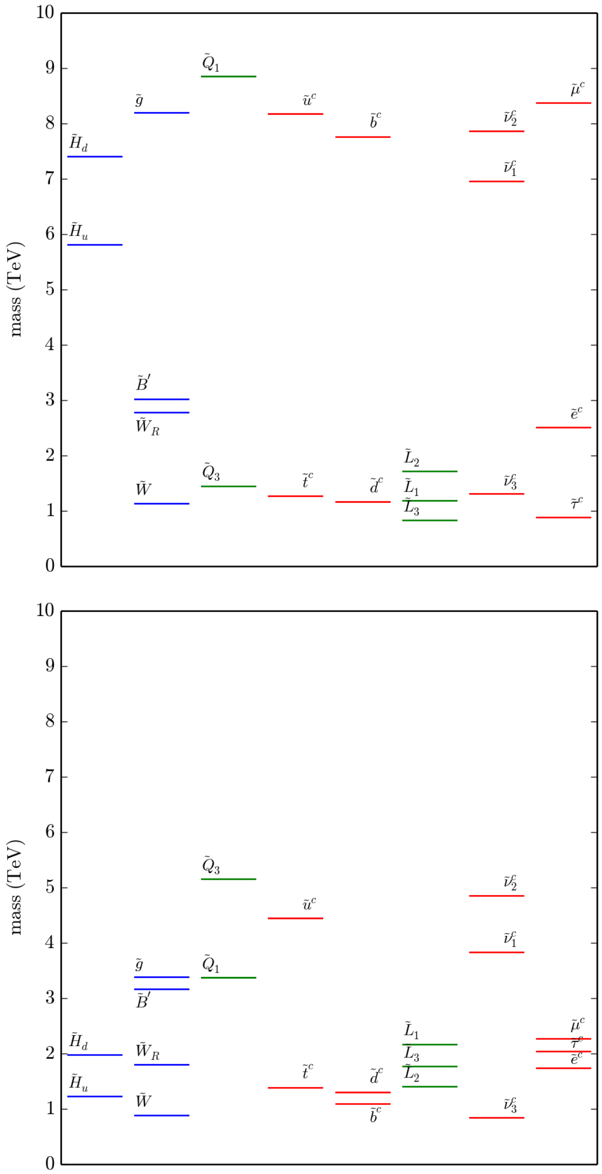

Figure 3.15: Example high-scale boundary conditions for the two valid points with the largest and smallest amount of splitting. The label $\tilde{Q}_1$ is actually labeling the nearly degenerate $\tilde{Q}_1$ and $\tilde{Q}_2$ soft masses. The labels $\tilde{u}^c$ and $\tilde{d}^c$ are similarly labeling the nearly degenerate first and second family masses.

the gluino mass yields

$$m_{H_u}^2 = -\frac{6}{16\pi^2}Y_t^2\left(m_{Q_3}^2 + m_{t^c}^2 + \frac{4}{3\pi^2}g_3^2M_3^2\ln\left(\frac{M_{\rm I}}{M_{\rm SUSY}}\right)\right) \times \ln\left(\frac{M_{\rm I}}{M_{\rm SUSY}}\right) + \cdots \ . \tag{3.15}$$

As discussed in Section 3.2.1, the stops and gluino have relatively high mass bounds from LHC searches. Additionally, as discussed in Appendix 6.2.2, satisfying the observed value of the Higgs mass tends to require heavy stops. This means that the stop and gluino soft mass contributions in Eq. (3.15) must be relatively large and give large contributions to the right-hand side of Eq. (3.13). For example, if $Y_t = 0.9$, $g_3^2 = 1$, $M_3 = m_{\tilde{q}_3} = m_{\tilde{t}^c} = 1$ TeV, $M_{\rm I} = 10^{15}$ GeV, and $M_{\rm SUSY} = 1$ TeV, these contributions are approximately equal to $-(2\text{ TeV})^2$. This must be almost exactly cancelled to yield the relatively small value of $M_Z^2 = (91.2\text{ GeV})^2$ on the left-hand side of Eq. (3.13). The cancellation usually comes from the μ^2, but can also come from the terms in the ellipsis or $m_{H_d}^2$.

As stated above, in the minimal $B-L$ extension of the MSSM there are additional contributions coming from the boundary condition on the Higgs soft masses at the $B-L$ scale, Eq. (2.80). Since $\tan\beta > 1$, the most important are the contributions to the H_u soft mass. These are proportional to M_{Z_R}. Since there is a lower bound of 2.5 TeV on M_{Z_R}, it is reasonable to suspect that these contributions to the H_u soft mass necessitate more delicate cancellation–thus worsening the little hierarchy problem. Rewritten in terms of M_{Z_R}, the associated boundary condition is

$$m_{H_u}^2(M_{B-L}^-) = m_{H_u}^2(M_{B-L}^+) - \frac{1}{2}\frac{g_R^2}{g_R^2 + g_{BL}^2}M_{Z_R}^2 \ . \tag{3.16}$$

The gauge couplings here, and in the remainder of this Section, are evaluated at M_{B-L} unless otherwise specified. Before concluding that this exacerbates the fine-tuning problem, we should replace the physical mass, M_{Z_R}, with more fundamental parameters of the theory, such as the soft masses evaluated at the intermediate scale. All of the scalar soft masses share in the generation of M_{Z_R} through the S-terms. Substituting Eq. (2.77) into Eq. (1.17) allows us to write the S-term contribution to M_{Z_R}. It is given by

$$M_{Z_R}^2 = \frac{1}{7}\frac{g_R^2 - g_R^2(M_{\rm I})}{g_R^2(M_{\rm I})}S_R(M_{\rm I}) - \frac{1}{8}\frac{g_{BL}^2 - g_{BL}^2(M_{\rm I})}{g_{BL}^2(M_{\rm I})}S_{B-L}(M_{\rm I}) + \cdots \ . \tag{3.17}$$

Substituting this into equation Eq. (3.16) yields S-term contributions to the H_u soft mass. In addition, the S-terms also influence the running of the H_u soft mass through the RGEs. Including both of these contributions, the value of $m^2_{H_u}$ at the SUSY scale is

$$\begin{aligned} m^2_{H_u}(M_{\text{SUSY}}) &= \frac{g_R^2}{g_R^2+g_{BL}^2}\left(\frac{1}{14}\frac{g_R^2-g_R^2(M_{\text{I}})}{g_R^2(M_{\text{I}})}S_R(M_{\text{I}})\right. \\ &\quad \left. -\frac{1}{16}\frac{g_{BL}^2-g_{BL}^2(M_{\text{I}})}{g_{BL}^2(M_{\text{I}})}S_{B-L}(M_{\text{I}})\right) \\ &\quad -\frac{1}{14}\frac{g_R^2-g_R^2(M_{\text{I}})}{g_R^2(M_{\text{I}})}S_R(M_{\text{I}})+\cdots\,. \end{aligned} \tag{3.18}$$

Consider a sample valid point with $S_R(M_{\text{I}}) < 0$ and $S_{B-L}(M_{\text{I}}) = -2S_R(M_{\text{I}})$. This case fits within the valid black points in Fig. 3.6. This arises physically if all scalar soft masses are universal with the exception that the the first- and second-family right-handed sneutrino soft masses–which are heavier. In this case, the S-term contributions to $m^2_{H_u}$ can be written as

$$\begin{aligned} m^2_{H_u}(M_{\text{SUSY}}) &= \left[\frac{g_R^2}{g_R^2+\frac{3}{2}g_{BL}^2}\left(\frac{1}{14}\frac{g_R^2-g_R^2(M_{\text{I}})}{g_R^2(M_{\text{I}})}\right.\right. \\ &\quad \left. +\frac{1}{8}\frac{g_{BL}^2-g_{BL}^2(M_{\text{I}})}{g_{BL}^2(M_{\text{I}})}\right) \\ &\quad \left. -\frac{1}{14}\frac{g_R^2-g_R^2(M_{\text{I}})}{g_R^2(M_{\text{I}})}\right]S_R(M_{\text{I}})+\cdots\,. \end{aligned} \tag{3.19}$$

Let us choose, for example, $M_{\text{SUSY}} = 1$ TeV and $M_{B-L} = 2.5$ TeV. Then the dimensionless coefficient of $S_R(M_{\text{I}})$ turns out to be -0.022. Since this value is considerably smaller than unity, it follows that the H_u soft mass is not–in fact–very sensitive to the fundamental parameters that set the Z_R mass. This remains true for all values of M_{SUSY} and M_{B-L} associated with valid points. Therefore, there is not a significant amount of new fine-tuning introduced in this way.

Fine-tuning in supersymmetric models has historically [99, 100, 101, 102] been quantified using the Barbieri-Giudice (BG) sensitivity, introduced in [103] and [104]. This quantifies the sensitivity of some observable quantity to changes in any of the fundamental parameters of a theory. The delicate cancellation between TeV-scale supersymmetry parameters in Eq. (3.13) results in the electroweak scale, M_Z, having a large BG sensitivity. The BG sensitivity of the electroweak scale is defined as

$$F_{a_i} = \left| \frac{a_i}{M_Z^2} \frac{\partial M_Z^2}{\partial a_i} \right| , \tag{3.20}$$

where a_i is any of the fundamental parameters of the theory. This says that a fractional change in a_i would produce a fractional change in M_Z^2 that is F_{a_i} times larger. The overall degree of fine-tuning is usually taken to be the largest of all the F_{a_i}'s ; that is,

$$F = \max(F_{a_i}) . \tag{3.21}$$

The BG sensitivity F will be used to quantify the fine-tuning required in the $B-L$ MSSM.

It is worth mentioning that some authors have pointed out drawbacks to the BG sensitivy and suggested other quantifications of fine-tuning. For example, as discussed in [101], the BG sensitivity and the overall degree of fine-tuning depend on how the fundamental parameters of the theory a_i are chosen. Furthermore, one could reasonably use the BG sensitivity of M_Z, rather than M_Z^2, as the indicator of fine-tuning. This would result in fine-tuning that is smaller by a factor of two. Such ambiguities in the way fine-tuning is calculated from the BG sensitivity suggest that it is not a precise way to quantify fine-tuning. A separate paper, [105], points out that the relationship between the proton mass and the strong coupling constant at a high scale exhibits high BG sensitivity, but is not actually finely tuned. They propose a more precise quantification of fine-tuning and show that the BG sensitivity actually overestimates the fine-tuning in some sample points in the MSSM.

Despite the possible shortcomings, the BG sensitivity remains the most widely used tool for making rough quantitative analyses of fine-tuning in supersymmetric models. We, therefore, proceed using the BG sensitivity to quantify fine-tuning in the $B-L$ MSSM. For each of the valid points, we compute F. We allow a_i to span all of the soft mass parameters of the theory, as well as μ. In the case of scalar soft masses, we take a_i to be the mass squared, while in the case of gaugino soft masses and μ we take a_i to be the mass to the first power. This choice corresponds to how these parameters appear in the Lagrangian. We then create a histogram of F for all of the valid points in our main scan. This data is shown as the blue line in Fig. 3.16. Note that the fine-tuning required by the highest percentage of valid points is $F \sim 5000$. Be that as it may, a reasonable number of valid points need significantly less fine-tuning–with about 2% requiring $F \lesssim 2000$. It is interesting to compare the amount of fine-tuning in the minimal $B-L$ extension of the MSSM model to the amount of fine-tuning required in an identical statistical scan of the R-parity invariant MSSM using $M = 2700$ GeV and $f = 3.3$. Due to the aforementioned ambiguities in how fine-tuning is quantified, it is critical that the fine-tuning be calculated the same way when two different models are being compared. Therefore, we use our own code, slightly modified, to produce a similar plot for the R-parity conserving MSSM. The results are shown as the green line in Fig. 3.16. Comparison of the blue and green lines in the figure show that the $B - L$ MSSM valid points tend to be slightly less finely tuned than valid points in the R-parity conserving MSSM. The difference is large enough to be apparent in the figure. However, due to the unresolved questions about how to properly quantify fine-tuning, we do not regard this difference between the $B - L$ MSSM and the MSSM to be significant.

With the fine-tuning of each randomly generated point in the $B - L$ MSSM now quantified, we are equipped to produce results for just the most natural points–that is, those requiring minimal fine-tuning. Figure 3.17 shows a histogram of the LSP's for those points with $F < 1000$, corresponding to the least fine-tuned $\sim 0.1\%$ of points, from a larger scan of four hundred million points. We refer to these points as "natural" valid points. There are three notable differences between Fig. 3.17 and Fig. 3.7. First, stop LSP's are more common. This includes both admixture and mostly right-handed stop LSP's. Stop LSP's are more common because heavy stops tend to cause fine-tuning, so low fine-tuning favors lighter stops and stop LSP's. Second, sbottom LSP's are more common. This is due to the fact that first, both the stop and sbottom masses depend on the soft mass $m^2_{Q_3}$ and second, because the right-handed stop and sbottom soft masses have similar terms in their RGE's. These two facts imply that favoring light stops tends to favor light sbottoms as well. Third, Fig. 3.17 does not have the gluino LSP's shown in Fig. 3.7, and it does have some $\tilde{d}_R$ LSP's not found in Fig. 3.7. However, the disappearance and appearance of these states in the $F < 1000$ histogram is not statistically significant and, hence, these states can be ignored. The prevalence of stop and sbottom LSP's is the only significant difference between the natural valid points and the valid points. Stop and sbottom LSP's are discussed in Chapter 4.

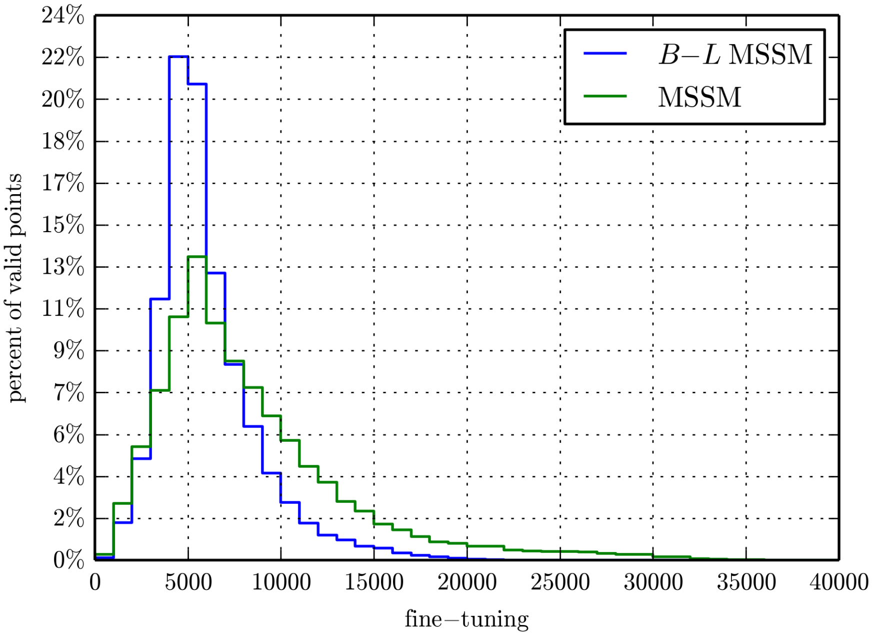

Figure 3.16: The blue line in the histogram shows the amount of fine-tuning required for valid points in the main scan of the $B - L$ MSSM. Similarly, the green line specifies the amount of fine-tuning necessary for the valid points of the R-parity conserving MSSM–computed using the same statistical procedure as for the $B - L$ MSSM with $M = 2700$ GeV and $f = 3.3$. The $B - L$ MSSM shows slightly less fine-tuning, on average, than the MSSM.

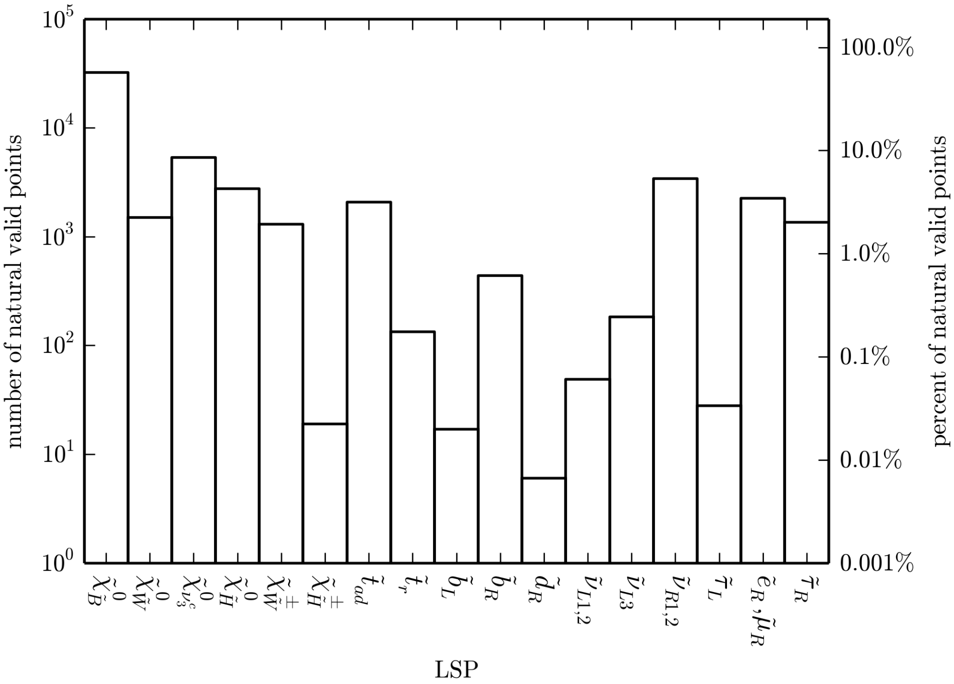

Figure 3.17: A histogram of the LSP's for the "natural" valid points with $F < 1000$. Sparticles which did not appear as LSP's are omitted. The y-axis has a log scale. The notation for the various states, as well as their most likely decay products, are given in Table 3.4. Note that the natural valid points favor stop and sbottom LSP's more than the valid points presented in Fig. 3.7. Note that we have combined left-handed first and second generation sneutrinos into one bin and each generation makes up about 50% of the LSP's. The same is true for the first and second generation right-handed sleptons and sneutrinos.

Chapter 4

Stop or Sbottom LSP's at the LHC

4.1 Overview

In the previous chapter, we established that stop and sbottom LSPs are not only possible in the $B - L$ MSSM but also strongly favored by considerations of fine-tuning. In this chapter we explore the specific predictions of a stop or sbottom LSP at the LHC. We begin with a discussion of R-parity violation and its role both in the formation of neutrino masses and in LSP decays. This will enable us to draw predictive connections between neutrino oscillations and LHC-observable physics. Additionally, we reinterpret LHC public data to place lower bounds on the masses of stop and sbottom LSPs. It should be noted that a more recent study from ATLAS [106] has greately improved these mass bounds.

4.2 R-parity Violation

R-parity violation in this model is best parameterized by the two flavorful parameters– v_{Li} and

$$\epsilon_i \equiv \frac{1}{\sqrt{2}} Y_{\nu i3} v_R \, . \tag{4.1}$$

The superpotential expanded around the vacuum now contains the R-parity violating terms

$$W \supset \epsilon_i \, L_i \, H_u - \frac{1}{\sqrt{2}} Y_{ei} \, v_{Li} \, H_d^- \, e_i^c \, , \tag{4.2}$$

which is similar to the so-called bilinear RPV scenario [42]. In addition, the Lagrangian contains various other bilinear terms, generated by v_{Li} and v_R, from the super-covariant derivative:

$$\begin{aligned}\mathcal{L} \;\supset\; & -\frac{1}{2}v_{L\,i}^{*}\left[g_2\left(\sqrt{2}\,e_i\tilde{W}^{+}+\nu_i\tilde{W}^{0}\right)-g_{BL}\nu_i\tilde{B}'\right] \\ & -\frac{1}{2}v_R\left[-g_R\nu_3^c\tilde{W}_R+g_{BL}\nu_3^c\tilde{B}'\right]+\text{h.c.}\end{aligned} \tag{4.3}$$

The calculations in this chapter will be carried out using the Lagrangian based on Eqs. (4.2) and (4.3). However, it is worthwhile to note that it is sometimes useful to rotate away the ϵ_i term in favor of the so-called trilinear R-parity violating terms. This is true when comparing to given bounds on various low-energy constraints on RPV, such as lepton number violating processes, and it makes approximating decays widths more straightforward. An example of each of these will be given in this section. Rotating ϵ_i away generates the following terms in the superpotential:

$$W_{TRPV}=\lambda_{ijk}L_iL_je_k^c+\lambda'_{ijk}Q_iL_jd_k^c, \tag{4.4}$$

where λ_{ijk} is antisymmetric under the interchange of i and j.[1] This is accomplished by considering H_d as a fourth generation lepton. In this case, the μ- and ϵ_i-terms can be combined to read $\mu_m\hat{L}'_mH_u$, where $m=0,\ldots,3$, $\hat{L}'_0=H_d$, $\hat{L}'_{1,2,3}=L_i$, $\mu_0=-\mu$ and $\mu_{1,2,3}=\epsilon_i$. The μ_m term can be perturbatively rotated so that only μ_0 is nonzero. This requires the rotation $\hat{L}'\to\hat{L}=R_\mu\hat{L}'$ with

$$R_\mu=\begin{pmatrix}1 & -\frac{\epsilon_1}{\mu} & -\frac{\epsilon_2}{\mu} & -\frac{\epsilon_3}{\mu}\\ \frac{\epsilon_1}{\mu} & 1 & 0 & 0\\ \frac{\epsilon_2}{\mu} & 0 & 1 & 0\\ \frac{\epsilon_3}{\mu} & 0 & 0 & 1\end{pmatrix}. \tag{4.5}$$

Implicit in this is that $\epsilon_i\ll\mu$, which follows from the fact that ϵ_i contributes to neutrino masses, as we shall see later. The rotation leaves only one bilinear between H_u and a linear combination of L'_m, which is, of course, mostly composed of H_d. This rotation must also be applied to H_d in the down-type quark Yukawa term, Y_d, and the charged lepton Yukawa coupling term, Y_e. The parameterization of λ_{ijk} and λ'_{ijk} can be read off from this rotation:

$$\lambda_{ijk}=\frac{1}{2}Y_{eik}\frac{\epsilon_j}{\mu}-\frac{1}{2}Y_{ejk}\frac{\epsilon_i}{\mu} \tag{4.6}$$

$$\lambda'_{ijk}=Y_{dik}\frac{\epsilon_j}{\mu}. \tag{4.7}$$

---

[1] Note that each L_i is an $SU(2)_L$ doublet. Hence, $L_iL_j=\epsilon_{AB}L_i^AL_j^B$ is antisymmetric in ij.

Because the charged lepton and down quark Yukawa matrices are dominated by the three-three component which gives mass to the tau lepton and bottom quark respectively, those matrices can be calculated to be $Y_e \sim$ diag$(0, 0, Y_\tau)$ and $Y_d \sim$ diag$(0, 0, Y_b)$. This means that the largest elements in the trilinear RPV Yukawas are $\lambda_{3i3} = -\lambda_{i33} = Y_\tau \epsilon_i/\mu$ and $\lambda'_{3i3} = Y_b \epsilon_i/\mu$.

As an application of this rotation, consider the lepton number violating decay $\mu \to e\gamma$. This places the following approximate bound on the trilinear R-parity violating couplings [107]:

$$|\lambda_{23k}\lambda_{13k}| \lesssim 2 \times 10^{-4} \left(\frac{m_{\tilde{\nu}_3}}{100\text{ GeV}}\right)^{-2} . \tag{4.8}$$

Using Eq. (4.6) yields

$$\left|\frac{\epsilon_1\epsilon_2}{\mu^2}\right| \lesssim 2.5 \times 10^{-3} \left(\frac{m_{\tilde{\nu}_3}}{100\text{ GeV}}\right)^{-2} \tag{4.9}$$

as the most stringent constraint. This corresponds to $\tan\beta = 55$, approximately the upper bound on $\tan\beta$ that keeps Y_τ perturbative up to the GUT scale. The dependence on $\tan\beta$ is due to the fact that the SUSY Yukawa coupling $Y_\tau = \sqrt{2}\, m_\tau/v_d$, where m_τ is the tau mass. This is negligible due to the suppression of the lepton Yukawa coupling and the μ term. One would expect ϵ_i values much lower than this bound due to constraints from neutrino masses, as we shall see later. It is worth noting that contributions to $\mu \to e\gamma$ also arise from the $e_i\tilde{W}^+$ term in Eq. (4.3). However, this is further suppressed due to the $\tilde{W}^+$-charged lepton mixing, which is proportional to lepton masses. See the approximate value in Eq. (6.132).

Using Eq. (4.7), the decay width of the stop LSP into a bottom quark and a charged lepton (henceforth, referred to as a bottom–charged lepton) is given by

$$\Gamma_{\tilde{t}_1 \to b\ell_i^+} \sim \frac{1}{16\pi} Y_b^2 \left|\frac{\epsilon_i}{\mu}\right|^2 m_{\tilde{t}_1}, \tag{4.10}$$

where $\tilde{t}_1$ indicates the lightest of the two physical stop states. While this neglects order one factors and the contributions from v_{Li}, it is useful for getting an impression of how the stop lifetime depends on the strength of R-parity violation. It will be shown later that ϵ_i is typically larger than v_{Li}, so that the contribution in Eq. (4.10) dominates the decay width. An order of magnitude approximation for the lifetime can be simply attained from the largest ϵ_i value, denoted ϵ_{max}, by

$$\tau_{\tilde{t}_1} \sim 1 \times 10^{-14} \left(\frac{\epsilon_{\text{max}}/\mu}{10^{-5}}\right)^{-2} \left(\frac{100}{1 + \tan^2\beta}\right) \left(\frac{500\text{ GeV}}{m_{\tilde{t}_1}}\right) \text{seconds}. \tag{4.11}$$

Taking representative values of $\mu, m_{\tilde{t}_1} = 500$ GeV and $\tan\beta = 10$, the lifetimes can be divided up into the following interesting regimes:

- Cosmologically significant ($\epsilon_{\text{max}} \lesssim 10^{-10}$ GeV): The decays of squarks with lifetimes greater than about 100 seconds would disrupt the predictions of big bang nucleosynthesis, see reference [108] for example, and would therefore be ruled out.
- Collider stability (10^{-10} GeV $\lesssim \epsilon_{\text{max}} \lesssim 10^{-7}$ GeV): In this regime, the decay length of the squark is longer than the radius of the LHC detectors, about ten meters in size. Such squarks would hadronize and are referred to as R-hadrons. These states would be detectable through their activity in the hadronic calorimeter of the detectors and have been studied in references [109, 110, 111, 112, 113, 114], for example.
- Displaced vertices (10^{-7} GeV $\lesssim \epsilon_{\text{max}} \lesssim 10^{-4}$ GeV): Squark decays inside an LHC detector with a decay length greater than a millimeter have a large enough displaced vertex from the squark origin to be measured. Such vertices, in a phenomenologically similar scenario, were discussed in [88]. Experimentally, some searches for displaced vertices have been performed in references [115, 116, 117].
- Prompt decays ($\epsilon_{\text{max}} \gtrsim 10^{-4}$ GeV): Decays in this case occur at an indistinguishable distance from the collision point at an LHC detector.

The physics associated with non-prompt decays is mostly dependent on the mass of the squark (through its production) and its decay length (displaced vertices or collider stable squarks). Such probes would not be the ideal way of studying the specific branching ratios of the squarks predicted in the model under consideration. In addition such signals have already been analyzed in the references above. We therefore continue this thesis considering prompt squark LSP decays only. As we shall see, this will intimately relate the neutrino sector to the stop decays.

The existence of this relationship is already suggested by Eqs. (4.2) and (4.3). These RPV bilinear terms mix fields with different R-parity number but the same spin and SM quantum numbers. Specifically, the neutrinos now mix with the neutralinos, Eq. (6.77), the charged leptons mix with the charginos, Eq. (6.119) and the Higgs fields mix with the sleptons. The neutrino/neutralino mixings are crucial because they generate tree-level Majorana neutrino masses through a seesaw mechanism. As a result of this, the bilinear R-parity violating terms cannot be too large. All R-parity violating effects will therefore be negligible compared to the R-parity conserving effects, except for the LSP, which now decays via RPV.

4.3 Neutrino Masses and R-parity Violation

Any model with right-handed neutrinos allows for Dirac neutrino masses through the Yukawa coupling between left- and right-handed neutrinos. In this model, Majorana masses are also possible due to the VEV of the right-handed sneutrino. As mentioned above, only one generation of right-handed sneutrino can attain a significant VEV [16, 32, 33]. This means that lepton number is only significantly violated in one generation of the right-handed neutrinos. It is only that generation of right-handed neutrinos that will attain a TeV-scale mass. This gives rise to a system of neutrinos with three layers: a TeV scale right-handed neutrino, the three active neutrinos and two light sterile neutrinos[2] Sterile neutrinos are typically sub-MeV fermions without SM quantum numbers. In this model, their masses must be at or below those of the left-handed, or active, neutrinos since their masses arise from Dirac Yukawa couplings to the left-handed neutrinos. Models with two sterile neutrinos are sometimes called 3+2 models in the literature, where the three represents the active neutrinos. .

Majorana masses for the active neutrinos are generated through an effective type I seesaw mechanism [118, 119, 120, 121] where the seesaw fields include the one heavy right-handed neutrino and the neutralinos. Once the heavy seesaw fields are integrated out, the Majorana contribution to the neutrino mass matrix is

$$m_{\nu ij} = A v_{L_i}^{*} v_{L_j}^{*} + B \left(v_{L_i}^{*} \epsilon_j + \epsilon_i v_{L_j}^{*} \right) + C \epsilon_i \epsilon_j \ . \tag{4.12}$$

The non-flavored parameters, A, B and C, are the results of integrating out the heavy fields. They, and more details, are given in Appendix 6.4. The Dirac neutrino mass contributions are simply given by the product of the up-type Higgs VEV and the neutrino Yukawa couplings that do not couple to the third generation right-handed neutrino: $\frac{1}{\sqrt{2}} Y_{\nu i, j \neq 3} v_u$.

One of the main tools at our disposal for probing the neutrino sector is the observation of neutrino oscillations. Such oscillations between two neutrinos are determined by the amount of mixing between the two neutrinos and their mass difference. In a purely Dirac neutrino case, the active-sterile mixing is maximal

---

[2]

but the mass difference is zero and, therefore, no active-sterile oscillations result. Here, in the pure Majorana case, the mass difference is significant but the mixing is negligible. A situation in which both Dirac and Majorana mass contributions are comparable would lead to large active-sterile oscillations which have not been observed and are therefore ruled out, *e.g.* [122, 123].

The question then remains, should this analysis assume that neutrinos receive their masses dominantly from Dirac or Majorana mass terms? Here, already, the connection to R-parity becomes important. Prompt LSP decays, which were argued to be of interest in the last section, will allow significant Majorana masses. Since these cannot coexist with significant Dirac masses, neutrinos must receive their masses dominantly from Majorana mass terms. This makes further study of the Majorana mass matrix, Eq. (4.12), fruitful.

As a first step, it is important to notice that the determinant of the neutrino mass matrix in Eq. (4.12) is zero. This is a consequence of the flavor structure and is independent of the A, B and C parameters. Closer observation reveals that only one eigenstate is massless. This constrains the neutrino masses to be either in the normal hierarchy (NH):

$$m_1 = 0 < m_2 \sim 8.7 \text{ meV} < m_3 \sim 50 \text{ meV} \tag{4.13}$$

or in the inverted hierarchy (IH):

$$m_1 \sim m_2 \sim 50 \text{ meV} > m_3 = 0 \tag{4.14}$$

where only the squared mass differences are measured in neutrino oscillation experiments.

The relevant seesaw contributions from A, B and C are also informative. For example, the term proportional to A in Eq. (4.12) is a contribution associated with the VEVs of the left-handed sneutrinos. It arises from neutrino-gaugino mixing such as in Eq. (4.3). The gauginos are naturally Majorana due to their soft masses and, therefore, integrating them out directly leads to Majorana mass terms for the neutrinos. One can therefore conclude that

$$A \sim \frac{1}{m_{\text{soft}}}, \tag{4.15}$$

where m_{soft} is some combination of gaugino and Higgsino masses. This conclusion can be verified with the full analytic expression for A in Appendix 6.4. The parameter C, on the other hand, arises through neutrino-Higgsino mixing because of the ϵ_i term. Higgsinos are not Majorana particles before electroweak symmetry breaking and only their electroweak mixings with the gauginos gives them a Majorana nature. Therefore, C must include at least two factors of Higgsino-gaugino mixing terms, each of which is proportional to the ratio of an electroweak VEV to m_{soft}:

$$C \sim \frac{v^2}{m_{\text{soft}}^3}. \tag{4.16}$$

A similar argument yields that $B \sim v/m_{\text{soft}}^2$ at lowest order. All of these conclusions can be verified with the full expressions in Appendix 6.4.

The neutrino mass matrix is diagonalized by the so-called PMNS matrix:

$$\begin{aligned} V_{\text{PMNS}} &= \begin{pmatrix} c_{12}c_{13} & s_{12}c_{13} & s_{13}e^{-i\delta} \\ -s_{12}c_{23} - c_{12}s_{23}s_{13}e^{i\delta} & c_{12}c_{23} - s_{12}s_{23}s_{13}e^{i\delta} & c_{13}s_{23} \\ s_{12}s_{23} - c_{12}c_{23}s_{13}e^{i\delta} & -c_{12}s_{23} - s_{12}c_{23}s_{13}e^{i\delta} & c_{13}c_{23} \end{pmatrix} \\ &\quad \times \text{diag}(1, e^{i\alpha/2}, 1), \end{aligned} \tag{4.17}$$

where $c_{ab}(s_{ab}) = \cos\theta_{ab}(\sin\theta_{ab})$. There are $N-1$ Majorana phases associated with N Majorana neutrinos. This translates into only one Majorana phase, α, in this case because one of the neutrinos is massless and, therefore, does not have a Majorana mass. The CP phase δ corresponds to the freedom in the three-by-three Y_ν matrix. In models that predict a massless neutrino, such as the one discussed here, the neutrino masses in terms of the mass squared differences in the *normal hierarchy* are

$$m_1 = 0, \quad m_2 = \sqrt{\Delta m_{21}^2}, \quad m_3 = \sqrt{\Delta m_{31}^2}, \tag{4.18}$$

while in the *inverted hierarchy* one has

$$m_1 = \sqrt{\Delta m_{31}^2}, \quad m_2 = \sqrt{\Delta m_{31}^2 + \Delta m_{21}^2}, \quad m_3 = 0. \tag{4.19}$$

The current values for the parameters in (4.17) and (4.18), (4.19) are given in [124, 125, 126]. We use the most recent values [127] from the collaboration of reference [125], which at one sigma are given by

$$\begin{aligned} \sin^2\theta_{12} &= 0.306^{+0.012}_{-0.012}, \\ \sin^2\theta_{23} &= 0.446^{+0.007}_{-0.007} \text{ or } 0.587^{+0.032}_{-0.037}, \\ \sin^2\theta_{13} &= 0.0229^{+0.0020}_{-0.0019}, \\ \Delta m_{21}^2(10^{-5}\text{ eV}^2) &= 7.45^{+0.19}_{-0.16}, \\ \Delta m_{31}^2(10^{-3}\text{ eV}^2) &= 2.417^{+0.013}_{-0.013}, \\ \delta(^\circ) &= 265^{+56}_{-61}. \end{aligned} \tag{4.20}$$

Note that at three sigma, δ spans its full range of $0° - 360°$ and that α has not been measured. The two values of θ_{23} represent a degeneracy in the best fit to the data.

One can solve for the flavorful parameters ϵ_i and v_{Li} by requiring that the diagonalization of the neutrino mass matrix, Eq. (4.12), yields the correct neutrino data specified in Eq. (4.20). A procedure for this is outlined in Appendix 6.4 in terms of a new set of variables E_i and V_i, where

$$v_{Li} = V_{\text{PMNS}\,il}\, V_l^*, \tag{4.21}$$

$$\epsilon_i = V^*_{\text{PMNS}\,il}\, E_l. \tag{4.22}$$

These imply that ϵ_i and v_{Li} should be on the order of magnitude of E_{max} and V_{max} respectively–where E_{max} and V_{max} are the largest of E_i and V_i–since the elements of V_{PMNS} are mostly of order one. In the normal hierarchy $E_1, V_1 = 0$ and Eqs. (6.109), (6.110), and (6.111) are used to calculate E_2 and $V_{2,3}$ in terms of E_3. Together, they imply that $V_{\text{max}} \sim (\mathcal{O}(1)\frac{B}{A} + \mathcal{O}(1)\sqrt{\frac{C}{A}})E_{\text{max}}$, where the coefficients are of order one as long as there are not finely tuned numerical cancellations between terms. The same conclusion holds in the inverted hierarchy. This in turn means that $v_{L_i} \sim (\mathcal{O}(1)\frac{B}{A} + \mathcal{O}(1)\sqrt{\frac{C}{A}})\epsilon_i$. Based on the approximations made above for A, B and C in Eqs. (4.15) and (4.16), it follows that

$$|\epsilon_i| \sim \frac{m_{\text{soft}}}{v} |v_{Li}| \,. \tag{4.23}$$

This means that ϵ_i typically dominates over v_{Li}. Quantitatively $|\epsilon_i| > |v_{Li}|$ is verified through the scan specified in Table 4.1, which is used to generate the numerical results in the next section. Indeed, we find that for 80% of the points $\epsilon_i > v_{Li}$ for all i and that the largest ϵ_i value is larger than the largest v_{Li} value ($\epsilon_{\text{max}} > v_{L\text{max}}$) in 97% of the points. Points that do not satisfy these conditions correspond to finely tuned cancellations between terms which, although unlikely, arise randomly in the scan. This indicates that ϵ_{max} typically approximates the amount of R-parity violation and that $|\epsilon_i|^2 \gg |v_{Li}|^2$ is a good approximation. This will be useful to obtain an analytic understanding of the numerical results.

4.4 Third Generation Squark LSP's

The previous two sections have reviewed various aspects of RPV and the neutrino sector. It was shown that there is a region of parameter space where 1) the strength of RPV corresponds to prompt LSP decays and 2) RPV is responsible for neutrino masses. We proceed to study these properties under the assumption that the LSP is a third generation squark; that is, for both a stop and sbottom LSP. In addition, we will place lower bounds on the masses of these sparticles using current publicly available LHC results. Since completing this work, ATLAS [106] has carried out a more sophisticated search using private data, placing stronger bounds on the mass of a stop LSP.

Squark LSP's are interesting in RPV for various reasons. First, they are not possible in RPC,[3] so this provides an opportunity to look beyond the typical SUSY LSP candidates and beyond the typical SUSY signatures. Specifically, squark LSP's behave like leptoquarks, meaning they are scalar particles that are pair produced and decay into a quark and a lepton. The stops and sbottoms have the following possible decays:

$$\tilde{t}_1 \to t\,\nu_i, \text{ or } \tilde{t}_1 \to b\,\ell_i^+ \,, \tag{4.24}$$

$$\tilde{b}_1 \to b\,\nu_i, \text{ or } \tilde{b}_1 \to t\,\ell_i^- \,, \tag{4.25}$$

where $\tilde{t}_1$ and $\tilde{b}_1$ are the lightest physical stop and sbottom respectively.

Colored particles are, furthermore, more abundantly produced at the LHC, so more aggressive bounds can be placed on them. Based on Chapter 3, the stob and sbottom are the most likely colered LSP's. From a phenomenological point of view, the first two generation of squarks should be relatively degenerate to avoid large disallowed contributions to flavor physics processes. This is known as the SUSY flavor problem. Light degenerate first and second generation squarks effectively double the expected number of events for a given process and will consequently have stronger bounds. Furthermore, the first two generations have additional contributions to their production cross section due to the presence of light quarks in the proton. This can, once again, increase the number of events. For these reasons, we continue our analysis focusing on third generation squark LSP's. Some general comments about the branching ratios of the first two generations will be made in the discussion.

Stop LSP's are especially compelling because of the central role they play in SUSY. Before discussing this further, we briefly review some basic stop phenomenology. More details can be found in Appendix 6.6. In the gauge eigenstate basis, the stop sector contains the $\tilde{t}$ field, which is the superpartner of the left-handed top and part of the squark $SU(2)_L$ doublet $\tilde{Q}$. Since it is a scalar, the stop has no actual chiral properties. The stop sector also contains the superpartner

---

[3] Squark LSP's are not allowed with R-parity conservation because they would be stable, resulting in a relic density of charged particles.

of the right-handed top, $\tilde{t}^c$, which is an $SU(2)_L$ singlet. Both have unrelated soft squared masses and are mixed through mass mixing terms. Diagonalization yields the physical stops $\tilde{t}_1$ and $\tilde{t}_2$, which are traditionally labeled so that $m_{\tilde{t}_1} < m_{\tilde{t}_2}$. The mass mixing term leads to what is usually referred to as the left-right mixing angle in the stop sector, θ_t, with the convention used here that $\theta_t = 0^\circ$ ($\theta_t = 90^\circ$) corresponds to a purely left-handed (right-handed) lightest stop, $\tilde{t}_1$. A purely left-handed $\tilde{t}_1$ cannot be the LSP because its $SU(2)_L$ partner, the left-handed sbottom, will always be lighter. This is because they share the same SUSY-breaking soft mass squared term and both get F-term contributions from their SM partner mass squared. That is, the sbottom mass gets a bottom mass squared contribution and the stop gets a top mass squared contribution. Since the top is much heavier than the bottom, the left-handed stop will always be heavier than the left-handed sbottom.

The stops in SUSY are important because they couple most strongly to the Higgs. This means they contribute most to the little hierarchy problem and provide a measure of the fine-tuning required in SUSY models. This is why, in Chapter 3, we found that a fine-tuning criterion favors stop LSP's. In RPC, stop decays can involve complicated decay chains with multi-particle final states making determination of the stop mass from the observation of such a decay difficult. As an LSP with R-parity violation, stop decays are very clean in the sense that each stop decays to only two particles. Therefore, such decays can be used to deduce the stop mass in a relatively straightforward way. This is especially true for the bottom–charged lepton channel, whose final states are both detectable. Neutrinos, on the other hand, escape the detector as missing energy. As we shall see, typically the bottom–charged lepton channel dominates the stop decays.

The issue of the little hierarchy problem is also strongly linked to the Higgs mass. In SUSY, the Higgs tree-level mass must be less than the Z mass. This can be increased at the loop level by radiative corrections to the Higgs mass which grow as the logarithms of the stop masses and also increase with stop mixing angle. This leads to a conflict between the heavy stops masses needed to make SUSY compatible with the recent Higgs discovery and the desire to keep the stops light so as to minimize fine-tuning in SUSY. The former seems to be an argument against a stop LSP. However, it is possible that only one stop is quite heavy while the second remains light–which will indeed be the case when the stop mixing angle is relatively large. This translates into an LSP stop that is composed of significant left- and right-handed components.

The stop partial widths into top neutrino and bottom–charged lepton are

$$\begin{aligned}\Gamma(\tilde{t}_1 \to t\,\nu_i) &= \frac{1}{16\pi}(|G^L_{\tilde{t}_1 t \chi^0_{6+i}}|^2 + |G^R_{\tilde{t}_1 t \chi^0_{6+i}}|^2) m_{\tilde{t}_1} \\ &\quad \times \left(1 - \frac{m_t^2}{m_{\tilde{t}_1}^2}\right)\sqrt{1 - 2\frac{m_t^2}{m_{\tilde{t}_1}^2} + \frac{m_t^4}{m_{\tilde{t}_1}^4}} \qquad (4.26) \\ \Gamma(\tilde{t}_1 \to b\,\ell_i^+) &= \frac{1}{16\pi}(|G^L_{\tilde{t}_1 b \chi^\pm_{2+i}}|^2 + |G^R_{\tilde{t}_1 b \chi^\pm_{2+i}}|^2) m_{\tilde{t}_1}, \qquad (4.27)\end{aligned}$$

where the G parameters are the coefficients of the relevant vertices, $\chi^0_{6+i} = \nu_i$ and $\chi^\pm_{2+i} = \ell_i^\pm$. They, as well as more details, can be found in Appendix 6.7. Parametrically, the $G^{L,R}_{\tilde{t}_1 t \chi^0_{6+i}}$ parameters contain the elements of the matrix that diagonalize the neutrino-neutralino sector and the $G^{L,R}_{\tilde{t}_1 b \chi^\pm_{2+i}}$ parameters contain the elements of the matrix that diagonalize the lepton-chargino sector and are, therefore, proportional to some combination of ϵ_i and v_{Li}. Also encoded in the G parameters is information about the stop left-right mixing angle, θ_t.

Before tackling a numerical study of stop LSP phenomenology, it is instructive to approximate the relative sizes of the different branching ratios. This can be done by perturbatively diagonalizing the neutrino-neutralino and charged lepton-chargino mass matrices, as is done in Appendices 6.4 and 6.5 and applied in Appenedix 6.7. For ease of comparison, the leading squared amplitudes for the different final states are given in the approximation that $M_{Z_R}^2 \gg m_{\text{soft}}^2 \gg v^2$. This is a phenomenologically relevant approximation because bounds on Z_R are much higher than electroweak gaugino and Higgsino bounds and both are above the electroweak scale itself. We also employ the results of the last section, $\epsilon_i^2 \gg v_{Li}^2$. The leading contributions to the square of the vertex amplitude, $|\mathcal{A}|^2 = |G^L|^2 + |G^R|^2$, are then

$$\begin{aligned}|\mathcal{A}(\tilde{t}_1 \to b\,\ell_i^+)|^2 &\sim c_t^2 Y_b^2 \left|\frac{\epsilon_i}{\mu}\right|^2 \qquad (4.28) \\ |\mathcal{A}(\tilde{t}_1 \to t\,\nu_i)|^2 &\sim \left[\frac{1}{8}c_t^2\left(\frac{g_2^2}{M_2} - \frac{g_{BL}^2 g_R^2}{3M_{\tilde{Y}}}\right)^2 + \frac{1}{18}s_t^2\frac{g_{BL}^4 g_R^4}{M_{\tilde{Y}}^2}\right] \\ &\quad \times \left|V_{\text{PMNS}\,ij}\left(\frac{v_d\,\epsilon_j}{\mu} + v_{Lj}^*\right)\right|^2, \qquad (4.29)\end{aligned}$$

where s_t (c_t) is $\sin\theta_t$ ($\cos\theta_t$), $M_{\tilde{Y}} \equiv g_R^2 M_{BL} + g_{BL}^2 M_R$ and there is an implicit sum over j. The top–neutrino channel is suppressed compared to the bottom–charged lepton channel both by helicity suppression to the term proportional to ϵ_i

and suppression by v_{Li} when the lightest stop is not purely right-handed. When the lightest stop is purely right-handed, the leading order bottom–charged lepton amplitude vanishes and the next order term becomes important:

$$|\mathcal{A}(\tilde{t}_1 \to b\,\ell_i^+)|^2\Big|_{\theta_t \sim 90^\circ} \sim Y_t^2 \left|\frac{m_{\ell_i}\,v_{Li}}{\mu\,v_d}\right|^2 . \tag{4.30}$$

This term is suppressed by both v_{Li} and the mass of the charged lepton in the final state, $m_{\ell i}$, indicating that, for the mostly right-handed stop, only the top–neutrino and bottom-tau channels are significant. The stop branching ratios, where branching ratio is defined as the partial width normalized to the total width, falls into two regimes of interest depending on the composition of the stop:

- Admixture stop LSP: Stop decays into into bottom–charged leptons dominate, $\sum_i \Gamma(\tilde{t}_1 \to b\ell_i^+) \gg \sum_i \Gamma(\tilde{t}_1 \to t\nu_i)$. We therefore approximated the total width as coming completely from the charged leptons, and the decays of the stop can be described by three branching ratios, which must satisfy

$$\text{Br}(\tilde{t}_1 \to b\,e^+) + \text{Br}(\tilde{t}_1 \to b\,\mu^+) + \text{Br}(\tilde{t}_1 \to b\,\tau^+) = 1. \tag{4.31}$$

- Right-handed stop LSP: Only the top–neutrino and bottom-tau channel are significant. We therefore approximate the width as coming completely from these two channels and the decays can be described by two branching ratios, which must satisfy:

$$\text{Br}(\tilde{t}_1 \to b\,\tau^+) + \text{Br}(\tilde{t}_1 \to t\,\nu) = 1. \tag{4.32}$$

Let us qualitatively understand these results, which may be a bit counterintuitive. Since ϵ_i mixes $\tilde{H}_u$ with L_i, one would expect the leading contributions to be proportional to the Y_t, since it couples the stops to $\tilde{H}_u$ and through it to the ϵ_i parameter. However, such decays are helicity suppressed by a factor of v^2/m_{soft}^2 (in Eq. (4.29)) and are, therefore, subdominant. The dominant channel to RPV then usually goes through $\tilde{H}_d$ and, therefore, includes a factor of $Y_b\epsilon_i$. This explains Eq. (4.28). The top–neutrino channel cannot, however, be accessed through $\tilde{H}_d$ and must, therefore, suffer the helicity suppression or be suppressed by v_{Li}, as are the two terms in Eq. (4.29). The right-handed stop also cannot access $\tilde{H}_d$. Its decay into bottom–charged lepton must go through $\tilde{H}_u - \tilde{H}_d$ mixing and finally through $Y_{e_i} v_{Li} \tilde{H}_d^- e_i^c$, which is the reason that Eq. (4.30) depends on the lepton mass.

4.4.1 Stop LSP Decays and the Neutrino Spectrum

The numerical procedure starts with the process in Appendix 6.4, which takes as input the unmeasured CP violating phases of the neutrino sector, the neutralino spectrum, the $B - L$ parameters, any one of the ϵ_i parameters, and two signs. It yields values for v_{Li} and the other two ϵ_i that are consistent with neutrino physics. These values are then used to numerically diagonalize the neutrino/neutralino and charged lepton/chargino mass matrices. These rotation matrices are then inputted into the Feynman rules in Appendix 6.7, which can be used in Eqs. (4.26) and (4.27) to calculate the partial widths. Because of the dependence on a variety of parameters, full analytic relationships between the input parameters and the stop decay branching ratios are complicated and not very illuminating. However, random scans in the space of the input parameters yield fairly simple behavior.

The parameters of our scan and their ranges are specified in Table 4.1. As mentioned above, the neutrino sector specifies all but one R-parity violating parameter, which we choose to be ϵ_i and we randomly choose the generation, i, of ϵ_i to avoid any bias in the scan. The sign factors, ζ_0 and ζ_3 are further discussed in Appendix 6.4. While only the gluino mass range is shown, we use the GUT inspired gaugino mass relation $M_R : M_{BL} : M_2 : M_3 \sim 1 : 1 : 2 : 5$ for the gaugino masses [1]. The lower ranges on M_3, M_{Z_R}, μ and $m_{\tilde{t}_1}$ roughly correspond to the lower bounds on those particles, while μ roughly corresponds to the mass of one of the physical chargino states. The lower and upper bounds on $\tan\beta$ are based on keeping all Yukawa couplings perturbative to the GUT scale. Meanwhile, the bounds on ϵ_i follow from requiring no fine-tuning in the neutrino sector, the conditions for which are described in Appendix 6.4. This fine-tuning depends on the actual parameter point and we find that non fine-tuned points lie in the range 10^{-4} GeV $< |\epsilon_i| < 1$ GeV, which is used in the scan.

In addition, the uncertainties on the neutrino parameters themselves can quantitatively alter the results. We, therefore, also scan over the three sigma range of the neutrino parameters based on their values and uncertainties given in Eq. (4.20). To do this, we need a probability distribution to describe the uncertainty in these parameters. A simple Gaussian will not do, because the uncertainties in some of the neutrino parameters are asymmetric. Instead we randomly select, with probability one half, which side of the central value a parameter will be on. Then a value for that parameter is randomly generated based on a Gaussian distribution whose standard deviation is equal to the 1σ uncertainty on the chosen side of that parameter's central value. The Gaussian distribution is curtailed a distance of three standard deviations away from the central value. No correlations between neutrino parameter ranges are taken into account here. Furthermore, the CP-violating phases, δ and α, are scanned over their full range and the central value of θ_{23} used is randomly chosen between the two ambiguous experimental values.

Since we are studying a stop LSP, points in the scan at which one of the neutralinos or charginos end up being lighter than the stop are rejected. It is also possible that some points in the scan may have a nearly purely left-handed lightest stop, which may be unable to be the LSP (see Appendix 6.6). A criterion for excluding such points from the scan would depend on parameters that do not effect the physics of this thesis, so we do not impose it here. Such a criterion would have no impact on the overall trends displayed by our scan, so it would not effect the conclusions of this thesis.

Parameter	Range
M_3 (TeV)	1.5 – 10
M_{Z_R} (TeV)	2.5 – 10
$\tan\beta$	2 – 55
μ (GeV)	150 – 1000
$m_{\tilde{t}_1}$ (GeV)	400 – 1000
$\theta_t(^\circ)$	0 – 90
$\|\epsilon_i\|$ (GeV)	10^{-4} – 10^0
$\arg(\epsilon_i)$	0 – 360
i	1 – 3
ζ_0, ζ_3	-1, 1
δ, $\alpha(^\circ)$	0 – 360
Neutrino Hierarchy	NH, IH

Table 4.1: Ranges for the parameter scan. The neutrino sector leaves only one unspecified R-parity violating parameter, which is chosen to be ϵ_i where the generational index, i, is also scanned to avoid any biases. The scanned gluino mass is shown here, while the other gaugino masses are extrapolated from the GUT relation $M_R : M_{BL} : M_2 : M_3 = 1 : 1 : 2 : 5$.

We note that due to the extra suppression in the decays of the right-handed stop, Eq. (4.30), the LSP stop lifetime increases by a significant amount when it approaches a purely right-handed stop composition. Using the scan from Table 4.1, we plot the decay length of the stop LSP versus stop mixing angle in Fig. 4.1. The figure shows that for a pure right-handed stop LSP, a significant number of points in the scan yield lifetimes long enough for displaced vertices

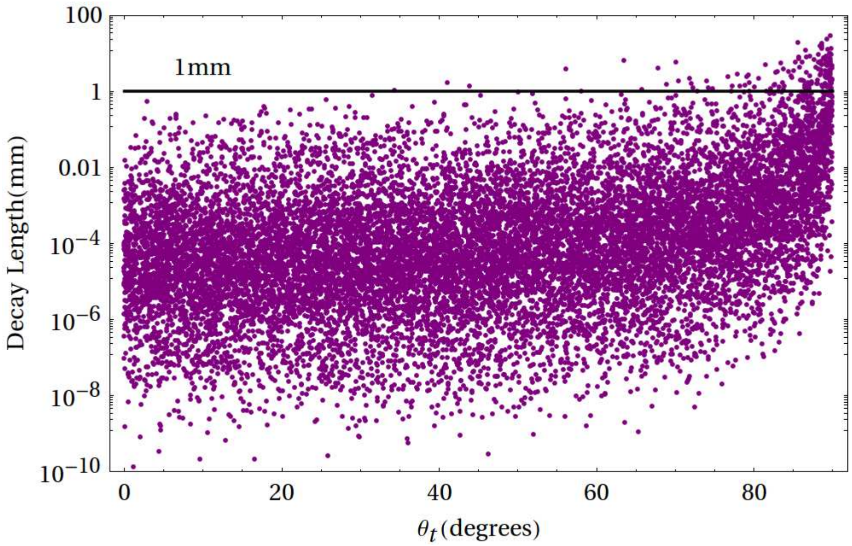

Figure 4.1: Stop LSP decay length in millimeters versus stop mixing angle. The decay length increases sharply past $80°$, where the stop is dominantly right-handed, due to the suppressed right-handed stop decays, Eq. (4.30).

(decay length greater than a millimeter). We continue our analysis focusing on prompt decays.

Figure 4.2 shows how Br$(\tilde{t}_1 \to t\nu)/$Br$(\tilde{t}_1 \to b\ell^+)$, where Br$(\tilde{t}_1 \to b\ell^+) \equiv \sum_{i=1}^{3}$ Br$(\tilde{t}_1 \to b\ell_i^+)$, depends on the stop mixing angle. This verifies the relationship between the stop mixing angle and branching ratios into bottom–charged lepton and top–neutrino derived from Eqs. (4.28) - (4.30). Figures 4.1 and 4.2 both show that the right-handed stop-like behavior, significant top–neutrino channel and longer lifetimes, turns on around $\theta_t = 80°$.

Perhaps the most striking result from this scan is the connection between the stop decays and the neutrino hierarchy. This connection is evident in Fig. 4.3 where the possible branching ratios are displayed in the Br$(\tilde{t}_1 \to b\,\tau^+)$ - Br$(\tilde{t}_1 \to b\,e^+)$ plane and where, for simplicity, we start with only the central values of the measured neutrino parameters, Eq. (4.20). The figure includes only points with Br$(\tilde{t}_1 \to t\nu) < 0.01$. Such points correspond to admixture stop LSP, according to Fig. 4.2. Using the top–neutrino branching ratio, instead of the stop mixing angle, to distinguish between the admixture and right-handed stop LSP is preferable because the top–neutrino branching is easier to measure. This means that

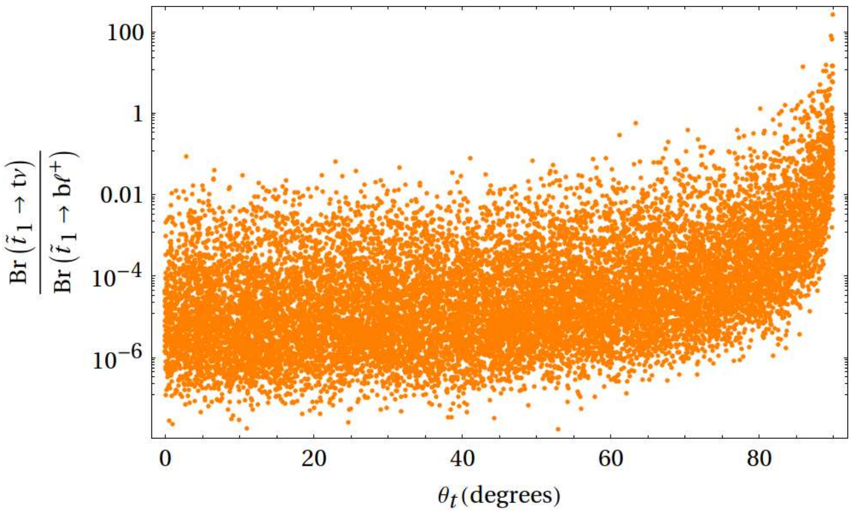

Figure 4.2: $\frac{\mathrm{Br}(\tilde{t}_1 \to t\nu)}{\mathrm{Br}(\tilde{t}_1 \to b\ell^+)}$ versus stop mixing angle, where $\mathrm{Br}(\tilde{t}_1 \to b\ell^+) \equiv \sum_{i=1}^{3} \mathrm{Br}(\tilde{t}_1 \to b\ell_i^+)$. For the admixture stop, the branching ratio to $b\ell^+$ is dominant and the branching ratio to $t\nu$ is insignificant for LHC purposes. For a mixing angle greater than about 80°, corresponding to a mostly right-handed stop, the branching ratio to $t\nu$ can be significant.

$\mathrm{Br}(\tilde{t}_1 \to b\,e^+) + \mathrm{Br}(\tilde{t}_1 \to b\,\mu^+) + \mathrm{Br}(\tilde{t}_1 \to b\,\tau^+) = 1$ (Eq. (4.31)), so that the $(0, 0)$ point on this plot corresponds to $\mathrm{Br}(\tilde{t}_1 \to b\,\mu^+) = 1$. The reader may observe that Fig. 4.3 includes a small number of points that do not follow the trend displayed by the bulk of the points, and are instead skewed in the direction of larger bottom–tau branching ratio. These rare points correspond to a transitional region between admixture stop and purely right-handed stop where Eq. (4.30) is starting to become valid, favoring a larger bottom–tau ratio due to the tau being the heaviest of the leptons. Points that do not satisfy the fine-tuning criteria of the neutrino sector, Eqs. (6.117) and (6.118), are excluded.

Figure 4.3 is divided into three quadrangles each corresponding to an area where one of the branching ratios is larger than the other two. In the top left quadrangle, the bottom–tau branching ratio is the largest; in the bottom left quadrangle the bottom–muon branching ratio is the largest; and in the bottom right quadrangle the bottom–electron branching ratio is the largest. Recall that the fit to the neutrino data allows two values of θ_{23}. One is shown in blue and and the other in green in the inverted hierarchy (where the impact on stop decays is most notable)

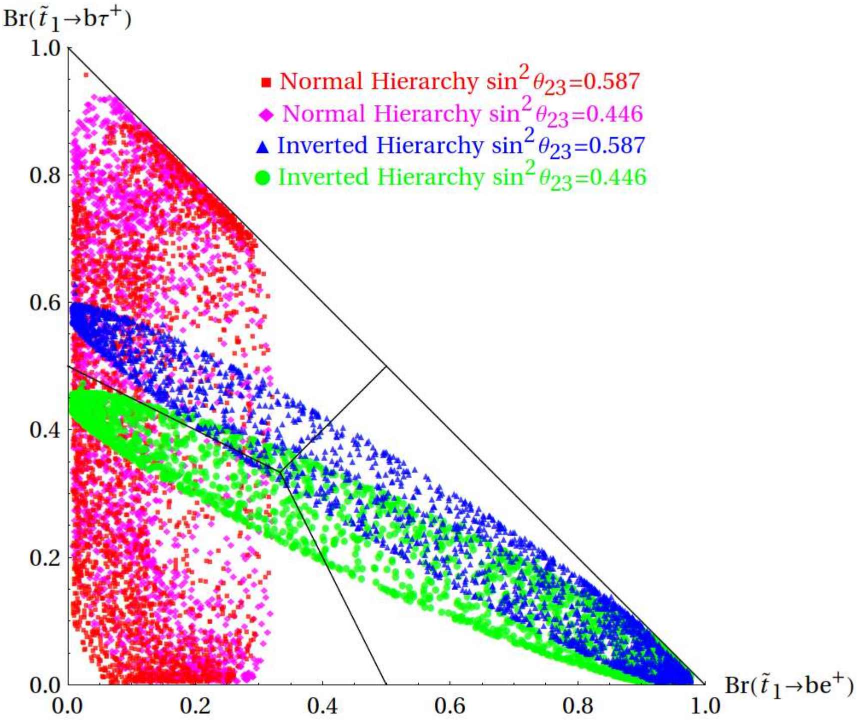

Figure 4.3: The results of the scan specified in Table 4.1, but with central values for the measured neutrino parameters in the Br$(\tilde{t}_1 \to b\,\tau^+)$ - Br$(\tilde{t}_1 \to b\,e^+)$ plane. The two different possible values of θ_{23} are shown in blue and green in the IH (where the difference is most notable) and red and magenta in the NH.

and in red and magenta in the normal hierarchy.

Figure 4.3 shows the strong connection between the stop branching ratios and the neutrino sector. The most interesting connection is to the neutrino mass hierarchy. If these decays were observed at the LHC and their branching ratios measured, then it might be possible to determine the neutrino hierarchy, an open question being actively pursued in neutrino physics today [128].

The full results including the three sigma scan over neutrino parameters are displayed in Fig. 4.4. The features of this figure are very similar to those of Fig. 4.3. While taking the three sigma range of the neutrino parameters into account has obscured things somewhat compared to Fig. 4.3, the connection to neutrino physics is still strong and very visual and the conclusions still of inter-

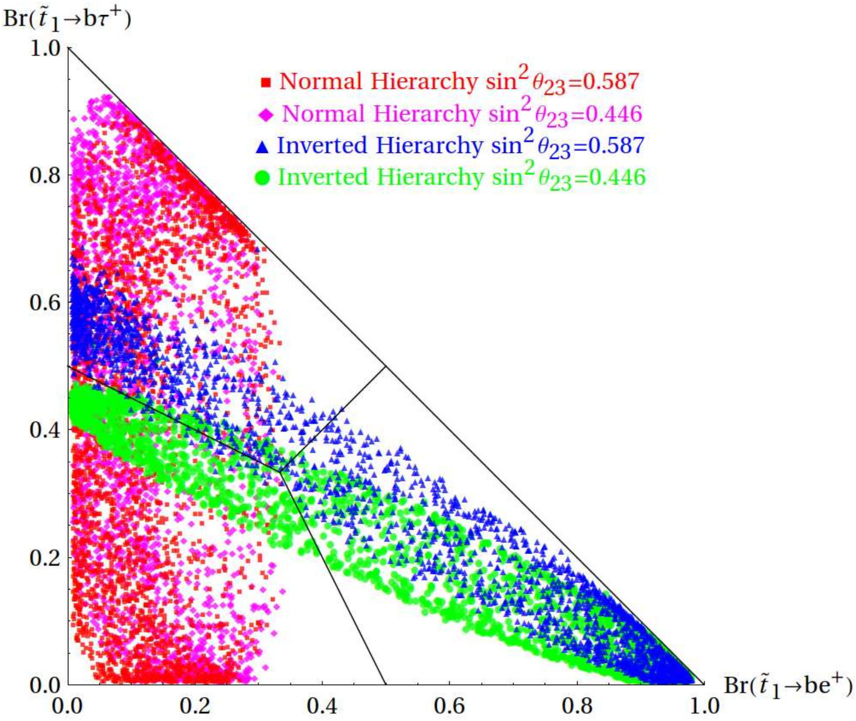

Figure 4.4: Same as Fig 4.3 except with a Gaussian distributed scan over the neutrino parameters as described in Eq (4.20).

est[4]. Therefore, assuming one is lucky enough to discover a particle decaying in this way at the LHC, one can then use the measured branching ratios to conclude the following.

- If the branching ratio to bottom–electron is the largest branching ratio, the neutrino mass hierarchy is likely to be the inverted hierarchy.

- If the branching ratio to bottom–muon is found to be highly dominant, then neutrino masses are likely to be in the normal hierarchy. If this branching ratio is only slightly dominant, the hierarchy cannot be determined from from this measurement alone, because it is compatible with both normal and inverted hierarchy. However, if the hierarchy were determined to be inverted from some other experiment, this measurement would favor the central value of $\sin^2\theta_{23} \sim 0.446$ over $\sin^2\theta_{23} \sim 0.587$.

---

[4] Note that the limited capability of the LHC detectors to precisely measure such branching ratios may also smear out this picture.

- The case where the branching ratio to bottom–tau is highly dominant, the normal hierarchy is favored. If it is only slightly dominant, neither hierarchy is favored, but the central value of $\sin^2\theta_{23} = 0.587$ would be slightly favored over $\sin^2\theta_{23} = 0.446$ if the hierarchy were determined to be inverted from some other experiment.

- A really lucky scenario would land the observer in the electron dominated quadrangle at the top of the blue points or the bottom of the green points. From this, one would be able to argue that the central value of $\sin^2\theta_{23}$ is closer to 0.587 for the former scenario and 0.446 for the latter in addition to an inverted hierarchy.

- Nature placing us in the white spaces would strongly suggest that this model is not the correct interpretation of the data. One caveat to this is the transition range between an admixture stop LSP and a purely right-handed stop LSP. This might allow some points in the upper white regions but, we found them to be rare in our scan.

The above conclusions are interesting because they relate decays that could be observable at the LHC to the neutrino mass hierarchy, which is currently at the forefront of neutrino physics with many experiments planned to investigate this issue [128]. Furthermore the hierarchy has important consequences for experiments seeking to measure neutrinoless double beta decay[5], which is more prominent in the inverted hierarchy. Measurement of stop LSP decays could allow a prediction of what hierarchy should be found by such experiments. Conversely, if neutrino experiments are able to determine the neutrino mass hierarchy, this could be used to further constrain the types of decays predicted for the LHC.

Much past the $\theta_t = 80^\circ$ mark, as seen in Figs. 4.1 and 4.2, the lightest stop is dominantly right-handed and the connection to neutrino physics is lost. This is because the branching ratios into the lighter generations of leptons are suppressed, and because the neutrino generation cannot, of course, be measured at the LHC. Still, in this case, there is an interesting connection between the two decay channels and $\tan\beta$ as can be seen from Eq. (4.30). From this, one would expect the bottom–tau channel to dominate at large $\tan\beta$ while the top neutrino channel dominates for low $\tan\beta$. Utilizing the same scan as in Table 4.1 but with $\theta_{\tilde{t}} = 90^\circ$ produces Fig. 4.5, which displays Br$(\tilde{t}_1 \to t\nu)/$Br$(\tilde{t}_1 \to b\tau^+)$ versus $\tan\beta$. The results confirm the relationship between the branching ratios and $\tan\beta$.

---

[5] A positive measurement of neutrinoless double beta decay is a clear measurement of lepton number violation and the Majorana nature of neutrinos.

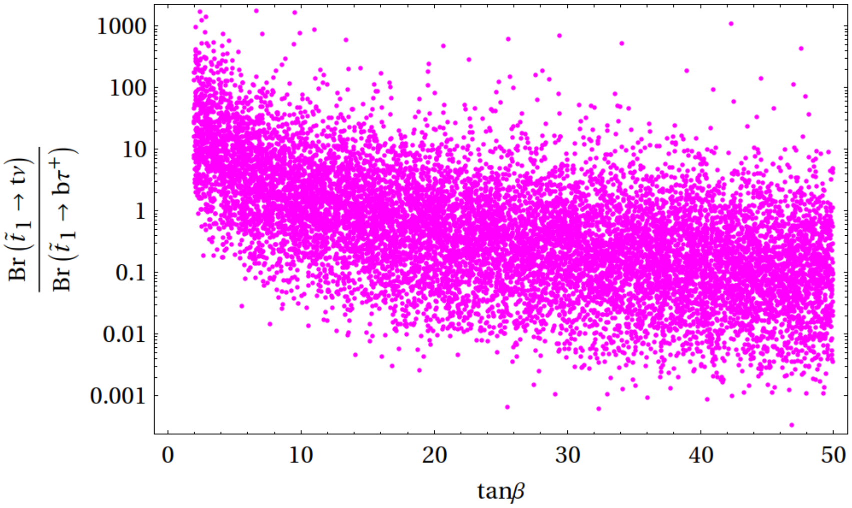

Figure 4.5: The ratio of the branching ratio of right-handed stops into top–neutrino to the branching ratio of right-handed stops to bottom–tau versus $\tan\beta$. Branching ratios to the lighter charged leptons are suppressed by their masses and therefore negligible in this case. The plot shows a dependence on $\tan\beta$ with small (large) $\tan\beta$ values corresponding to dominant top neutrino (bottom–tau) branching ratio.

4.4.2 Stop LSP Lower Bounds

LHC searches that place limits on one of the final states discussed previously can be reinterpreted to place lower bounds on the stop mass. Naively, bounds on the stop mass can be placed based on the number of expected events, for a given mass, as compared to the number of observed events. Of course, realistically, one must also take the background for the process into account as well various detector level details. Putting these aside for the moment, the number of expected events depends only on the mass of the stop, its branching ratios and the center of mass energy. Squarks are always pair produced in this model and, in the admixture case, result in the final state $b\bar{b}\ell_i^-\ell_j^+$. The number of such events is given by

$$L \times (2-\delta_{ij}) \times \sigma_{pp\to\tilde{t}_1\bar{\tilde{t}}_1} \times \mathrm{Br}(\tilde{t}_1 \to b\ell_i^+) \times \mathrm{Br}(\tilde{t}_1 \to b\ell_j^+), \tag{4.33}$$

where L is the luminosity (the most recent LHC run has 20^{-1} fb of luminosity) and $\sigma_{pp\to\tilde{t}_1\bar{\tilde{t}}_1}$ is the hadron level cross section, which results from summing partonic contributions. These partonic contributions are a product of the parton level cross section and the appropriate parton distribution function (PDF) integrated over the parton's momentum fraction of the hadron's momentum. For LHC stop production, the leading order parton contributions come from gluon fusion and quark-quark fusion. The parton-level cross section formulas can be found in [129]. Here we plot the production cross section at next to leading order in α_S, including resummation at next-to-leading log, as calculated by the ATLAS, CMS and LPCC SUSY working group [130, 131], as a function of stop mass at both a 7 and 8 TeV LHC, in Fig. 4.6.

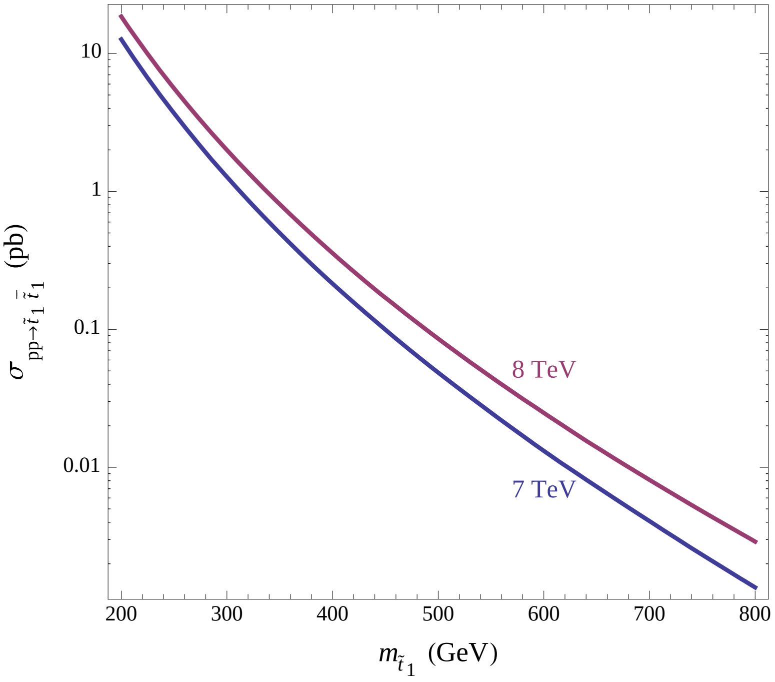

Figure 4.6: Stop pair production cross section at the 7 and 8 TeV LHC as calculated by the ATLAS, CMS and LPCC SUSY working group.

Leptoquarks exists in various extensions of the standard model, such as unification and partial unification models, and have been searched for in this context [132]. Since stop LSP's in our scenario decay like leptoquarks, one can set bounds on them based on previous leptoquark searches. However, many analyses have not yet been updated to include 8 TeV data [133, 134, 135, 136, 137, 138][6].

---

[6] For interpretation of these results for stop decays in explicit trilinear R-parity violation see [94].

Searches in the top–neutrino channel, which has the same signal as a stop decaying into a top and a massless neutralino in the R-parity conserving MSSM with a neutralino LSP, has been updated to include the full 8 TeV dataset with preliminary results [139, 140, 141], as has the jet–muon leptoquark search at CMS [142].

The current ATLAS and CMS leptoquark analyses search for final states with opposite signed, same flavor leptons. This yields upper limits on the $\tilde{t}_1$-$\bar{\tilde{t}}_1$ production cross section for each of the three possible flavors. The cross section upper limits from the ATLAS and CMS searches are used directly; no additional detector simulation is performed. The upper limit on the cross section is easily translated into a lower bound on the stop LSP mass, since the cross section depends only on the mass and center of mass energy and falls off steeply as the mass increases.

Although the ATLAS and CMS analyses assume branching ratios of unity to a given family, we can generalize their results to arbitrary branching ratios. This is accomplished by rescaling the expected cross section limit[7] from each search by dividing it by the appropriate branching ratio squared. It is then compared to the calculated production cross section as a function of stop LSP mass, which yields the lower bound on the stop LSP mass from that search. For a given choice of branching ratios, the search with the strongest expected mass bound is selected. Then the observed cross section limit from that search is rescaled in the same way and, finally, compared to the calculated production cross section as a function of stop LSP mass. This yields the lower bound on the stop LSP mass. No combination of the ATLAS or CMS results is attempted. No special treatment of signal contamination in control regions is taken into account here.

For the admixture stop LSP, the three relevant channels are the bottom–charged lepton channels. It should be noted that the exclusion results presented here have been improved upon by a more recent study from ATLAS [106] using private data and more sophisticated analysis methods such as combination of different decay channels and b-tagging. The exclusion results can be plotted on a two-dimensional plot since the sum of all three branching ratios is unity. This is done in the form of lines of constant stop mass lower bound in Fig. 4.7 in the Br$(\tilde{t}_1 \to b\tau^+)$ - Br$(\tilde{t}_1 \to be^+)$ plane, the same plane as in Fig. 4.3. The absolute lowest bound, 424 GeV, occurs at Br$(\tilde{t}_1 \to be^+) = 0.23$, Br$(\tilde{t}_1 \to b\mu^+) = 0.15$, Br$(\tilde{t}_1 \to b\tau^+) = 0.62$. It is marked by a dot. The bounds are stronger in the three corners of the plot where one of the branching ratios is unity. The strongest of

---

[7] For a small number of searches, the expected upper limit is not publicly available. As these searches do not observe an excess, the observed limit is used as an approximation of the expected limit.

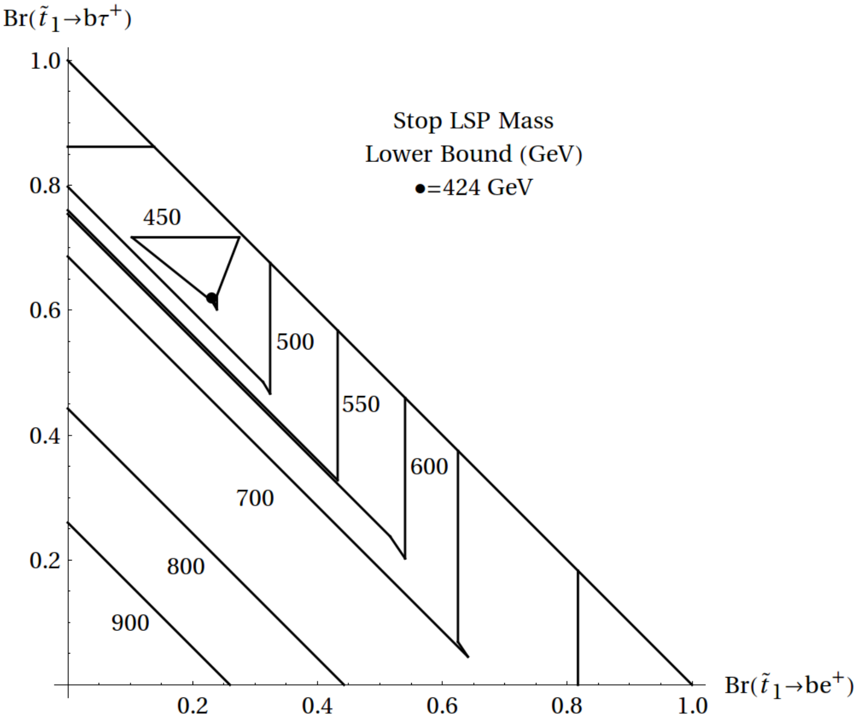

Figure 4.7: Lines of constant stop lower bound in GeV in the Br($\tilde{t}_1 \to b\,\tau^+$) - Br($\tilde{t}_1 \to b\,e^+$) plane for an admixture stop LSP. The strongest bounds arise when the bottom–muon branching ratio is largest, while the weakest arise when the bottom–tau branching ratio is largest.

these three bounds corresponds to decays purely to bottom–muon. This reflects the fact that this is the easiest of the three channels to detect and the search has been performed with the most data (20 fb^{-1}) and at the highest energy (8 TeV). The weakest of these bounds corresponds to decays purely to bottom–tau because this channel is the hardest to detect. The contours are each composed of several connected straight line segments. The straightness of the segments is due to the fact that the bound is always coming from a single channel (the one with the strongest expected bound) and so only depends on one of the three significant branching ratios. Cross referencing Fig. 4.7 with Fig. 4.4 shows that the lowest stop mass bounds overlap the part of the normal hierarchy with a large branching ratio to bottom-tau and an inverted hierarchy with a large θ_{23} and a large branching ratio to bottom-tau.

For the right-handed stop, the production cross section limit is determined

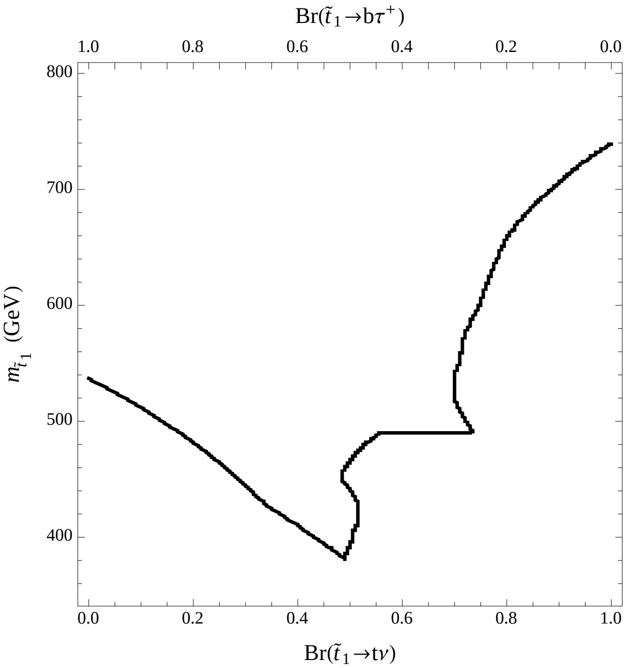

Figure 4.8: The lower mass bound on a mostly right-handed stop–which decays predominantly into a bottom-charged lepton and a top-neutrino. It is plotted as a function of the branching ratio into top neutrino (bottom axis) and bottom–tau (top axis). The lowest allowed mass is at about 380 GeV for Br $\left(\tilde{t}_1 \to t\nu\right) \approx 0.5$.

only by the stop mass and one of its branching ratios. In Fig. 4.8 the stop mass lower bound is plotted versus the branching ratio, with bottom–tau branching ratio on the top axis and top neutrino branching ratio on the bottom axis. Values below the plotted line are ruled out–with the exception of two pockets of allowed masses where the blue line is double valued; for example, between $0.70 \lesssim \mathrm{Br}(\tilde{t}_1 \to t\nu) \lesssim 0.75$. The lowest allowed mass is at about 380 GeV for Br $\left(\tilde{t}_1 \to t\nu\right) \approx 0.5$. There is also a small allowed window, around 30 GeV wide, for the stop to have a mass similar to the top, when the branching ratio to top–neutrino dominates. This is not displayed in Fig. 4.8.

4.4.3 Sbottom LSP

In this Section, an analysis similar to that of the stop is conducted for a sbottom LSP; namely investigating its branching ratios and mass lower bound. Because many of the key points parallel the stop analysis, the discussion of both the sbottom decays and lower bound are combined here into a single short subsection.

The allowed decay channels for a sbottom LSP were given in Eq. (4.25). The associated partial widths are found to be

$$\Gamma(\tilde{b}_1 \to b\,\nu_i) = \frac{1}{16\pi}(|G^L_{\tilde{b}_1 b \chi^0_{6+i}}|^2 + |G^R_{\tilde{b}_1 b \chi^0_{6+i}}|^2) m_{\tilde{b}_1} \tag{4.34}$$

$$\begin{aligned} \Gamma(\tilde{b}_1 \to t\,\ell^-_i) &= \frac{1}{16\pi}(|G^L_{\tilde{b}_1 t \chi^\pm_{2+i}}|^2 + |G^R_{\tilde{b}_1 t \chi^\pm_{2+i}}|^2) m_{\tilde{b}_1} \\ &\quad \times \left(1 - \frac{m_t^2}{m^2_{\tilde{b}_1}}\right)\sqrt{1 - 2\frac{m_t^2}{m^2_{\tilde{b}_1}} + \frac{m_t^4}{m^4_{\tilde{b}_1}}}, \end{aligned} \tag{4.35}$$

where the G parameters are given in Appendix 6.7, $\chi^0_{6+i} = \nu_i$ and $\chi^\pm_{2+i} = \ell_i$. Both the left- and right-handed sbottom couple directly to $\tilde{H}_d$, which leads to the largest RPV widths. However, one can still separate the phenomenology based on the composition of the LSP sbottom. Unlike the stop LSP, a sbottom LSP can have any left–right composition while remaining the LSP. That is, the sbottom mixing angle can span the entire range $\theta_b = 0^\circ - 90^\circ$. Also, unlike the stop, the sbottom is expected to be mostly left– or right–handed (that is, $\theta_b \approx 0^\circ$ or $\theta_b \approx 90^\circ$) because the off-diagonal element of the sbottom mass mass matrix is suppressed by the mass of the bottom quark (this can be seen from Eq. 6.138). An exception to this is when the soft masses for the third generation squark doublet, m_{Q_3}, and the right-handed sbottom, m_{b^c}, are very close (order 100 GeV for TeV scale masses and a small soft trilinear term, a_b, see Eq. (6.138)). Regardless, in the interest of being completely general, all values of the sbottom mixing angle will be considered.

The leading order amplitudes squared for the admixture sbottom LSP, as well as the purely right-handed sbottom LSP, are approximately

$$|\mathcal{A}(\tilde{b}_1 \to b\nu_i)|^2 \sim Y_b^2 \left| V_{\text{PMNS}\,ji}\frac{\epsilon_j}{\mu}\right|^2 \tag{4.36}$$

$$|\mathcal{A}(\tilde{b}_1 \to t\ell^-_i)|^2 \sim s_b^2 Y_b^2 \left|\frac{\epsilon_i}{\mu}\right|^2, \tag{4.37}$$

where s_b is $\sin\theta_b$ and there is an implicit sum over j. Note that $\theta_b = 0^\circ$ ($\theta_b = 90^\circ$) corresponds to a left-handed (right-handed) lightest sbottom. The term in Eq. (4.36) is independent of mixing angle since there is a contribution from both the left- and right-handed sbottoms of relatively the same size. At this order, the mostly left-handed sbottom LSP ($\theta_b \approx 0^\circ$) amplitude to top–charged lepton is suppressed and one must go to the next order term

$$|\mathcal{A}(\tilde{b}_1 \to t\ell_i^-)|^2\Big|_{\theta_b \sim 0^\circ} \sim Y_t^2 \left|\frac{m_{\ell_i}\, v_{Li}}{\mu\, v_d}\right|^2 . \qquad (4.38)$$

From this one can conclude:

- Admixture and purely right-handed sbottom LSP: here the branching ratios to bottom–neutrino and top–charged lepton should be of the same order of magnitude. Generically, the bottom–neutrino should be somewhat larger. However, in the purely right-handed sbottom case the two branching ratios will be fairly similar.
- Mostly left-handed sbottom LSP: in this case, the top–charged lepton channel is suppressed by both v_{Li} and the charged lepton masses. However the decay to bottom–neutrino is not suppressed and, hence, will dominate this case.

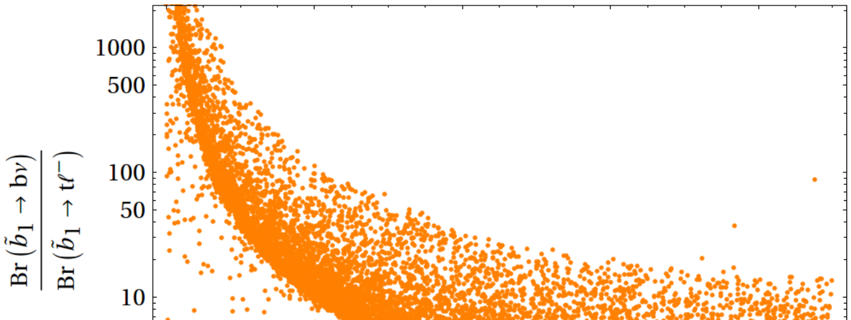

Figure 4.9: The ratio of the branching ratio of sbottom to bottom–neutrino to the branching ratio of sbottom to top–charged lepton versus the left-right mixing angle in the sbottom sector. A 0° (90°) angle corresponds to a left-handed (right-handed) sbottom. Typically, one expects to be at one of the extremes of this plot as sbottom mixing is suppressed by the bottom mass.

The approximate analytic results are verified by the numerical results. These are calculated implementing the same scanning ranges as in Table 4.1, but with θ_t replaced by θ_b and $m_{\tilde{t}_1}$ replaced by $m_{\tilde{b}_1}$. The ratio Br$(\tilde{b}_1 \to b\nu)/$Br$(\tilde{b}_1 \to t\ell^-)$, where Br$(\tilde{b}_1 \to t\ell^-) \equiv \sum_{i=1}^{3}$ Br$(\tilde{b}_1 \to t\ell_i^-)$, versus the sbottom mixing angle is displayed in Fig. 4.9. The results closely match the approximate analytic conclusions. Sbottom lifetimes are relatively independent of the sbottom mixing angle and are typically far below the displaced vertex threshold of 1 millimeter, similar to the left-hand side of Fig. 4.1.

We now want to produce an analogue of Fig. 4.4. That figure was possible due to the suppressed top–neutrino channel. To produce such a figure here, where the bottom–neutrino channel is significant or even dominant, we define a new variable, the lepton branching ratio (LBr), given by

$$\text{LBr}(\tilde{b}_1 \to t\ell_i^-) \equiv \frac{\Gamma(\tilde{b}_1 \to t\ell_i^-)}{\sum\limits_{i=1}^{3} \Gamma(\tilde{b}_1 \to t\ell_i^-)} \,. \tag{4.39}$$

This can be understood as the width of the sbottom into a single lepton generation normalized by the total width to all charged lepton generations. Note that, by definition, the three lepton branching ratios sum to unity. This allows a plot similar to Fig. 4.4 to be produced, so that one can compare the results. The sbottom situation, however, is more difficult experimentally than for the stop LSP. This is because the bottom–neutrino branching ratio can overwhelm the top–charged lepton branching ratios to the point where they are too small to be measured at the LHC. This will be the case for the mostly left-handed sbottom, as can be seen from Fig. 4.9. Furthermore, here one must measure three of the four branching ratios and infer the fourth, while in the case of the admixture stop one need only measure two branching ratios to infer the third.

We display the lepton branching ratios in the LBr$(\tilde{b}_1 \to t\tau)$-LBr$(\tilde{b}_1 \to te)$ plane in Fig. 4.10, in analogy to Fig. 4.4. The two figures have the same features and, therefore, one can make the same conclusions as in the stop case once three of the branching ratios are measured. We will comment on this connection in the next section. In Fig. 4.10 we include only points for which Br$(\tilde{b}_1 \to b\nu) < 0.99$. This excludes points where the bottom–neutrino branching ratio dwarfs the top–charged lepton branching ratio, thus making the latter unobservable. It follows from Fig. 4.9 that the plot excludes mostly left-handed sbottom LSP's. In analogy with the stop LSP case, it is preferable to base our exclusion criteria on the bottom–neutrino branching ratio instead of the mixing angle, since the former is easier to observe. Points that do not satisfy the fine-tuning criteria, Eqs. (6.117) and (6.118), are excluded from Fig. 4.10.

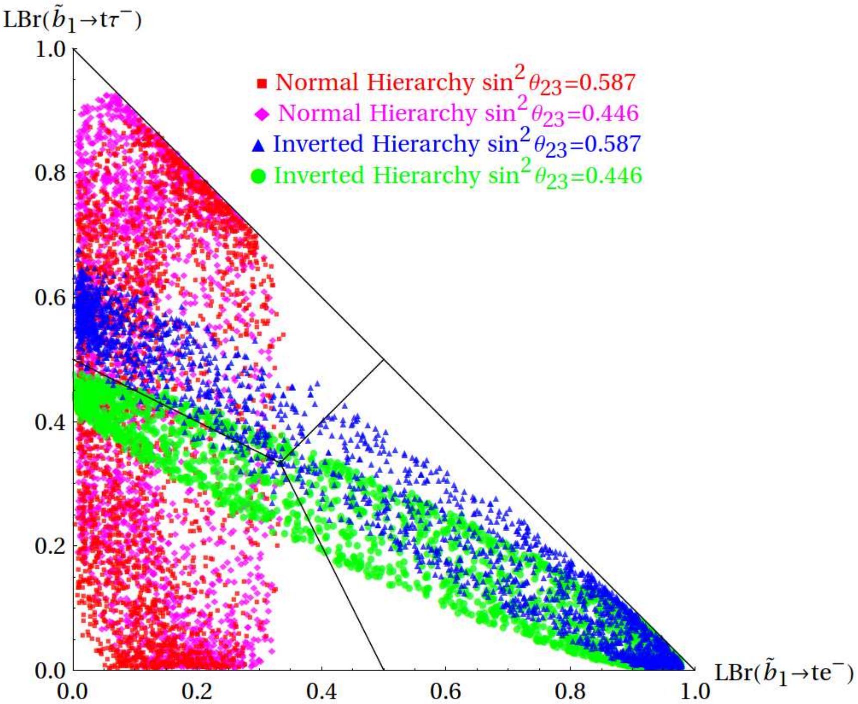

Figure 4.10: Results of a scan over the parameters described in Table 4.1, with θ_t replaced by θ_b and $m_{\tilde{t}_1}$ replaced by $m_{\tilde{b}_1}$, are displayed in the LBr($\tilde{b}_1 \to t\tau$)-LBr($\tilde{b}_1 \to te$) plane where LBr is defined in Eq. (4.39). The details and findings of this plot are very similar to those of Fig. 4.4.

In analogy to searches for the R-parity conserving decays of a stop into a top and a neutralino, searches have been conducted for the R-parity conserving decays of a sbottom into a bottom and a neutralino at both ATLAS [143] and CMS [144] with the full 2012 data set. For massless neutralinos, these searches can be directly reinterpreted to place lower bounds on the sbottom decay to bottom-neutrino in our model, as we did for the stops in Sec. 4.4.2. These bounds are displayed in Fig. 4.11 versus Br $\left(\tilde{b}_1 \to b\nu\right)$, which ranges in our model from 0.5 (when the sbottom is mostly right-handed) to 1 (where the sbottom is mostly left-handed), as can be seen from Fig. 4.9. Values below the plotted line are ruled out. The stop pair production cross sections from Fig. 4.6 are used for the sbottom pair production as well. This is possible since both the stop and sbottom pair production cross sections are dominantly through color interactions, and both stop and sbottom have the same color quantum number.

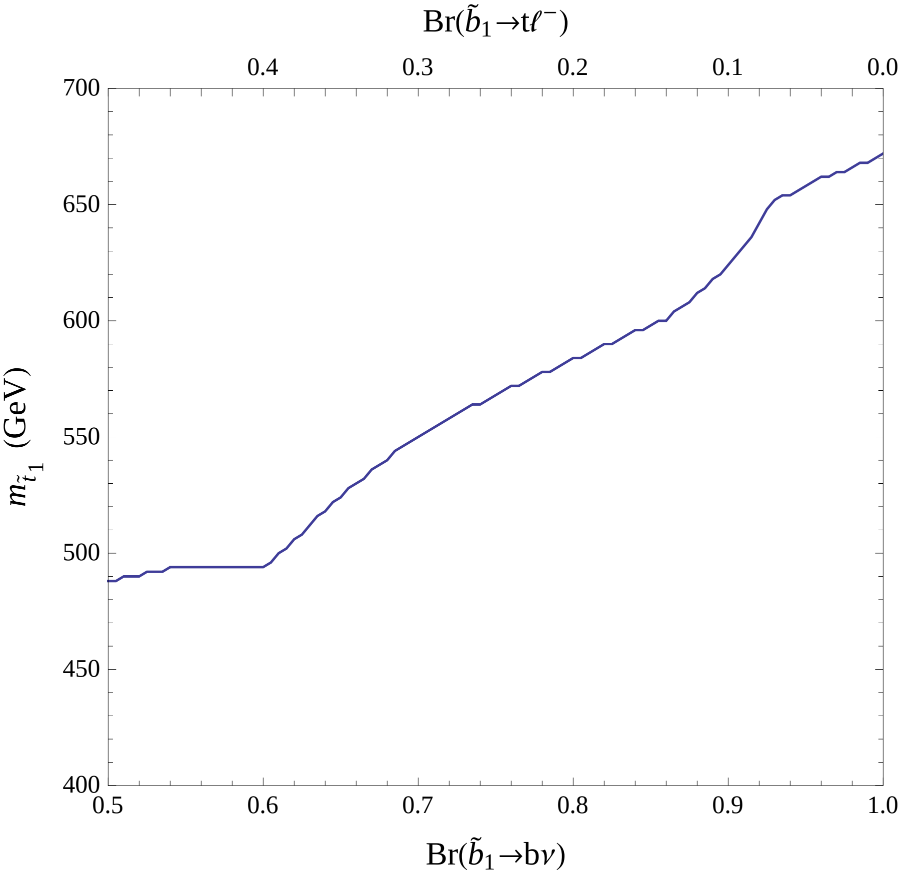

Figure 4.11: Lower bound on the sbottom mass versus $\mathrm{Br}\left(\tilde{b}_1 \to b\nu\right)$ on the bottom axis and $\mathrm{Br}\left(\tilde{b}_1 \to t\ell^-\right)$ on the top axis. This bound is derived from LHC searches for the RPC decays of a sbottom to a bottom and a neutralino, reinterpreted to be our bottom-neutrino decays.

4.5 Discussion

One of the interesting results in this thesis is the connection between the LSP decays and the neutrino hierarchy. As was shown in Figs. 4.4 and 4.10, this connection is very similar in the stop and sbottom LSP scenarios. This relationship, and the similarity, are fairly straightforward to explain and can be understood by examining the relationships in Appendix 6.4 and recalling some of the analytical conclusions of the last sections. The latter of these is that the ϵ_i parameters are the dominant source of RPV and, therefore, when the decay into charged leptons is large, the amplitude to $\ell_i^{\pm}$ is proportional to ϵ_i/μ, see Eqs. (4.28) and (4.37). This yields the following approximate branching ratios and lepton branching ratios:

$$\text{Br}(\tilde{t}_1 \to b\ell_i^+) \sim \frac{|\epsilon_i|^2}{\sum\limits_{j=1}^{3} |\epsilon_j|^2} \tag{4.40}$$

$$\text{LBr}(\tilde{b}_1 \to t\ell_i^-) \sim \frac{|\epsilon_i|^2}{\sum\limits_{j=1}^{3} |\epsilon_j|^2}. \tag{4.41}$$

The similarity between these two equations already explains why Figs. 4.4 and 4.10 are similar.

The connection between the neutrino parameters and the relative sizes of ϵ_i can be qualitatively understood without appeal to random scans. Appendix 6.4 relates the ϵ_i parameters to linear combinations of E_l parameters weighted by the elements of the PMNS matrix,

$$\epsilon_i = V^*_{\text{PMNS}\,il} E_l. \tag{4.42}$$

Two of the E_l parameters can be solved for based on the neutrino masses and mixings, but their actual values are not so important here. Let us first consider the case of a stop LSP. In the NH, $E_1 = 0$. Varying the relative size of E_2 and E_3 and calculating the branching ratios according to Eq. (4.40) traces out ellipses in the $\text{Br}(\tilde{t}_1 \to b\tau^+)$ - $\text{Br}(\tilde{t}_1 \to be^+)$ plane. This can be done for both values of θ_{23}. In the IH, $E_3 = 0$. Varying the relative size of E_1 and E_2 and calculating the branching ratios according to Eq. (4.40) again traces out ellipses in the $\text{Br}(\tilde{t}_1 \to b\tau^+)$ - $\text{Br}(\tilde{t}_1 \to be^+)$ plane. This can be done for both values of θ_{23}. The results, using central values for the neutrino parameters and no CP violation in the neutrino sector, are shown in Fig. 4.12 superimposed over the numerical results in Fig. 4.3.

In the case of a sbottom LSP, we find, now calculating the branching ratios using Eq. (4.41), similar results with identical conclusions.

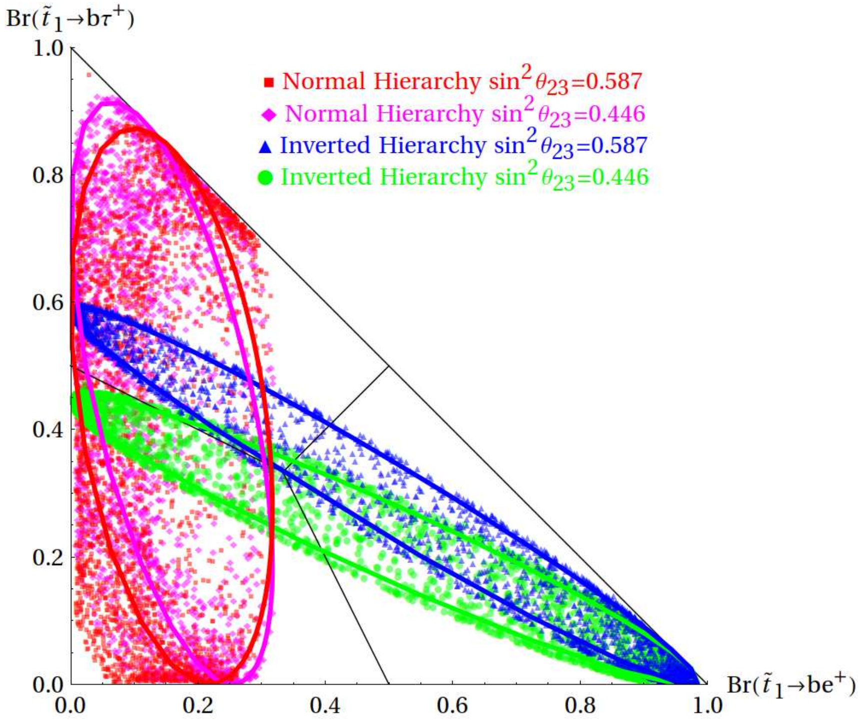

Figure 4.12: Analytic results for the branching ratios using Eqs. (4.40) and (4.42) superimposed on the results from Fig. 4.3.

Varying the CP violating phases in the neutrino sector will move the ellipses in such a way that they fill out the same regions that were filled by the scan, thereby demonstrating the agreement between the analytic approximation and the numerical results. The same analysis would also apply to the v_{Li} parameters in cases where they dominate the decays (an example of which will be discussed shortly). The crucial features of this theory that lead to these predictions are that the R-parity violation is controlled by the flavorful parameters ϵ_i and v_{Li}, which also give rise to neutrino masses and mixing, and that one of the neutrinos is massless.

This analytical understanding is quite powerful since it indicates that the results displayed in Fig. 4.4, the bullet points associated with this figure and Fig. 4.10 are fairly independent of many of the assumptions that have been made in this thesis–which could, therefore, be relaxed or altered. These assumptions are briefly summarized here.

- GUT gaugino relations: The $SO(10)$ GUT relationships for the gaugino masses has been assumed: $M_R : M_{BL} : M_2 : M_3 \sim 1 : 1 : 2 : 5$. However, according to the analytical analysis conducted here, this would have very little impact on the relationship between the neutrino hierarchy and the branching ratios. Therefore, a bottom-up approach that does not assume this relationship would yield similar results.
- Squark LSP's: Third generation squark LSP's were studied here. However, the same connection between the neutrino hierarchy and the LSP branching ratios would hold true for the first two generations as well. One difference is that the first two generations do not couple to the Higgs fields very strongly. Therefore, their dominant decay channels will be due to gauginos mixing with the neutrinos and charged leptons. This also means their lifetimes will be, on average, longer and there might be more points in parameter space with displaced vertices. Another difference is that left-right mixing angles in these generations are expected to be negligible, suppressed by the corresponding fermion mass. Therefore, one will only have the purely right- or left-handed LSP's.
- The parameter scan, Table 4.1: While we only scanned a finite parameter space, the analytical arguments given in this section indicate that extending the parameter space of the scan will result in similar behavior.

Chapter 5

Conclusion

The most minimal $B - L$ extension of the MSSM must always spontaneously break R-parity and, in addition, predicts the existence of a TeV scale neutral gauge boson, Z_R, two light sterile neutrinos and a Majorana contribution to neutrino masses coming from R-parity violation. Such a model is well-motivated by string theory.

In this paper, we presented a novel approach for relating UV physics to TeV scale physics and applied this analysis to the minimal SUSY $B - L$ model. This approach hypothesizes that all SUSY breaking parameters are about an order of magnitude away from a characteristic SUSY breaking mass scale. Practically, this translates into conducting an analysis where all relevant soft SUSY mass parameters are independently scanned over the same range at the UV scale, and then RG evolved to the TeV scale. This program lends itself especially well to the string realization of the minimal $B - L$ MSSM model. However, our results are relevant for any high scale soft SUSY breaking minimal SUSY $B - L$ model with gauge coupling unification.

A central result of this work is the general region of initial parameter space that leads to radiative $B - L$ symmetry breaking. While this depends on multiple parameters of the theory, it can be expressed in terms of the two S-parameters and is presented in this context in Fig. 3.4. A subsequent figure, Fig 3.6, shows how additional constraints, such as electroweak symmetry breaking and lower bounds on new sparticle masses, depend on the S-parameters. These two plots indicate that a significant amount of the initial parameter space leads to experimentally viable results. They are followed by various spectrum graphs which show that acceptable spectra are relatively general and do not depend on a specific hierarchy of initial masses.

The phenomenology of a given point at the LHC strongly depends on the identity of the LSP. Therefore, another central result of this paper is the calculation of the probability that a given SUSY particle can be the LSP. This was addressed in Fig. 3.7. As might be expected, a mostly bino neutralino is the most likely candidate. However, since binos cannot be directly produced at the LHC, signals associated with bino LSPs also depend on the rest of the SUSY spectrum. Therefore, an interesting future direction might be to investigate the phenomenology of mostly wino or Higgsino neutralinos. Mostly wino or Higgsino neutralinos can be directly produced at the LHC, independently of the rest of the SUSY spectrum, and have relatively large cross sections for colorless particles. The signals associated with different LSPs are summarized in Table 3.4.

The fine-tuning associated with this statistical scan was investigated. While it is not drastically different from the fine-tuning in the MSSM with a similar UV completion, one might think that the new mass scale associated with $B - L$ breaking could introduce new contributions to fine-tuning. We showed that it does not. In fact, a given point in this model is typically less fine-tuned than a similar point in the MSSM. In addition, we explored possible LSPs for points with fine-tuning better than one part per thousand–in a way analogous to Fig. 3.7. We found that stops and sbottoms become much more likely LSP candidates, as one might expect–see Fig. 3.17.

Finally, this thesis examined the phenomenology of third generation squark LSP's within the context of this model. Because of R-parity violation, these LSP's can now decay. Due to the connection between R-parity violation and neutrino masses, one can potentially make statements about the neutrino mass hierarchy based on the LSP branching ratios. The relevant results for the stop and sbottom LSP's are shown in Fig. 4.4 and Fig. 4.10 respectively. If these quantities are measured at the LHC, their location on the plots potentially can extract information about the neutrino hierarchy.

Chapter 6

Appendices

6.1 Renormalization Group Equations

This Appendix lists the RGEs used in this study. Most RGEs are derived with the help of reference [51], unless otherwise stated.

The RGEs for gauge couplings were presented in Section 2.3, but are repeated here for completeness. The RGE for a general gauge coupling is

$$\frac{d}{dt}\alpha_a^{-1} = -\frac{b_a}{2\pi}. \tag{6.1}$$

where t is the logarithm of the renormalization scale and the index a runs over the different gauge factors. The slope factors are different in each of the different scaling regimes:

- Intermediate regime: $b_3 = 10,\ b_2 = 14,\ b_R = 14,\ b_{B-L} = 19.$
- $B-L$ MSSM: $b_3 = -3,\ b_2 = 1,\ b_{3R} = 7,\ b_{B-L} = 6.$
- MSSM: $b_3 = -3,\ b_2 = 1,\ b_1 = \frac{33}{5}.$
- Non-SUSY $B-L$: $b_3 = -7,\ b_2 = -\frac{19}{6},\ b_{3R} = \frac{53}{12},\ b_{B-L} = \frac{33}{8}.$
- SM: $b_3 = -7,\ b_2 = -\frac{19}{6},\ b_1 = \frac{41}{10}$

The gaugino soft mass RGE is

$$\frac{d}{dt}M_a = \frac{b_a\alpha_a M_a}{2\pi}, \tag{6.2}$$

where the b_a are the same slope factors given in Eqs. (2.20 - 2.23). It is helpful to observe that the gaugino mass renormalization group equation admits a rather compact analytic solution:

$$M_a(t) = \frac{M_a(M_{\rm U})}{\alpha_{\rm U}}\alpha_a(t), \tag{6.3}$$

for all gaugino masses associated with $SO(10)$ and

$$M_1(t) = \frac{M_1(M_{B-L})}{\alpha_1(M_{B-L})}\alpha_1(t), \tag{6.4}$$

for the bino.

There are three significant Yukawa couplings for RGE analysis: y_t, y_b and y_τ. In the SM scaling regime their RGEs can be found in [145], for example, and are given by

$$\begin{aligned}
\frac{d}{dt}y_t &= \frac{1}{16\pi^2}y_t\left(\frac{3}{2}(y_t^2 - y_b^2) + 3(y_t^2 + y_b^2) + y_\tau^2 - 8g_3^2 - \frac{9}{4}g_2^2 - \frac{17}{20}g_1^2\right) && (6.5)\\
\frac{d}{dt}y_b &= \frac{1}{16\pi^2}y_b\left(\frac{3}{2}(y_b^2 - y_t^2) + 3(y_t^2 + y_b^2) + y_\tau^2 - 8g_3^2 - \frac{9}{4}g_2^2 - \frac{1}{4}g_1^2\right) && (6.6)\\
\frac{d}{dt}y_\tau &= \frac{1}{16\pi^2}y_\tau\left(\frac{3}{2}y_\tau^2 + 3(y_t^2 + y_b^2) + y_\tau^2 - \frac{9}{4}g_2^2 - \frac{9}{4}g_1^2\right). && (6.7)
\end{aligned}$$

In the $U(1)$ extended SM regime of the upside-down case, the Yukawa coupling RGEs are

$$\begin{aligned}
\frac{d}{dt}y_t &= \frac{1}{16\pi^2}y_t\left(\frac{3}{2}(y_t^2 - y_b^2) + 3(y_t^2 + y_b^2) + y_\tau^2\right.\\
&\qquad \left. -8g_3^2 - \frac{9}{4}g_2^2 - \frac{3}{4}g_R^2 - \frac{1}{4}g_{BL}^2\right) && (6.8)\\
\frac{d}{dt}y_b &= \frac{1}{16\pi^2}y_b\left(\frac{3}{2}(y_b^2 - y_t^2) + 3(y_t^2 + y_b^2) + y_\tau^2\right.\\
&\qquad \left. -8g_3^2 - \frac{9}{4}g_2^2 - \frac{3}{4}g_R^2 - \frac{1}{4}g_{BL}^2\right) && (6.9)\\
\frac{d}{dt}y_\tau &= \frac{1}{16\pi^2}y_\tau\left(\frac{3}{2}y_\tau^2 + 3(y_t^2 + y_b^2) + y_\tau^2\right.\\
&\qquad \left. -\frac{9}{4}g_2^2 - \frac{3}{4}g_R^2 - \frac{9}{4}g_{BL}^2\right). && (6.10)
\end{aligned}$$

The boundary condition at the $B-L$ scale is trivial. At the SUSY scale, however, the boundary condition is nontrivial:

$$\begin{aligned} y_t(M_{\text{SUSY}}) &= Y_t(M_{\text{SUSY}})\sin\beta \\ y_{b,\tau}(M_{\text{SUSY}}) &= Y_{b,\tau}(M_{\text{SUSY}})\cos\beta. \end{aligned} \tag{6.11}$$

The Yukawa couplings above the SUSY scale will be denoted by Y instead of y. This condition applies both in the upside-down case and in the right-side-up case. In the MSSM scaling regime of the right-side-up case the RGEs are

$$\frac{d}{dt}Y_t = \frac{1}{16\pi^2}Y_t\left(6Y_t^2+Y_b^2-\frac{16}{3}g_3^2-3g_2^2-\frac{16}{15}g_1^2\right) \tag{6.12}$$

$$\frac{d}{dt}Y_b = \frac{1}{16\pi^2}Y_b\left(6Y_b^2+Y_\tau^2+Y_t^2-\frac{16}{3}g_3^2-3g_2^2-\frac{4}{15}g_1^2\right) \tag{6.13}$$

$$\frac{d}{dt}Y_\tau = \frac{1}{16\pi^2}Y_\tau\left(3Y_b^2+4Y_\tau^2-3g_2^2-\frac{12}{5}g_1^2\right).$$

In the $B-L$ MSSM scaling regime the RGEs are

$$\frac{d}{dt}Y_t = \frac{1}{16\pi^2}Y_t\left(6Y_t^2+Y_b^2-\frac{16}{3}g_3^2-3g_2^2-\frac{1}{6}g_{BL}^2-g_R^2\right) \tag{6.14}$$

$$\frac{d}{dt}Y_b = \frac{1}{16\pi^2}Y_b\left(6Y_b^2+Y_\tau^2+Y_t^2-\frac{16}{3}g_3^2-3g_2^2-\frac{1}{6}g_{BL}^2-g_R^2\right) \tag{6.15}$$

$$\frac{d}{dt}Y_\tau = \frac{1}{16\pi^2}Y_\tau\left(3Y_b^2+4Y_\tau^2-3g_2^2-\frac{3}{2}g_{BL}^2-g_R^2\right). \tag{6.16}$$

The fact that these RGEs are non-linear means that the analytic solutions are much more cumbersome if they can be found at all. We use numerical integration techniques instead, yielding numerical values for the Yukawa couplings at any scale up to the intermediate scale, M_{I}. These solutions will be subsequently used in the running of the soft tri-scalar couplings and some of the scalar soft masses because the RGEs of those parameters depend on the Yukawa couplings. The Yukawa couplings do not need to be evolved above the intermediate scale since the couplings that depend on them will not be evolved above the intermediate scale.

Tri-linear couplings are generated at the intermediate scale and evolved to the

SUSY scale. Their RGEs in the $B-L$ MSSM scaling regime are

$$\begin{aligned}\frac{d}{dt}a_t &= \frac{1}{16\pi^2}a_t\left(8^2+Y_b^2-\frac{16}{3}g_3^2-3g_2^2-\frac{1}{6}g_{BL}^2-g_R^2\right)\\ &\quad+\frac{1}{16\pi^2}Y_t\left(10a_uY_t+2Y_ba_b+\frac{32}{3}g_3^2M_3\right.\\ &\quad\left.+6g_2^2M_2+\frac{1}{3}g_{BL}^2M_{B-L}+2g_R^2M_R\right)\end{aligned}\tag{6.17}$$

$$\begin{aligned}\frac{d}{dt}a_b &= \frac{1}{16\pi^2}a_b\left(8Y_b^2+Y_\tau^2+Y_t^2-\frac{16}{3}g_3^2-3g_2^2-\frac{1}{6}g_{BL}^2-g_R^2\right)\\ &\quad+\frac{1}{16\pi^2}Y_b\left(10a_bY_b+2a_\tau Y_\tau+2Y_ta_u+\frac{32}{3}g_3^2M_3\right.\\ &\quad\left.+6g_2^2M_2+\frac{1}{3}g_{BL}^2M_{B-L}+2g_R^2M_R\right)\end{aligned}\tag{6.18}$$

$$\begin{aligned}\frac{d}{dt}a_\tau &= \frac{1}{16\pi^2}a_\tau\left(3Y_b^2+6Y_\tau^2-3g_2^2-\frac{3}{2}g_{BL}^2-g_R^2\right)\\ &\quad+\frac{1}{16\pi^2}Y_\tau\left(6a_bY_b+6a_\tau Y_\tau+6g_2^2M_2+3g_{BL}^2M_{B-L}+2g_R^2M_R\right)\end{aligned}\tag{6.19}$$

In the right-side-up case, the $B-L$ scale is above the SUSY scale so these parameters will also be run through the MSSM scaling regime from the $B-L$ scale to the SUSY scale. The RGEs in the MSSM scaling regime are

$$\begin{aligned}\frac{d}{dt}a_t &= \frac{1}{16\pi^2}a_t\left(8^2+Y_b^2-\frac{16}{3}g_3^2-3g_2^2-\frac{13}{15}g_1^2\right)\\ &\quad+\frac{1}{16\pi^2}Y_t\left(10a_uY_t+2Y_ba_b+\frac{32}{3}g_3^2M_3+6g_2^2M_2+\frac{26}{15}g_1^2M_1\right)\end{aligned} \tag{6.20}$$

$$\begin{aligned}\frac{d}{dt}a_b &= \frac{1}{16\pi^2}a_b\left(8Y_b^2+Y_\tau^2+Y_t^2-\frac{16}{3}g_3^2-3g_2^2-\frac{7}{15}g_1^2\right)\\ &\quad+\frac{1}{16\pi^2}Y_b\left(10a_bY_b+2a_\tau Y_\tau+2Y_ta_u+\frac{32}{3}g_3^2M_3\right.\\ &\quad\left.+6g_2^2M_2+\frac{14}{15}g_1^2M_1\right)\end{aligned} \tag{6.21}$$

$$\begin{aligned}\frac{d}{dt}a_\tau &= \frac{1}{16\pi^2}a_\tau\left(3Y_b^2+6Y_\tau^2-3g_2^2-\frac{9}{5}g_1^2\right)\\ &\quad+\frac{1}{16\pi^2}Y_\tau\left(6a_bY_b+6a_\tau Y_\tau+6g_2^2M_2+\frac{18}{5}g_1^2M_1\right).\end{aligned} \tag{6.22}$$

These equations are also do not yield tractable analytic solutions, of course.

Scalar soft mass squared parameters are also inputted at the intermediate scale and evolved down to the SUSY scale. In the case of the right-side-up hierarchy, this will involve running through the $B-L$ scale and the brief MSSM scaling regime. The boundary condition at the $B-L$ scale is nontrivial because D-term interactions between the third-family right-handed sneutrino and the other scalars give rise to a new contribution to the soft masses when the third-family right-handed sneutrino acquires a VEV, Eq. (2.80). As discussed in Section 3.2.2, we take the soft masses to be flavor diagonal in order to satisfy flavor constraints.

Before writing the scalar soft mass RGEs, it is useful to define the S-terms,

$$S_{B-L} = \mathrm{Tr}\,(2m_{\tilde{Q}}^2-m_{\tilde{u}^c}^2-m_{\tilde{d}^c}^2-2m_{\tilde{L}}^2+m_{\tilde{\nu}^c}^2+m_{\tilde{e}^c}^2) \tag{6.23}$$

$$S_R = m_{H_u}^2-m_{H_d}^2+\mathrm{Tr}\,\left(-\frac{3}{2}m_{\tilde{u}^c}^2+\frac{3}{2}m_{\tilde{d}^c}^2-\frac{1}{2}m_{\tilde{\nu}^c}^2+\frac{1}{2}m_{\tilde{e}^c}^2\right) \tag{6.24}$$

$$S_Y = m_{H_u}^2-m_{H_d}^2+\mathrm{Tr}\,\left(m_{\tilde{Q}}^2-2m_{\tilde{u}^c}^2+m_{\tilde{d}^c}^2+m_{\tilde{L}}^2-m_{\tilde{e}^c}^2\right), \tag{6.25}$$

where the traces are over generational indices. It can be shown, using the scalar soft mass RGEs, that the S-terms obey the RGEs:

$$\frac{d}{dt}S_a = \frac{b_a\alpha_aS_a}{2\pi}, \tag{6.26}$$

which admit the simple analytic solution

$$S_a(t) = \frac{g_a^2(t)}{g_a^2(M_{\mathrm{I}})} S_a(M_{\mathrm{I}}), \tag{6.27}$$

for S_R or S_{B-L} and

$$S_Y(t) = \frac{g_Y^2(t)}{g_Y^2(M_{\mathrm{SUSY}})} S_Y(M_{\mathrm{SUSY}}), \tag{6.28}$$

It is perhaps useful to separate the scalar mass RGEs into those that are analytically tractable and those that are not. In the $B-L$ MSSM scaling regime, the first- and second-family and sneutrino soft mass RGEs, analytically solvable, are

$$\begin{aligned}
16\pi^2 \frac{d}{dt} m_{\tilde{Q}_{1,2}}^2 &= -\frac{32}{3} g_3^2 M_3^2 - 6 g_2^2 M_2^2 - \frac{1}{3} g_{BL}^2 M_{B-L}^2 + \frac{1}{4} g_{BL}^2 S_{B-L} && (6.29) \\
16\pi^2 \frac{d}{dt} m_{\tilde{u}_{1,2}^c}^2 &= -\frac{32}{3} g_3^2 M_3^2 - \frac{1}{3} g_{BL}^2 M_{B-L}^2 - 2 g_R^2 M_R^2 \\
&\quad -\frac{1}{4} g_{BL}^2 S_{B-L} - g_R^2 S_R && (6.30) \\
16\pi^2 \frac{d}{dt} m_{\tilde{d}_{1,2}^c}^2 &= -\frac{32}{3} g_3^2 M_3^2 - \frac{1}{3} g_{BL}^2 M_{B-L}^2 - 2 g_R^2 M_R^2 \\
&\quad -\frac{1}{4} g_{BL}^2 S_{B-L} + g_R^2 S_R && (6.31) \\
16\pi^2 \frac{d}{dt} m_{\tilde{L}_{1,2}}^2 &= -6 g_2^2 M_2^2 - 3 g_{BL}^2 M_{B-L}^2 - \frac{3}{4} g_{BL}^2 S_{B-L} && (6.32) \\
16\pi^2 \frac{d}{dt} m_{\tilde{\nu}_{1,2,3}^c}^2 &= -3 g_{BL}^2 M_{B-L}^2 - 2 g_R^2 M_R^2 + \frac{3}{4} g_{BL}^2 S_{B-L} - g_R^2 S_R && (6.33) \\
16\pi^2 \frac{d}{dt} m_{\tilde{e}_{1,2}^c}^2 &= -3 g_{BL}^2 M_{B-L}^2 - 2 g_R^2 M_R^2 + \frac{3}{4} g_{BL}^2 S_{B-L} + g_R^2 S_R . && (6.34)
\end{aligned}$$

In the MSSM scaling regime, which is only relevant to the case of the right-side-up hierarchy, the RGEs are

$$16\pi^2 \frac{d}{dt} m^2_{\tilde{Q}_{1,2}} = -\frac{32}{3} g_3^2 M_3^2 - 6 g_2^2 M_2^2 - \frac{2}{15} g_1^2 M_1^2 + \frac{1}{5} g_1^2 S_Y \tag{6.35}$$

$$16\pi^2 \frac{d}{dt} m^2_{\tilde{u}^c_{1,2}} = -\frac{32}{3} g_3^2 M_3^2 - \frac{32}{15} g_1^2 M_1^2 - \frac{4}{5} Y g_1^2 S_Y \tag{6.36}$$

$$16\pi^2 \frac{d}{dt} m^2_{\tilde{d}^c_{1,2}} = -\frac{32}{3} g_3^2 M_3^2 - \frac{8}{15} g_1^2 M_1^2 + \frac{2}{5} Y g_1^2 S_Y \tag{6.37}$$

$$16\pi^2 \frac{d}{dt} m^2_{\tilde{L}_{1,2}} = -6 g_2^2 M_2^2 - \frac{6}{5} g_1^2 M_1^2 - \frac{3}{5} Y g_1^2 S_Y \tag{6.38}$$

$$16\pi^2 \frac{d}{dt} m^2_{\tilde{\nu}^c_{1,2}} = 0 \tag{6.39}$$

$$16\pi^2 \frac{d}{dt} m^2_{\tilde{e}^c_{1,2}} = -\frac{6}{5} Y^2 g_1^2 M_1^2 + \frac{3}{5} Y g_1^2 S_Y \tag{6.40}$$

The right-handed sneutrinos masses do not run in this regime because they are not charged under the MSSM gauge group. In the upside-down case the the right-handed sneutrinos are present in the brief scaling regime between M_{SUSY} and M_{B-L}. Their soft mass RGEs are

$$16\pi^2 \frac{d}{dt} m^2_{\tilde{\nu}^c_{1,2,3}} = \frac{3}{4} g_{BL}^2 (m^2_{\tilde{\nu}^c_1} + m^2_{\tilde{\nu}^c_2} + m^2_{\tilde{\nu}^c_3}). \tag{6.41}$$

For the third family sfermions (excluding the sneutrinos) and for the MSSM Higgs, all of which are not analytically solvable, the RGEs In the $B-L$ MSSM scaling regime are

$$\begin{aligned} 16\pi^2 \frac{d}{dt} m_{H_u}^2 &= 6Y_t^2(m_{H_u}^2 + m_{\tilde{Q}_3}^2 + m_{\tilde{t}^c}^2) + 6a_t^2 \\ &\quad -6g_2^2 M_2^2 - 2g_R^2 M_R^2 + g_R^2 S_R \end{aligned} \tag{6.42}$$

$$\begin{aligned} 16\pi^2 \frac{d}{dt} m_{H_d}^2 &= 6Y_d^2(m_{H_d}^2 + m_{\tilde{Q}_3}^2 + m_{\tilde{b}^c}^2) \\ &\quad +2Y_\tau^2(m_{H_d}^2 + m_{\tilde{L}_3}^2 + m_{\tilde{\tau}^c}) + 6a_b^2 + 2a_\tau^2 \\ &\quad -6g_2^2 M_2^2 - 2g_R^2 M_R^2 - g_R^2 S_R \end{aligned} \tag{6.43}$$

$$\begin{aligned} 16\pi^2 \frac{d}{dt} m_{\tilde{Q}_3}^2 &= 2Y_t^2(m_{H_u}^2 + m_{\tilde{Q}_3}^2 + m_{\tilde{t}^c}^2) \\ &\quad +2Y_b^2(m_{H_d}^2 + m_{\tilde{Q}_3}^2 + m_{\tilde{b}^c}) + 2a_t^2 + 2a_b^2 \\ &\quad -\frac{32}{3}g_3^2 M_3^2 - 6g_2^2 M_2^2 - \frac{1}{3}g_{BL}^2 M_{BL}^2 + \frac{1}{4}g_{BL}^2 S_{B-L} \end{aligned} \tag{6.44}$$

$$\begin{aligned} 16\pi^2 \frac{d}{dt} m_{\tilde{L}_3}^2 &= 2Y_\tau^2(m_{H_d}^2 + m_{\tilde{L}_3}^2 + m_{\tilde{\tau}^c}^2) + 2a_\tau^2 \\ &\quad -6g_2^2 M_2^2 - 3g_{BL}^2 M_{BL}^2 - \frac{3}{4}g_{BL}^2 S_{B-L} \end{aligned} \tag{6.45}$$

$$\begin{aligned} 16\pi^2 \frac{d}{dt} m_{\tilde{t}^c}^2 &= 4Y_t^2(m_{H_u}^2 + m_{\tilde{Q}_3}^2 + m_{\tilde{t}^c}) + 4a_t^2 \\ &\quad -\frac{32}{3}g_3^2 M_3^2 - \frac{1}{3}g_{BL}^2 M_{BL}^2 - 2g_R^2 M_R^2 - \frac{1}{4}g_{BL}^2 S_{B-L} - g_R^2 S_R \end{aligned} \tag{6.46}$$

$$\begin{aligned} 16\pi^2 \frac{d}{dt} m_{\tilde{b}^c}^2 &= 4Y_b^2(m_{H_d}^2 + m_{\tilde{Q}_3}^2 + m_{\tilde{b}^c}^2) + 4a_b^2 \\ &\quad -\frac{32}{3}g_3^2 M_3^2 - \frac{1}{3}g_{BL}^2 M_{BL}^2 - 2g_R^2 M_R^2 - \frac{1}{4}g_{BL}^2 S_{B-L} + g_R^2 S_R \end{aligned} \tag{6.47}$$

$$\begin{aligned} 16\pi^2 \frac{d}{dt} m_{\tilde{\tau}^c}^2 &= 4Y_\tau^2(m_{H_d}^2 + m_{\tilde{L}_3}^2 + m_{\tilde{\tau}^c}^2) + 4a_\tau^2 \\ &\quad -3g_{BL}^2 M_{BL}^2 - 2g_R^2 M_R^2 + \frac{3}{4}g_{BL}^2 S_{B-L} + g_R^2 S_R. \end{aligned} \tag{6.48}$$

In the MSSM scaling regime they are

$$\begin{aligned}16\pi^2 \frac{d}{dt} m^2_{H_u} &= 6Y_t^2(m^2_{H_u} + m^2_{\tilde{Q}_3} + m^2_{\tilde{t}^c}) + 6a_t^2 \\ &\quad -6g_2^2 M_2^2 - \frac{6}{5} g_1^2 M_1^2 + \frac{3}{5} g_1^2 S_Y \end{aligned} \tag{6.49}$$

$$\begin{aligned}16\pi^2 \frac{d}{dt} m^2_{H_d} &= 6Y_d^2(m^2_{H_d} + m^2_{\tilde{Q}_3} + m^2_{\tilde{b}^c}) \\ &\quad +2Y_\tau^2(\tilde{m}^2_{H_d} + m^2_{\tilde{L}_3} + m_{\tilde{\tau}^c}) + 6a_b^2 + 2a_\tau^2 \\ &\quad -6g_2^2 M_2^2 - \frac{6}{5} g_1^2 M_1^2 + \frac{3}{5} g_1^2 S_Y \end{aligned} \tag{6.50}$$

$$\begin{aligned}16\pi^2 \frac{d}{dt} m^2_{\tilde{Q}_3} &= 2Y_t^2(m^2_{H_u} + m^2_{\tilde{Q}_3} + m^2_{\tilde{t}^c}) \\ &\quad +2Y_b^2(\tilde{m}^2_{H_d} + m^2_{\tilde{Q}_3} + m_{\tilde{b}^c}) + 2a_t^2 + 2a_b^2 \\ &\quad -\frac{32}{3} g_3^2 M_3^2 - 6g_2^2 M_2^2 - \frac{2}{15} g_1^2 M_1^2 + \frac{1}{5} g_1^2 S_Y \end{aligned} \tag{6.51}$$

$$\begin{aligned}16\pi^2 \frac{d}{dt} m^2_{\tilde{L}_3} &= 2Y_\tau^2(m^2_{H_d} + m^2_{\tilde{L}_3} + m^2_{\tilde{\tau}^c}) + 2a_\tau^2 \\ &\quad -6g_2^2 M_2^2 - \frac{12}{5} g_1^2 M_1^2 - \frac{3}{5} g_1^2 S_Y \end{aligned} \tag{6.52}$$

$$\begin{aligned}16\pi^2 \frac{d}{dt} m^2_{\tilde{t}^c} &= 4Y_t^2(m^2_{H_u} + m^2_{\tilde{Q}_3} + m_{\tilde{t}^c}) + 4a_t^2 \\ &\quad -\frac{32}{3} g_3^2 M_3^2 - \frac{16}{5} g_1^2 M_1^2 - \frac{4}{5} g_1^2 S_Y \end{aligned} \tag{6.53}$$

$$\begin{aligned}16\pi^2 \frac{d}{dt} m^2_{\tilde{b}^c} &= 4Y_b^2(m^2_{H_d} + m^2_{\tilde{Q}_3} + m^2_{\tilde{b}^c}) + 4a_b^2 \\ &\quad -\frac{32}{3} g_3^2 M_3^2 - \frac{8}{15} g_1^2 M_1^2 - \frac{2}{15} g_1^2 S_Y \end{aligned} \tag{6.54}$$

$$\begin{aligned}16\pi^2 \frac{d}{dt} m^2_{\tilde{\tau}^c} &= 4Y_\tau^2(m^2_{H_d} + m^2_{\tilde{L}_3} + m^2_{\tilde{\tau}^c}) + 4a_\tau^2 \\ &\quad -\frac{12}{5} g_1^2 M_1^2 + \frac{3}{5} g_1^2 S_Y \end{aligned} \tag{6.55}$$

The soft mass parameters are used in the calculation of the physical sparticle masses, discussed in the next appendix.

6.2 Physical Masses

In this Appendix, we discuss how the physical masses of the sparticles and the Higgs are determined from the running parameters.

6.2.1 Sparticle Masses

Because the first- and second-family Yukawa and tri-scalar couplings are negligible, mixing among the first- and second-family sfermions and the sneutrinos is negligible, greatly simplifying the relationship between physical masses and soft masses. However, there are electroweak D-term contributions associated with the electroweak scale. Although these are numerically small, they have the effect of splitting the masses of the otherwise degenerate $SU(2)_L$ doublets, which has implications for the lightest supersymmetric particle (see Section 3.4):

$$\Delta_\phi = M_Z^2 \left(T_3 - Q \sin^2 \theta_W\right) \cos 2\beta, \tag{6.56}$$

where θ_W is the weak mixing angle ($\sin^2 \theta_W \approx 0.23$) and T_3 and Q are the left-handed isospin and electric charge of the scalar ϕ. Here we lay out the physical masses with the electroweak D-term contributions, along with the notation for the physical masses.

$$\begin{aligned}
m_{\tilde{u}_L} &= m_{\tilde{u}} + \Delta_{\tilde{Q}_1}, & m_{\tilde{u}_R} &= m_{\tilde{u}^c} + \Delta_{\tilde{u}^c},\\
m_{\tilde{c}_L} &= m_{\tilde{c}} + \Delta_{\tilde{Q}_2}, & m_{\tilde{c}_R} &= m_{\tilde{c}^c} + \Delta_{\tilde{s}^c},\\
m_{\tilde{d}_L} &= m_{\tilde{d}} + \Delta_{\tilde{Q}_1}, & m_{\tilde{d}_R} &= m_{\tilde{d}^c} + \Delta_{\tilde{d}^c},\\
m_{\tilde{s}_L} &= m_{\tilde{s}} + \Delta_{\tilde{Q}_2}, & m_{\tilde{s}_R} &= m_{\tilde{s}^c} + \Delta_{\tilde{s}^c},\\
m_{\tilde{\nu}_{L1}} &= m_{\tilde{\nu}_1} + \Delta_{\tilde{L}_1}, & m_{\tilde{\nu}_{R1}} &= m_{\tilde{\nu}_1^c} + \Delta_{\tilde{\nu}_1^c},\\
m_{\tilde{\nu}_{L2}} &= m_{\tilde{\nu}_2} + \Delta_{\tilde{L}_2}, & m_{\tilde{\nu}_{R2}} &= m_{\tilde{\nu}_2^c} + \Delta_{\tilde{\nu}_2^c},\\
m_{\tilde{\nu}_{L3}} &= m_{\tilde{\nu}_3} + \Delta_{\tilde{L}_3}, & m_{\tilde{\nu}_R^c} &= M_{Z_R},\\
m_{\tilde{e}_L} &= m_{\tilde{e}} + \Delta_{\tilde{L}_1}, & m_{\tilde{e}_R} &= m_{\tilde{e}^c} + \Delta_{\tilde{e}^c},\\
m_{\tilde{\mu}_L} &= m_{\tilde{\mu}} + \Delta_{\tilde{L}_2}, & m_{\tilde{\mu}_R} &= m_{\tilde{\mu}^c} + \Delta_{\tilde{\mu}^c}.
\end{aligned} \tag{6.57}$$

The third-family right-handed sneutrino physical state (referred to as $\tilde{\nu}_R^c$) mass is different because it acquires mass through the $B - L$ symmetry breaking mechanism and is degenerate with the Z_R mass.

The Yukawa and tri-scalar couplings associated with third-family squarks and charged sleptons contribute non-negligible mixing terms among these scalars.

These effects are captured in the stop, sbottom, and stau mixing matrices. Here we use the conventional notation $a_{t,b,\tau} = Y_{t,b,\tau}A_{t,b,\tau}$. The stop mixing matrix in the basis $(\tilde{t}, \tilde{t}^{c*})$ is[1]

$$\mathcal{M}^2_{\tilde{t}} = \begin{pmatrix} m^2_{\tilde{Q}_3} + M_t^2 + \Delta_{\tilde{Q}_3} & M_t\left(A_t - \frac{\mu}{\tan\beta}\right) \\ M_t\left(A_t - \frac{\mu}{\tan\beta}\right) & m^2_{\tilde{t}^c} + M_t^2 + \Delta_{\tilde{t}^c} \end{pmatrix}. \tag{6.58}$$

The eigenstates of this matrix will be referred to as $\tilde{t}_1$ and $\tilde{t}_2$ with mass eigenvalues defined such that $m_{\tilde{t}_1} < m_{\tilde{t}_2}$. The sbottom mixing matrix in the basis $(\tilde{b}, \tilde{b}^{c*})$ is

$$\mathcal{M}^2_{\tilde{b}} = \begin{pmatrix} m^2_{\tilde{Q}_3} + M_b^2 + \Delta_{\tilde{Q}_3} & M_b\left(A_b - \mu\tan\beta\right) \\ M_b\left(A_b - \mu\tan\beta\right) & m^2_{\tilde{b}^c} + M_b^2 + \Delta_{\tilde{b}^c} \end{pmatrix}. \tag{6.59}$$

The eigenstates of this mass matrix will be referred to similarly to the stops. The stau mixing matrix in the basis $(\tilde{\tau}, \tilde{e}^{c*})$ is

$$\mathcal{M}^2_{\tilde{\tau}} = \begin{pmatrix} m^2_{\tilde{L}_3} + M_\tau^2 + \Delta_{\tilde{L}_3} & M_\tau\left(A_\tau - \mu\tan\beta\right) \\ M_\tau\left(A_\tau - \mu\tan\beta\right) & m^2_{\tilde{\tau}^c} + M_\tau^2 + \Delta_{\tilde{\tau}^c} \end{pmatrix}. \tag{6.60}$$

The eigenstates of this matrix will be referred to similarly to the stops and sbottoms. All of the running parameters in these matrices are evaluated at the SUSY scale.

For any of these matrices,

$$\begin{pmatrix} L_{\tilde{f}} & X_{\tilde{f}} \\ X_{\tilde{f}} & R_{\tilde{f}} \end{pmatrix}, \tag{6.61}$$

the relevant mixing angle is given by

$$\tan 2\theta_{\tilde{f}} = \frac{-2|X_f|}{L_{\tilde{f}} - R_{\tilde{f}}}, \tag{6.62}$$

where the angle $\theta_{\tilde{f}}$ may always be chosen to be between $0°$ and $90°$. Defined this way, a mixing angle close to zero means the lighter mass eigenstate consists of mostly the left-handed gauge eigenstate and a mixing angle close to $90°$ means the lighter state is mostly right-handed.

---

[1] We present these matrices in terms of the fermion masses $M_{t,b,\tau}$ for simplicity. However, for numerical evaluation these fermion masses are replaced with the appropriate Higgs VEV times Yukawa coupling evaluated at the SUSY scale.

The chargino content is identical to that of the MSSM in the approximation of vanishing R-parity violation. This is a good approximation for calculating masses but the mixing with the charged leptons need to be take into account when calculating decays, see [2] for example. Continuing with the approximation of vanishing R-parity violation, the results of [38] may be used. Those results, in our own notation, are

$$\begin{aligned} m^2_{\tilde{\chi}^\pm_1} &= \frac{1}{2}(M_2^2+\mu^2+2M_W^2 \\ &\quad -\sqrt{(M_2^2+\mu^2+2M_W^2)^2-4(\mu M_2-M_W^2\sin 2\beta)^2}) \qquad (6.63) \\ m^2_{\tilde{\chi}^\pm_2} &= \frac{1}{2}(M_2^2+\mu^2+2M_W^2 \\ &\quad +\sqrt{(M_2^2+\mu^2+2M_W^2)^2-4(\mu M_2-M_W^2\sin 2\beta)^2}). \qquad (6.64) \end{aligned}$$

In the basis $(\nu, \tilde{W}_R, \tilde{B}', \tilde{W}^0, \tilde{H}^0_u, \tilde{H}^0_d)$, the neutralino mass matrix is

$$\begin{pmatrix} 0 & -c_{\theta_R}M_{Z_R} & s_{\theta_R}M_{Z_R} & 0 & 0 & 0 \\ -c_{\theta_R}M_{Z_R} & M_R & 0 & 0 & -c_\beta s_{\theta_W}M_Z & s_\beta s_{\theta_W}M_Z \\ s_{\theta_R}M_{Z_R} & 0 & M_{BL} & 0 & 0 & 0 \\ 0 & 0 & 0 & M_2 & c_\beta c_{\theta_W}M_Z & -s_\beta c_{\theta_W}M_Z \\ 0 & -c_\beta s_{\theta_W}M_Z & 0 & c_\beta c_{\theta_W}M_Z & 0 & -\mu \\ 0 & s_\beta s_{\theta_W}M_Z & 0 & -s_\beta c_{\theta_W}M_Z & -\mu & 0 \end{pmatrix}, \qquad (6.65)$$

where $c_\theta \equiv \cos\theta$ and $s_\theta \equiv \sin\theta$ etc. As with the charginos, we have assumed that mixing with the left-handed neutrinos, due to R-parity violation is 0. This is good approximation for calculating masses and will be used here, but cannot be used when calculating decay rates. As discussed in Section 2.4 some of the eigenstates of this matrix have masses associated with the $B-L$ scale while others have masses associated with the SUSY scale. A conventional approach to this situation would be to perturbatively diagonalize the matrix in the limit $M_{\text{SUSY}} \gg M_{B-L}$ for the right-side-up case or $M_{B-L} \gg M_{\text{SUSY}}$ for the upside-down case. However, these two scales may be comparable so the entire mass matrix must be diagonalized without the use of perturbative methods. This has the potential to introduce errors since it doesn't account for the fact that some states should be integrated out at different scales. However, the errors will always be small because the $B-L$ and SUSY scales are always of comparable size. We choose to evaluate all of the running parameters in this matrix at the SUSY scale. The error introduced by doing this should be smaller than the error introduced by associating the entire SUSY spectrum with a single scale, M_{SUSY}. The mass eigenstates are referred to as $\tilde{\chi}^0_1 \cdots \tilde{\chi}^0_6$ in a mass ordered basis with eigenvalues $m_{\tilde{\chi}^0_1} \cdots m_{\tilde{\chi}^0_6}$.

The physical gluino mass, $M_{\tilde{g}}$ is simply equal to the running gluino mass evaluated at the SUSY scale.

$$M_{\tilde{g}} = M_3(M_{\text{SUSY}}). \tag{6.66}$$

6.2.2 Higgs Masses

Supersymmetric models such as the MSSM and this $B - L$ MSSM contain five Higgs particles. The most important for the present discussion is the lightest neutral SM-like Higgs, h^0, which we refer to as "the Higgs" throughout this thesis. This one is important because its mass is known and can be used to constrain some of the SUSY parameter space. The other four Higgses are the heavy Higgs, H^0, the Higgs pseudoscalar, A^0, and the charged Higgses, $H^{\pm}$.

The Higgs mass is calculated using methods discussed in [56, 57, 58]. The physical Higgs mass is

$$m_{h^0} = \sqrt{\lambda} v, \tag{6.67}$$

with the Higgs quartic coupling, λ, evaluated at the scale of the physical Higgs mass. Above the SUSY scale, λ comes from the D-terms and is thereby fixed. Below the SUSY scale, RGE effects will cause λ to deviate from its supersymmetric value. These effects come mainly from one-loop graphs involving the top quark. They are contained in the RGE for λ in the SM scaling regime. We employ results from [58]. Here we re-state the relevant equations in our own notation. The supersymmetric boundary condition on λ is

$$\lambda(M_{\text{SUSY}}) = \frac{1}{4}\left(g_L^2 + \frac{3}{5} g_1^2\right)\cos^2 2\beta + \delta\lambda. \tag{6.68}$$

The parameter $\delta\lambda$ contains threshold corrections applied at the SUSY scale. Including only the dominant stop contributions from [58],

$$16\pi^2 \delta\lambda = 3Y_t^4\left(2\frac{X_t^2}{m_{\tilde{t}_1} m_{\tilde{t}_2}} F\left(\frac{m_{\tilde{t}_1}}{m_{\tilde{t}_2}}\right) - \frac{1}{6}\frac{X_t^4}{m_{\tilde{t}_1}^2 m_{\tilde{t}_2}^2} G\left(\frac{m_{\tilde{t}_1}}{m_{\tilde{t}_2}}\right)\right), \tag{6.69}$$

where we define $X_t = A_t - \mu\cot\beta$ (note that this definition is different from that used in [58]) and

$$\begin{aligned} F(x) &= \frac{2x\ln x}{x^2 - 1} && (6.70)\\ G(x) &= \frac{12x^2(1 - x^2 + (1 + x^2)\ln x)}{(x^2 - 1)^3}. && (6.71) \end{aligned}$$

The RGE for λ in the SM regime is

$$\begin{aligned} \frac{d}{dt}\lambda &= 4\lambda(3y_t^2 + 3y_b^2 + y_\tau^2) - 9\lambda(\frac{1}{5}g_1^2 + g_2^2) \\ &\quad -4(3y_t^4 + 3y_b^4 + y_\tau^4) + \frac{27}{100}g_1^4 + \frac{9}{10}g_2^2g_1^2 + \frac{9}{4}g_2^4 + 12\lambda^2, \quad (6.72) \end{aligned}$$

and in the upside-down case between M_{SUSY} and M_{B-L} it is

$$\begin{aligned} \frac{d}{dt}\lambda &= 4\lambda(3y_t^2 + 3y_b^2 + y_\tau^2) - 9\lambda(\frac{1}{3}g_R^2 + g_2^2) \\ &\quad -4(3y_t^4 + 3y_b^4 + y_\tau^4) + \frac{3}{4}g_R^4 + \frac{3}{2}g_2^2g_R^2 + \frac{9}{4}g_2^4 + 12\lambda^2. \quad (6.73) \end{aligned}$$

Since this depends on the Yukawa couplings, which are solved numerically, this must also be solved numerically. The dominant contributions come from the terms involving y_t. These terms are present because both stops are integrated out at M_{SUSY}. This has the potential to introduce errors because the stops generally do not have the same mass. The errors introduced by this are minimized when the SUSY scale is chosen to be $M_{\text{SUSY}} = \sqrt{m_{\tilde{t}_1}m_{\tilde{t}_2}}$. We find this method of calculating the Higgs mass is the best compromise between transparency and accuracy.

Regarding the masses of the other four Higgses, the tree level results from [38] apply and are sufficient for the present purposes. We re-state them here.

$$m_{A^0}^2 = 2b/\sin(2\beta) = 2\mu^2 + m_{H_u}^2 + m_{H_d}^2 \quad (6.74)$$

$$m_{H^0}^2 = \frac{1}{2}\left(m_{A^0}^2 + M_Z^2 + \sqrt{(m_{A^0}^2 - M_Z^2)^2 + 4M_Z^2m_{A^0}^2\sin^2(2\beta)}\right) \quad (6.75)$$

$$m_{H^\pm}^2 = m_{A^0}^2 + M_W^2. \quad (6.76)$$

6.3 Application of the Checks and Iterative Procedure

In this Appendix, we describe–for a single randomly generated initial point–two things: 1) the precise algorithm by which the checks described in Table 3.3 are applied and 2) the iterative numerical method used to solve for the $B - L$ and SUSY scales. It is necessary to discuss these simultaneously since, as will become clear, they are interrelated. We include this Appendix to give the reader insight into the details of our statistical method and to elucidate technical comments made in the main text.

Before proceeding, it is helpful to note several things. A "point" here refers to a randomly generated choice of the parameters listed in Table 3.2. For each point, we make working "guesses" of the initial values of M_{SUSY} and M_{B-L}. These will be iteratively improved using a simple numerical method. For a fixed choice of randomly generated parameters and the two scales M_{SUSY} and M_{B-L} specified, there is a unique solution for all of the RGEs and physical masses. That unique solution is found by our code using a combination of analytic solutions (discussed throughout this thesis) and numerical methods (not discussed in this thesis). For the purposes of this Appendix, it is sufficient to know that the solution can indeed be calculated. It is also useful to note that, with the exception of the spill and convergence checks, the checks in Table 3.3 are applied sequentially. For example, a point is subjected to the EW breaking check if and only if it passes the preceding $B-L$ breaking and Z_R bound checks. This means that a point that fails a particular check a) has implicitly passed all previous checks and b) is immediately discarded and never subjected to subsequent checks. The sequential nature of these checks is what enables us to define the survival rates given in Table 3.3. The spill checks and the convergence check, however, are different because they are not necessarily applied in a particular order and may even be applied multiple times to a single point. Nevertheless, if any point fails a spill or convergence check, at any step in the iterative process, we count that point as having passed all spill checks that appear above the failed check in Table 3.3. This removes any ambiguity about how to define survival rates for the spill and convergence checks.

Now we are prepared to discuss the main goals of this Appendix. For each randomly generated point, the initial guesses for M_{SUSY} and M_{B-L} are always taken to be 1 TeV and 2.5 TeV respectively. If the point with these initial guesses does not satisfy $B-L$ breaking, then we count it as failing the $B-L$ breaking check. If the point does not satisfy the Z_R lower bound, then it is so counted. If it does not satisfy EW breaking, then it is so counted. If it does not satisfy the non-tachyonic stops check, it is so counted.

If the guess for the $B-L$ scale satisfies its definition, that is, if the RG calculation of $M_{Z_R} = M_{B-L}$, to within 1%, and the guess for the SUSY scale satisfies its definition, that is, the RG calculation of $m_{\tilde{t}_1}$, $m_{\tilde{t}_2}$ satisfies $\sqrt{m_{\tilde{t}_1} m_{\tilde{t}_2}} = M_{\text{SUSY}}$ to within 1%, then "convergence" has occurred and the steps in the next two paragraphs are skipped.

If the guess for the $B-L$ scale satisfies its definition to within 1%, then the rest of the steps in this paragraph are skipped. If not, the guess for the $B-L$ scale is changed to M_{Z_R}. Using the same value for M_{SUSY}, and the new choice of M_{B-L}, we again run the RGEs for the same initial point. If M_{Z_R} not within 1%

of M_{B-L}, then the process is repeated. If the steps in this paragraph are repeated more than 300 times[2] without success, then we count the point as having failed the convergence check.

If the guess for the SUSY scale satisfies its definition to within 1%, the rest of the steps in this paragraph are skipped. If not, the guess for the SUSY scale is changed to $\sqrt{m_{\tilde{t}_1}(M_{\text{SUSY}})m_{\tilde{t}_2}(M_{\text{SUSY}})}$ and we rerun the RGEs. If the point now does not satisfy EW breaking, it is counted as failing the EW breaking spill check. If the point now does not satisfy the non-tachyonic stops check, it is counted as failing the non-tachyonic stops spill check. If it does pass these checks, but M_{SUSY} does not satisfy its definition to within 1%, then the steps in this paragraph are repeated. If they have been repeated more than 300 times without success, the point is counted as failing the convergence check.

Having successfully passed all of the previous criterion, we now must check the remaining checks. If the point does not satisfy the Z_R bound, it is counted as failing the $B-L$ bound spill check. If the point does not satisfy the sparticle bounds, it is so counted. If the point does not satisfy the Higgs mass check, it is so counted. If it does, however, satisfy all of these experimental checks, it is a valid point.

The procedure described in the previous five paragraphs is represented pictorially by the “flow chart” in Fig. 6.1.

---

[2] a conveniently chosen number which provides adequate opportunity for the iteration to converge.

6.4 Neutralinos and Neutrinos:

R-parity violation allows all fermions with the same quantum numbers to mix and form physical states which are linear combinations of the original fields. In the basis $\left(\tilde{W}_R,\ \tilde{W}^0,\ \tilde{H}_d^0,\ \tilde{H}_u^0,\ \tilde{B}',\ \nu_3^c,\ \nu_i\right)$ with $i = 1, ..., 3$, the neutralino mass

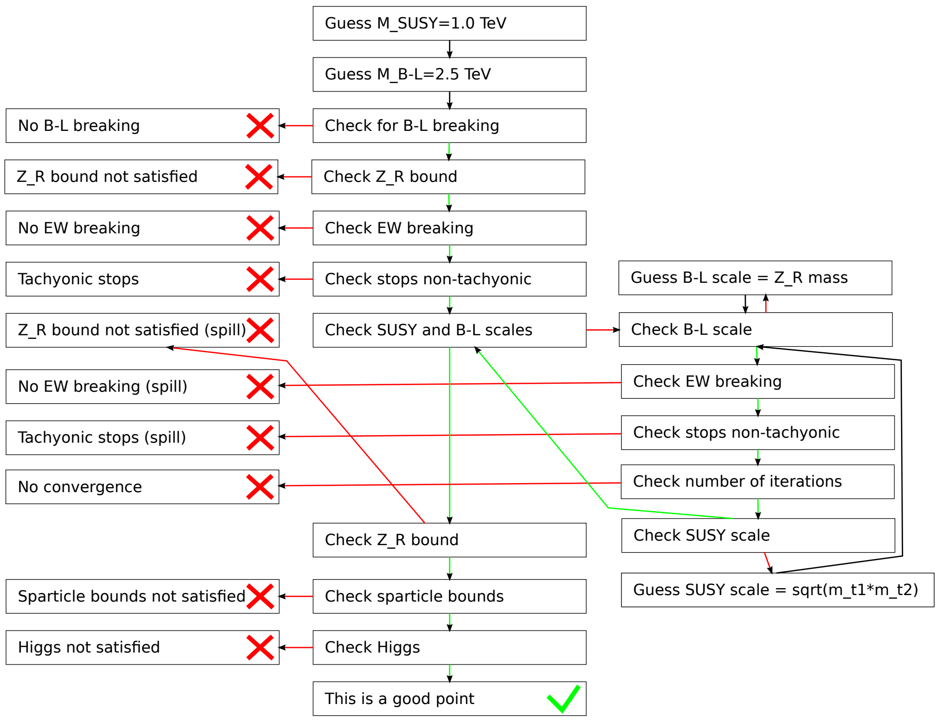

Figure 6.1: A "flow chart" showing how the checks are applied and how the iterative process of solving for the $B - L$ and SUSY scales works. Every block that begins with the word "Check" has an outgoing red and green arrow. The green arrow is followed if the check is satisfied and the red arrow is followed if the check is not satisfied.

matrix is given by

$$\mathcal{M}_{\chi^0} = \begin{pmatrix} M_R & 0 & -\frac{1}{2}\, g_R\, v_d & \frac{1}{2}\, g_R\, v_u & 0 & -\frac{1}{2} g_R v_R & 0_{1\times 3} \\ 0 & M_2 & \frac{1}{2}\, g_2\, v_d & -\frac{1}{2}\, g_2\, v_u & 0 & 0 & \frac{1}{2}\, g_2\, v_{L}{}_i^* \\ -\frac{1}{2}\, g_R\, v_d & \frac{1}{2}\, g_2\, v_d & 0 & -\mu & 0 & 0 & 0_{1\times 3} \\ \frac{1}{2}\, g_R\, v_u & -\frac{1}{2}\, g_2\, v_u & -\mu & 0 & 0 & 0 & \epsilon_i \\ 0 & 0 & 0 & 0 & M_{BL} & \frac{1}{2}\, g_{BL}\, v_R & -\frac{1}{2}\, g_{BL}\, v_{L}{}_i^* \\ -\frac{1}{2} g_R v_R & 0 & 0 & 0 & \frac{1}{2}\, g_{BL}\, v_R & 0 & \frac{1}{\sqrt{2}}\, Y_{\nu\, i3}\, v_u \\ 0_{3\times 1} & \frac{1}{2}\, g_2\, v_{L}{}_j^* & 0_{3\times 1} & \epsilon_j & -\frac{1}{2}\, g_{BL}\, v_{L}{}_j^* & \frac{1}{\sqrt{2}}\, Y_{\nu\, j3}\, v_u & 0_{3\times 3} \end{pmatrix}, \tag{6.77}$$

where

$$\epsilon_i \equiv \frac{1}{\sqrt{2}} Y_{\nu i3} v_R \tag{6.78}$$

are the parameters of the induced bilinear R-parity violating terms. We have suppressed terms that are quadratic in the neutrino mass parameter, *e.g.* $v_{Li} Y_{\nu ij}$.

The neutralino mass matrix, Eq. (6.77), has the schematic form

$$\mathcal{M}_{\chi^0} = \begin{pmatrix} M_{\chi^0} & m_D \\ m_D^T & 0_{3\times 3} \end{pmatrix}, \tag{6.79}$$

where M_{χ^0} is a six-by-six matrix of order a TeV and m_D is six-by-three matrix of order an MeV. This allows the mass matrix to be diagonalized perturbatively. The diagonal neutralino mass matrix is

$$\mathcal{M}^D_{\chi^0} = \mathcal{N}^* \mathcal{M}_{\chi^0} \mathcal{N}^\dagger \tag{6.80}$$

with

$$\mathcal{N} = \begin{pmatrix} N & 0_{3\times 3} \\ 0_{3\times 3} & V^\dagger_{\text{PMNS}} \end{pmatrix} \begin{pmatrix} 1_{6\times 6} & -\xi_0 \\ \xi_0^\dagger & 1_{3\times 3} \end{pmatrix}, \tag{6.81}$$

where the second matrix on the right-hand side rotates away the neutrino/neutralino mixing. This quantity is of interest since it is ultimately used in the Feynman Rules given in Appendix 6.7 used to calculate the third generation squark decay widths. The first matrix diagonalizes the neutralino states and the neutrino states. Equation (6.80) specifies the relationship between the gauge eigenstates, ψ^0, and the mass eigenstates χ^0:

$$\chi^0 = \mathcal{N} \psi^0, \tag{6.82}$$

where the first six states in χ^0 are the TeV scale neutralino states labeled from lightest to heaviest and the last three are the physical neutrino states.

Equation (6.80) can be used to solve for the six-by-three matrix ξ_0:

$$\xi_0 = M^{-1}_{\chi^0} m_D. \tag{6.83}$$

The rows of ξ_0 are the gaugino gauge eigenstates and the columns correspond to the neutrino gauge eigenstates. These are explicitly labeled and presented below:

$$\xi_{0\tilde{W}_R\nu_i} = \frac{g_R\mu}{8d_{\chi^0}}\left[2M_{BL}v_u\left(g_2^2 v_d v_u - 2M_2\mu\right)\epsilon_i - g_{BL}^2 M_2 v_R^2\left(v_d\epsilon_i + \mu v_{L_i}^*\right)\right] \tag{6.84}$$

$$\xi_{0\tilde{W}_2\nu_i} = \frac{g_2\mu}{8d_{\chi^0}}\left[2g_R^2 M_{BL}v_d v_u^2\epsilon_i + M_{\tilde{Y}}v_R^2\left(v_d\epsilon_i + \mu v_{L_i}^*\right)\right] \tag{6.85}$$

$$\xi_{0\tilde{H}_d^0\nu_i} = \frac{1}{16d_{\chi^0}}\left[M_{\tilde{\gamma}}v_R^2 v_u\left(v_d\epsilon_i - \mu v_{L_i}^*\right) - 4M_2\mu\left(M_{\tilde{Y}}v_R^2 + g_R^2 M_{BL}v_u^2\right)\epsilon_i\right] \tag{6.86}$$

$$\xi_{0\tilde{H}_u^0\nu_i} = \frac{1}{16d_{\chi^0}}\left[M_{\tilde{\gamma}}v_R^2 v_d\left(v_d\epsilon_i + \mu v_{L_i}^*\right) + 4g_R^2\mu M_2 M_{BL}v_d v_u\epsilon_i\right] \tag{6.87}$$

$$\begin{aligned}\xi_{0\tilde{B}'\nu_i} = -\frac{1}{8d_{\chi^0}}&\left[g_{BL}g_R^2 M_2\mu v_R^2\left(v_d\epsilon_i + \mu v_{L_i}^*\right)\right.\\ &\left.+2g_{BL}\mu v_u\left(\left(g_R^2 M_2 + g_2^2 M_R\right)v_d v_u - 2M_R M_2\mu\right)\epsilon_i\right]\end{aligned} \tag{6.88}$$

$$\begin{aligned}\xi_{0\nu_3^c\nu_i} = \frac{\mu}{8v_R d_{\chi^0}}&\left[\left(M_{\tilde{\gamma}}v_R^2 v_d v_u - 2g_{BL}^2 M_R M_2\mu v_R^2\right)v_{L_i}^*\right.\\ &+ 2M_{BL}\left(M_2\left(g_R^2 v_R^2 v_d - 4M_R\mu v_u\right)\right.\\ &\left.\left.+2\left(g_R^2 M_2 + g_2^2 M_R\right)v_d v_u^2\right)\epsilon_i\right],\end{aligned} \tag{6.89}$$

where

$$d_{\chi^0} \equiv \frac{1}{4}M_2 M_{\tilde{Y}}\mu^2 v_R^2 - \frac{1}{8}M_{\tilde{\gamma}}\mu v_R^2 v_d v_u \tag{6.90}$$

$$M_{\tilde{\gamma}} \equiv g_R^2 g_{BL}^2 M_2 + g_2^2 g_R^2 M_{BL} + g_2^2 g_{BL}^2 M_R \tag{6.91}$$

$$M_{\tilde{Y}} \equiv g_R^2 M_{BL} + g_{BL}^2 M_R\ . \tag{6.92}$$

Using Eqs. (6.80) and (6.83), or simply integrating out the heavy states, yields the neutrino mass matrix

$$m_{\nu ij} = Av_{L_i}^* v_{L_j}^* + B\left(v_{L_i}^*\epsilon_j + \epsilon_i v_{L_j}^*\right) + C\epsilon_i\epsilon_j\ , \tag{6.93}$$

with

$$A = \frac{\mu\, M_{\tilde{\gamma}}}{2\, M_{\tilde{\gamma}} v_u v_d - 4 M_2 M_{\tilde{Y}} \mu} \tag{6.94}$$

$$B = \frac{M_{\tilde{\gamma}} v_d \left(2 M_{Z_R}^2 + g_{Z_R}^2 v_u^2\right) - 2 g_{Z_R}^2 g_{BL}^2 M_2 M_R\, \mu\, v_u}{4 M_{Z_R}^2 (M_{\tilde{\gamma}} v_u v_d - 2 M_{\tilde{Y}} M_2 \mu)} \tag{6.95}$$

$$\begin{aligned} C = {} & (2 g_{Z_R}^4 M_2 M_{BL} M_R\, \mu^2 v_u^2 \\ & \quad - g_{Z_R}^2 M_{BL} \mu \left(g_2^2\, g_{Z_R}^2 M_R v_u^2 + g_R^2 M_2 \left(4 M_{Z_R}^2 + g_{Z_R}^2 v_u^2\right)\right) v_d v_u) \\ & \quad / (4 M_{Z_R}^4 \mu \,(2 M_{\tilde{Y}} M_2\, \mu - M_{\tilde{\gamma}} v_d v_u)) \\ & \quad - \frac{M_{\tilde{\gamma}} v_d^2}{2\mu\, (2 M_{\tilde{Y}} M_2\, \mu - M_{\tilde{\gamma}} v_d v_u)} \,, \end{aligned} \tag{6.96}$$

and where

$$g_{Z_R}^2 \equiv g_{BL}^2 + g_R^2 \,. \tag{6.97}$$

The diagonal neutrino mass matrix is then given by

$$\begin{aligned} m_{\nu\; ij}^D &= \left(V_{\text{PMNS}}^T\, m_\nu\, V_{\text{PMNS}}\right)_{ij} \\ &= A V_i V_j + B\, (V_i E_j + E_i V_j) + C E_i E_j \,, \end{aligned} \tag{6.98}$$

where

$$v_{Li} = V_l^*\, V_{\text{PMNS}\, il} \,, \tag{6.99}$$

$$\epsilon_i = E_l\, V_{\text{PMNS}\, il}^* \,, \tag{6.100}$$

and

$$\begin{aligned} V_{\text{PMNS}} \quad = \quad & \begin{pmatrix} c_{12} c_{13} & s_{12} c_{13} & s_{13} e^{-i\delta} \\ -s_{12} c_{23} - c_{12} s_{23} s_{13} e^{i\delta} & c_{12} c_{23} - s_{12} s_{23} s_{13} e^{i\delta} & c_{13} s_{23} \\ s_{12} s_{23} - c_{12} c_{23} s_{13} e^{i\delta} & -c_{12} s_{23} - s_{12} c_{23} s_{13} e^{i\delta} & c_{13} c_{23} \end{pmatrix} \\ & \times \text{diag}(1, e^{i\alpha/2}, 1) \,, \end{aligned} \tag{6.101}$$

with $c_{ab}(s_{ab}) = \cos\theta_{ab}(\sin\theta_{ab})$.

Equations (6.98) - (6.100) can be used to solve for five of the six v_{Li} and ϵ_i parameters in terms of the the neutrino parameters, modulo two signs. The determinant of Eq. (6.93) is zero, so at tree-level there is one massless neutrino. In this case, the solutions to Eqs. (6.98) - (6.100) depend on whether the neutrino mass hierarchy is normal or inverted:

- Normal Hierarchy

In a theory with one massless neutrino, such as the one analyzed in this thesis, the neutrino masses in the normal hierarchy are

$$m_1 = 0\,, \qquad m_2 = \sqrt{\Delta m_{21}^2}\,, \qquad m_3 = \sqrt{\Delta m_{31}^2}\,. \tag{6.102}$$

Loop effects will contribute mass to the massless neutrino, but we continue in the limit where these contributions are negligible. For the normal hierarchy, Equation (6.98) then breaks down into the following six equations:

$$AV_1^2 + 2BV_1E_1 + CE_1^2 = 0\,, \tag{6.103}$$

$$AV_1V_2 + B\left(V_1E_2 + V_2E_1\right) + CE_1E_2 = 0\,, \tag{6.104}$$

$$AV_1V_3 + B\left(V_1E_3 + V_3E_1\right) + CE_1E_3 = 0\,, \tag{6.105}$$

$$AV_2V_3 + B\left(V_2E_3 + V_3E_2\right) + CE_2E_3 = 0\,, \tag{6.106}$$

$$AV_2^2 + 2BV_2E_2 + CE_2^2 = m_2\,, \tag{6.107}$$

$$AV_3^2 + 2BV_3E_3 + CE_3^2 = m_3\,. \tag{6.108}$$

Equations. (6.103) - (6.105) force $V_1, E_1 = 0$. The remaining system of equations, (6.106) - (6.108), can be solved for with respect to E_3:

$$E_2 = \zeta_1\sqrt{-\frac{m_2}{m_3}\left(E_3^2 + \frac{Am_3}{R}\right)}\,, \tag{6.109}$$

$$V_2 = \frac{1}{A}\left(-BE_2 + \zeta_2\sqrt{R\left(E_2^2 + \frac{Am_2}{R}\right)}\right)\,, \tag{6.110}$$

$$V_3 = \frac{1}{A}\left(-BE_3 + \zeta_3\sqrt{R\left(E_3^2 + \frac{Am_3}{R}\right)}\right)\,, \tag{6.111}$$

where

$$R \equiv B^2 - AC \tag{6.112}$$

and ζ_1, ζ_2 and ζ_3 are the usual sign factors (± 1) associated with solving a quadratic equation. These sign factors, however, are not all independent. They are related by

$$\zeta_2 = \zeta_1\zeta_3\frac{\sqrt{-\frac{m_2}{m_3}RE_3^2}\,\sqrt{R\left(E_3 + \frac{Am_3}{R}\right)}}{RE_3\sqrt{-\frac{m_2}{m_3}\left(E_3^2 + \frac{Am_3}{R}\right)}}\,. \tag{6.113}$$

Inverting Eqs. (6.99) and (6.100) translates these solutions in E_i and V_i to ϵ_i and v_{Li}.

Using Eqs. (6.100) and (6.109), E_3 can be expressed in terms of any one of the ϵ_i. This is advantageous because the ϵ_i are more transparently related to stop decay branching ratios and are the more fundamental parameters in the Lagrangian. This allows one to specify one of the ϵ_i as the input parameters. Substituting Eq. (6.109) and $E_1 = 0$ into Eq. (6.100) and squaring it yields a quadratic equation for E_3. It is solved by

$$\begin{aligned} E_3 = {} & (\epsilon_i V^*_{\text{PMNS}_{i3}} \\ & + \zeta_0 \sqrt{-\frac{m_2}{m_3}(V^*_{\text{PMNS}_{i2}})^2\epsilon_i^2 - \frac{Am_2}{R}(V^*_{\text{PMNS}_{i2}})^2\left((V^*_{\text{PMNS}_{i3}})^2 + \frac{m_2}{m_3}(V^*_{\text{PMNS}_{i2}})^2\right)}\,) \\ & /((V^*_{\text{PMNS}_{i3}})^2 + \frac{m_2}{m_3}(V^*_{\text{PMNS}_{i2}})^2). \end{aligned} \tag{6.114}$$

This introduces a new sign $\zeta_0 = \pm 1$ into the procedure, as well as a new constraint on the sign variables. Substituting Eq. (6.109) into Eq. (6.100) yields

$$\zeta_1 = \frac{(\epsilon_i - V^*_{\text{PMNS}_{i3}} E_3)}{\sqrt{-\frac{m_2}{m_3}\left(E_3^2 + \frac{Am_3}{R}\right)}\, V^*_{\text{PMNS}_{i2}}}. \tag{6.115}$$

The result is that specifying the SUSY and $B - L$ parameters, as well as any one of the ϵ_i and the two signs ζ_0 and ζ_2, specifies the v_{L_i} and the other two ϵ_i.

- Inverted Hierarchy

  The neutrino masses in the inverted hierarchy are

  $$m_1 = \sqrt{\Delta m_{31}^2}\,, \qquad m_2 = \sqrt{\Delta m_{31}^2 + \Delta m_{21}^2}\,, \qquad m_3 = 0\,. \tag{6.116}$$

  In this case, the procedure above is modified in the following ways: $m_1 \leftrightarrow m_3$, $E_1 \leftrightarrow E_3$, $V_1 \leftrightarrow V_3$. Thus, solving for V_i and E_i one obtains $V_3, E_3 = 0$ and the solutions above with the appropriate substitutions.

In both the normal and inverted neutrino hierarchies, since the dimensionful parameters ϵ_i are responsible for neutrino masses, there is a relationship between their overall scales. We understand this in terms of two fine-tuning criteria, and use it to inform our choice of the range of ϵ_i in our scans defined in Table 4.1. We then use these fine-tuning criteria to exclude finely tuned points from Figs. 4.3, 4.4, and 4.10. Relaxing these criteria does not significantly change the trends displayed in those figures. In the normal hierarchy, the first criterion is that the last terms on the left hand sides of Eqs. (6.107),(6.108) should not be much bigger than the right hand sides. Were they to be, this would require a delicate cancellation between the terms on the left hand sides to produce the correct neutrino masses. Specifically, the criterion is

$$|CE_i^2| < 10 \cdot m_i \,, \tag{6.117}$$

where $i = 2, 3$. The second criterion is that none of the ϵ_i should be much smaller than the E_i, since the former are just linear combinations of the latter. That is, take

$$10 \cdot |\epsilon_i| > |E_j| \tag{6.118}$$

for all $i = 1, 2, 3$ and $j = 2, 3$. In the invented hierarchy, these conditions are the same except with the appropriate replacements: $m_1 \leftrightarrow m_3$, $E_1 \leftrightarrow E_3$, $V_1 \leftrightarrow V_3$.

6.5 Charginos and Charged Leptons:

The charginos mix with the charged leptons due to R-parity violation. The chargino mass matrix, in the basis $\left(\tilde{W}^+,\ \tilde{H}_u^+, e_i^c,\ \tilde{W}^-,\ \tilde{H}_d^-,\ e_i\right)$, is given by

$$\mathcal{M}_{\tilde{\chi}^\pm} = \begin{pmatrix} 0_{5\times5} & \mathcal{X}^T \\ \mathcal{X} & 0_{5\times5} \end{pmatrix}, \tag{6.119}$$

with

$$\mathcal{X} = \begin{pmatrix} M_2 & \frac{1}{\sqrt{2}}g_2 v_u & 0 & 0 & 0 \\ \frac{1}{\sqrt{2}}g_2 v_d & \mu & -\frac{v_{L1}}{v_d}m_e & -\frac{v_{L2}}{v_d}m_\mu & -\frac{v_{L3}}{v_d}m_\tau \\ \frac{1}{\sqrt{2}}\, g_2 v_{L1}^* & -\epsilon_1 & m_e & 0 & 0 \\ \frac{1}{\sqrt{2}}\, g_2 v_{L2}^* & -\epsilon_2 & 0 & m_\mu & 0 \\ \frac{1}{\sqrt{2}}\, g_2 v_{L3}^* & -\epsilon_3 & 0 & 0 & m_\tau \end{pmatrix} \tag{6.120}$$

This has the schematic form

$$\mathcal{X} = \begin{pmatrix} X & \Gamma \\ G^T & m_{\ell i} \end{pmatrix}, \tag{6.121}$$

where X is on the order of the SUSY soft mass scale and Γ, G are proportional to RPV and, therefore, much smaller. The chargino mass matrix is diagonalized as

$$\mathcal{X}^D = \mathcal{U}^* \mathcal{X} \mathcal{V}^\dagger, \tag{6.122}$$

where $\mathcal{V}$ diagonalizes the positively charged charginos and $\mathcal{U}$ the negatively charged charginos. The relationships between the gauge eigenstates, $\psi^\pm$, and the mass eigenstates, $\chi^\pm$, are

$$\chi^- = \mathcal{U}\psi^-, \tag{6.123}$$

$$\chi^+ = \mathcal{V}\psi^+. \tag{6.124}$$

The first two components of the mass eigenstates are the physical chargino TeV scale states and the last three are the physical charged lepton states.

As with the neutralinos, the chargino/charged lepton mixing can be perturbatively rotated away. The mixing matrix that does this is used in the Feynman rules in Appendix 6.7 to calculate the decay widths for the third generation squarks. Following a similar procedure as for the neutralinos, the negative chargino mixing matrix is

$$\mathcal{U} = \begin{pmatrix} U & 0_{2\times3} \\ 0_{3\times2} & 1_{3\times3} \end{pmatrix} \begin{pmatrix} 1_{2\times2} & -\xi_- \\ \xi_-^\dagger & 1_{3\times3} \end{pmatrix} . \tag{6.125}$$

Successful diagonalization requires

$$\xi_- = -\left(X^T\right)^{-1} G. \tag{6.126}$$

Technically, the rows of ξ_- are the negative chargino gauge eigenstates and the columns are the charged lepton gauge eigenstates. However, the latter are very close to the mass eigenstates and will, therefore, be labeled accordingly:

$$(\xi_-)_{\tilde{W}^- \ell_i} = -\frac{g_2}{\sqrt{2} d_X} \left(v_d \epsilon_i + \mu v_{L_i}^*\right) \tag{6.127}$$

$$(\xi_-)_{\tilde{H}_d^- \ell_i} = \frac{1}{2 d_X} \left(2 M_2 \epsilon_i + g_2 v_u v_{L_i}^*\right), \tag{6.128}$$

where

$$d_X = M_2 \mu - \frac{1}{2} g_2^2 v_d v_u \tag{6.129}$$

is the determinant of X.

The positive chargino mixing matrix is

$$\mathcal{V} = \begin{pmatrix} V & 0_{2\times3} \\ 0_{3\times2} & 1_{3\times3} \end{pmatrix} \begin{pmatrix} 1_{2\times2} & -\xi_+ \\ \xi_+^\dagger & 1_{3\times3} \end{pmatrix} . \tag{6.130}$$

Solving from diagonalization yields

$$\xi_+ = -\left(X\right)^{-1}\Gamma, \tag{6.131}$$

where the components of ξ_+ are

$$\left(\xi_+\right)_{\tilde{W}^+\ell_i} = -\frac{1}{\sqrt{2}d_X} g_2 \tan\beta\, m_{\ell i} v_{Li} \tag{6.132}$$

$$\left(\xi_+\right)_{\tilde{H}_u^+\ell_i} = \frac{1}{d_X}\frac{M_2 m_{\ell i} v_{Li}}{v_d}\,. \tag{6.133}$$

6.6 Squarks

In a general SUSY scenario, all six up-type squarks mix with each other and all six down-type squarks mix with each other as well. However, flavor physics dictates that there should be little mixing between the first and second generations. Furthermore, left-right mixing in a given generation is suppressed by the corresponding fermion mass. Therefore, it is generally assumed that significant mixing only exists in the third generation, as assumption adopted in this thesis as well. The sfermion masses have different D-term contributions in this model than in the MSSM and are therefore presented here. The mass matrices $\mathcal{M}^2_{\tilde{t}}$ and $\mathcal{M}^2_{\tilde{b}}$, in the basis $\left(\tilde{t},\ \tilde{t}^{c*}\right)$ and $\left(\tilde{b},\ \tilde{b}^{c*}\right)$, are

$$\mathcal{M}^2_{\tilde{t}} = \begin{pmatrix} m^2_{\tilde{Q}_3} + m_t^2 + \frac{1}{2}c_W^2 c_{2\beta} M_Z^2 + \frac{1}{6}s_R^2 M^2_{Z_R} & m_t\left(A_t - \frac{\mu}{\tan\beta}\right) \\ m_t\left(A_t - \frac{\mu}{\tan\beta}\right) & m^2_{\tilde{t}^c} + m_t^2 + \left(\frac{1}{2} - \frac{2}{3}s_R^2\right) M^2_{Z_R} \end{pmatrix}, \tag{6.134}$$

$$\mathcal{M}^2_{\tilde{b}} = \begin{pmatrix} m^2_{\tilde{Q}_3} + m_b^2 - \frac{1}{2}c_W^2 c_{2\beta} M_Z^2 + \frac{1}{6}s_R^2 M^2_{Z_R} & m_b\left(A_b - \tan\beta\,\mu\right) \\ m_b\left(A_b - \tan\beta\,\mu\right) & m^2_{\tilde{b}^c} + m_b^2 + \left(\frac{1}{3}s_R^2 - \frac{1}{2}\right) M^2_{Z_R} \end{pmatrix}, \tag{6.135}$$

where $c_{2\beta} \equiv \cos 2\beta$, $c_W \equiv \cos\theta_W$, θ_W is the weak mixing angle and $s_R \equiv \sin\theta_R = g_{BL}/\sqrt{g_{BL}^2 + g_R^2}$. This latter quantity is technically a free parameter from a low energy perspective. However, in the UV physics discussed in reference [1], it takes the value $s_R^2 \sim 0.6$. In this thesis, the numerical work was carried out by scanning over the physical masses of the squarks and, therefore, this parameter is not used. Here, $m_t,\ m_b$ are the top and bottom masses and $Y_t A_t$, $Y_b A_b$ are the trilinear a-terms.The physical states are related to the gauge states by

$$\begin{pmatrix} \tilde{f}_1 \\ \tilde{f}_2 \end{pmatrix} = \begin{pmatrix} \cos\theta_f & \sin\theta_f \\ -\sin\theta_f & \cos\theta_f \end{pmatrix} \begin{pmatrix} \tilde{f} \\ \tilde{f}^{c*} \end{pmatrix} , \tag{6.136}$$

where $\tilde{f}$ represent either $\tilde{t}$ or $\tilde{b}$ and $m_{\tilde{f}_1} < m_{\tilde{f}_2}$. The lightest sfermion is purely left-handed (right-handed) when its mixing angle is 0° (90°). The mixing angles are given by

$$\tan 2\theta_t = \frac{2m_t\left(A_t - \frac{\mu}{\tan\beta}\right)}{m_{\tilde{Q}_3}^2 + \frac{1}{2}c_W^2 c_{2\beta} M_Z^2 - m_{\tilde{t}^c}^2 + \left(-\frac{1}{2} + \frac{5}{6}s_R^2\right) M_{Z_R}^2}, \tag{6.137}$$

$$\tan 2\theta_b = \frac{2m_b\left(A_b - \mu\tan\beta\right)}{m_{\tilde{Q}_3}^2 - \frac{1}{2}c_W^2 c_{2\beta} M_Z^2 - m_{\tilde{b}^c}^2 + \left(\frac{1}{2} - \frac{1}{6}s_R^2\right) M_{Z_R}^2}, \tag{6.138}$$

when $\mathcal{M}_{\tilde{t}\,11}^2 > \mathcal{M}_{\tilde{t}\,22}^2$ and $\mathcal{M}_{\tilde{b}\,11}^2 > \mathcal{M}_{\tilde{b}\,22}^2$. When $\mathcal{M}_{\tilde{t}\,11}^2 < \mathcal{M}_{\tilde{t}\,22}^2$, θ_t is shifted by $-\pi/2$ and when $\mathcal{M}_{\tilde{b}\,11}^2 < \mathcal{M}_{\tilde{b}\,22}^2$, θ_b is shifted by $-\pi/2$.

It is worthwhile to note that a purely left-handed lightest stop ($\theta_t = 0$) cannot be the LSP. This is because both the left-handed stop and the left-handed sbottom get some of their mass from the $m_{\tilde{Q}_3}^2$ soft mass parameter (as shown in Eqs. (6.134),(6.135)) and their respective fermion masses, m_t and m_b. Since $m_t^2 > m_b^2$, $m_{\tilde{t}_1}^2 > m_{\tilde{b}_1}^2$ for a purely left-handed lightest stop. It is possible that mixing in the sbottom sector could change this, but those effects are expected to be small since they are proportional to m_b (see the off-diagonal elements of Eq. (6.135)). For a mostly left-handed stop ($\theta_t \approx 0$), the lightest stop can be the LSP for certain values of some parameters that do not effect the physics studied in this thesis.

6.7 Feynman Rules

In this Appendix, the Feynman rules for the interactions between third generation squarks, quarks and neutralinos, and charginos are listed in the physical basis. The physical neutralinos and charginos are labeled by the subscript n. For the neutralinos, $\chi_n^0 = (\chi_1, ..., \chi_6, \nu_i)$ where the first six states are the TeV scale neutralinos and the last three states are the physical neutrinos labeled by i. For the charginos $\chi_n^\pm = (\chi_1^\pm, \chi_2^\pm, \ell_i)$ where the first two states are the TeV scale charginos and the lass three states are the charged leptons labeled by i. In this case, the physical i^{th} neutrino is given by χ_{6+i}^0 and the physical i^{th} charged lepton is $\chi_{2+i}^\pm$.

The Feynman rule for each process will be followed by an approximation of that Feynman rule relevant for the R-parity violating decays discussed in the paper; namely, leptoquark-like decays. This approximation will be given in the limit $M_{Z_R}^2 \gg m_{\text{soft}}^2 \gg v_{d,u}^2$ using the perturbative diagonalizations presented in Appendices 6.4 and 6.5. We also employ the fact that $\epsilon_i^2 \gg {v_{L}}_i^2$ in general. This is useful for an analytic understanding of the strengths of the different decay channels.

6.7.1 Stops

For the lightest stop vertex $\tilde{t}_1\, t\, \tilde{\chi}_n^0$:

$$g_{\tilde{t}_1 t \chi_n^0} = G^L_{\tilde{t}_1 t \chi_n^0} P_L + G^R_{\tilde{t}_1 t \chi_n^0} P_R \;, \tag{6.139}$$

where

$$G^L_{\tilde{t}_1 t \chi_n^0} = \frac{1}{\sqrt{2}} g_R s_{\theta_t} \mathcal{N}^*_{n1} + \frac{1}{3\sqrt{2}} g_{BL} s_{\theta_t} \mathcal{N}^*_{n5} - Y_t c_{\theta_t} \mathcal{N}^*_{n4} \;, \tag{6.140}$$

$$G^R_{\tilde{t}_1 t \chi_n^0} = -\frac{1}{\sqrt{2}} g_2 c_{\theta_t} \mathcal{N}_{n2} - \frac{1}{3\sqrt{2}} g_{BL} c_{\theta_t} \mathcal{N}_{n5} - Y_t s_{\theta_t} \mathcal{N}_{n4} \;. \tag{6.141}$$

and $P_{\frac{L}{R}} = \frac{1}{2}(1 \pm \gamma_5)$. For the neutrino components of the physical neutralinos, $\chi_{6+i} = \nu_i$, these G parameters are approximated by

$$\begin{aligned} G^L_{\tilde{t}_1 t \nu_i} \approx (V_{\text{PMNS}})_{ji} \Bigg[& \frac{1}{\sqrt{2}} g_R s_{\theta_t} \left(-g_R \frac{4M_{BL}\mu v_u + g_{BL}^2 v_R^2 v_d}{2M_{\tilde{Y}} \mu v_R^2} \epsilon_j - \frac{g_R g_{BL}^2}{2M_{\tilde{Y}}} {v_L}_j^* \right) \\ & - \frac{1}{3\sqrt{2}} g_{BL} s_{\theta_t} \left(g_{BL} \frac{g_R^2 v_R^2 v_d - 4M_R \mu v_u}{2M_{\tilde{Y}} \mu v_R^2} \epsilon_j + \frac{g_{BL} g_R^2}{2M_{\tilde{Y}}} {v_L}_j^* \right) \\ & - Y_t c_{\theta_t} \left(\frac{M_{\tilde{\gamma}} v_R^2 v_d^2 + 4 g_R^2 M_2 M_{BL} \mu v_d v_u}{4M_{\tilde{Y}} M_2 v_R^2 \mu^2} \epsilon_j + \frac{v_d M_{\tilde{\gamma}}}{4M_{\tilde{Y}} M_2 \mu} {v_L}_j^* \right) \Bigg] \end{aligned} \tag{6.142}$$

$$
\begin{aligned}
G^R_{\tilde{t}_1 t\nu_i} \approx (V_{\text{PMNS}})^*_{ji} \Bigg[& -\frac{1}{\sqrt{2}} g_2 c_{\theta_t} \left(\frac{g_2 v_d}{2M_2 \mu} \epsilon_j^* + \frac{g_2}{2M_2} v_{Lj} \right) \\
& + \frac{1}{3\sqrt{2}} g_{BL} c_{\theta_t} \left(g_{BL} \frac{g_R^2 v_R^2 v_d - 4M_R \mu v_u}{2M_{\tilde{Y}} \mu v_R^2} \epsilon_j^* + \frac{g_{BL} g_R^2}{2M_{\tilde{Y}}} v_{Lj} \right) \\
& - Y_t s_{\theta_t} \left(\frac{M_{\tilde{\gamma}} v_R^2 v_d^2 + 4 g_R^2 M_2 M_{BL} \mu v_d v_u}{4M_{\tilde{Y}} M_2 v_R^2 \mu^2} \epsilon_j^* + \frac{v_d M_{\tilde{\gamma}}}{4M_{\tilde{Y}} M_2 \mu} v_{Lj} \right) \Bigg] .
\end{aligned}
\tag{6.143}
$$

For the lightest stop vertex $\tilde{t}_1 \, b \, \tilde{\chi}_n^-$:

$$
g_{\tilde{t}_1 b \chi_n^\pm} = G^L_{\tilde{t}_1 b \chi_n^\pm} P_L + G^R_{\tilde{t}_1 b \chi_n^\pm} P_R \, , \tag{6.144}
$$

with

$$
G^L_{\tilde{t}_1 b \chi_n^\pm} = Y_b c_{\theta_t} \mathcal{U}^*_{n2} \, , \tag{6.145}
$$

$$
G^R_{\tilde{t}_1 b \chi_n^\pm} = -\frac{1}{\sqrt{2}} g_2 c_{\theta_t} \mathcal{V}_{n1} + Y_t s_{\theta_t} \mathcal{V}_{n2} \, . \tag{6.146}
$$

For the charged lepton components of the physical charginos, $\chi^\pm_{2+i} = \ell_i$, these G parameters are approximated as

$$
G^L_{\tilde{t}_1 b \ell_i} \approx Y_b c_{\theta_t} \frac{1}{\mu} \epsilon_i \tag{6.147}
$$

$$
G^R_{\tilde{t}_1 b \ell_i} \approx Y_t s_{\theta_t} \frac{m_{\ell_i}}{\sqrt{2} v_d \mu} v_{Li}^* \, . \tag{6.148}
$$

The approximations show that the top–neutrino channel is suppressed either by factors of $v_{d,u}/m_{\text{soft}}$ or by v_{Li} compared to the bottom-charged lepton channel. Therefore, the bottom-charged lepton channel dominates except for the case were the stop is mostly right-handed.

6.7.2 Sbottoms

For the lightest sbottom vertex $\tilde{b}_1 \, b \, \tilde{\chi}_n^0$:

$$
g_{\tilde{b}_1 b \chi_n^0} = G^L_{\tilde{b}_1 b \chi_n^0} P_L + G^R_{\tilde{b}_1 b \chi_n^0} P_R \, , \tag{6.149}
$$

where n labels the combined neutralinos (charginos) and neutrinos (charged leptons), and

$$G^L_{\tilde{b}_1 b \chi^0_n} = -\frac{1}{\sqrt{2}} g_R s_{\theta_b} \mathcal{N}^*_{n1} + \frac{1}{3\sqrt{2}} g_{BL} s_{\theta_b} \mathcal{N}^*_{n5} - Y_b c_{\theta_b} \mathcal{N}^*_{n3} \ , \tag{6.150}$$

$$G^R_{\tilde{b}_1 b \chi^0_n} = \frac{1}{\sqrt{2}} g_2 c_{\theta_b} \mathcal{N}_{n2} - \frac{1}{3\sqrt{2}} g_{BL} c_{\theta_b} \mathcal{N}_{n5} - Y_b s_{\theta_b} \mathcal{N}_{n3} \ . \tag{6.151}$$

For the neutrino components of the physical neutralinos, $\chi_{6+i} = \nu_i$, these G parameters are approximated by

$$G^L_{\tilde{b}_1 b \nu_i} \approx V_{\text{PMNS}\,ji} Y_b c_{\theta_b} \frac{\epsilon^*_j}{\mu} \ , \tag{6.152}$$

$$G^R_{\tilde{b}_1 b \nu_i} \approx V_{\text{PMNS}}{}^*_{ji} Y_b s_{\theta_b} \frac{\epsilon_i}{\mu} \ . \tag{6.153}$$

For the lightest sbottom vertex $\tilde{b}_1 \, t \, \tilde{\chi}^-_n$:

$$g_{\tilde{b}_1 t \tilde{\chi}^-_n} = G^L_{\tilde{b}_1 t \tilde{\chi}^-_n} P_L + G^R_{\tilde{b}_1 t \tilde{\chi}^-_n} P_R \ , \tag{6.154}$$

with

$$G^L_{\tilde{b}_1 t \tilde{\chi}^\pm_n} = Y_t c_{\theta_b} V^*_{n2} \ , \tag{6.155}$$

$$G^R_{\tilde{b}_1 t \tilde{\chi}^\pm_n} = -g_2 c_{\theta_b} U_{n1} + Y_b s_{\theta_b} U_{n2} \ . \tag{6.156}$$

For the charged lepton components of the physical charginos, $\chi^\pm_{2+i} = \ell_i$, these G parameters are approximated as

$$G^L_{\tilde{b}_1 t \ell_i} \approx Y_t c_{\theta_b} \frac{m_{\ell_i}}{v_d \mu} v_{Li} \ , \tag{6.157}$$

$$G^R_{\tilde{b}_1 t \ell_i} \approx Y_b s_{\theta_b} \frac{\epsilon^*_i}{\mu} \ . \tag{6.158}$$

In the sbottom sector, the bottom–neutrino and top–charged lepton channels are both unsuppressed except in the case of the mostly left-handed sbottom in which case the bottom–neutrino channel dominates.

Bibliography

[1] B. A. Ovrut, A. Purves and S. Spinner, "Wilson Lines and a Canonical Basis of SU(4) Heterotic Standard Models," JHEP **1211**, 026 (2012) [arXiv:1203.1325 [hep-th]].

[2] Z. Marshall, B. A. Ovrut, A. Purves and S. Spinner, "Spontaneous R-Parity Breaking, Stop LSP Decays and the Neutrino Mass Hierarchy," Phys. Lett. B **732**, 325 (2014) [arXiv:1401.7989 [hep-ph]].

[3] Z. Marshall, B. A. Ovrut, A. Purves and S. Spinner, "LSP Squark Decays at the LHC and the Neutrino Mass Hierarchy," Phys. Rev. D **90**, 015034 (2014) [arXiv:1402.5434 [hep-ph]].

[4] B. A. Ovrut, A. Purves and S. Spinner, "A Statistical Analysis of the Minimal SUSY B-L Theory," arXiv:1412.6103 [hep-ph].

[5] B. A. Ovrut, A. Purves and S. Spinner, arXiv:1503.01473 [hep-ph].

[6] L. M. Krauss and F. Wilczek, "Discrete Gauge Symmetry in Continuum Theories," Phys. Rev. Lett. **62**, 1221 (1989).

[7] A. Font, L. E. Ibanez and F. Quevedo, "Does Proton Stability Imply the Existence of an Extra Z0?," Phys. Lett. B **228**, 79 (1989).

[8] S. P. Martin, "Some simple criteria for gauged R-parity," Phys. Rev. D **46**, 2769 (1992) [hep-ph/9207218].

[9] C. S. Aulakh, A. Melfo, A. Rasin and G. Senjanovic, "Seesaw and supersymmetry or exact R-parity," Phys. Lett. B **459** (1999) 557 [hep-ph/9902409].

[10] C. S. Aulakh, B. Bajc, A. Melfo, A. Rasin and G. Senjanovic, "SO(10) theory of R-parity and neutrino mass," Nucl. Phys. B **597** (2001) 89 [hep-ph/0004031].

[11] K. S. Babu and R. N. Mohapatra, "Minimal Supersymmetric Left-Right Model," Phys. Lett. B **668**, 404 (2008) [arXiv:0807.0481 [hep-ph]].

[12] D. Feldman, P. Fileviez Perez and P. Nath, "R-parity Conservation via the Stueckelberg Mechanism: LHC and Dark Matter Signals," arXiv:1109.2901 [hep-ph].

[13] P. Fileviez Perez and M. B. Wise, "Low Energy Supersymmetry with Baryon and Lepton Number Gauged," Phys. Rev. D **84**, 055015 (2011) [arXiv:1105.3190 [hep-ph]].

[14] C. S. Aulakh and R. N. Mohapatra, "Neutrino as the Supersymmetric Partner of the Majoron," Phys. Lett. B **119**, 136 (1982).

[15] M. J. Hayashi and A. Murayama, "Radiative Breaking of $SU(2)_R X U(1)_{(B-L)}$ Gauge Symmetry Induced by Broken $N = 1$ Supergravity in a Left-right Symmetric Model," Phys. Lett. B **153**, 251 (1985).

[16] R. N. Mohapatra, "Mechanism For Understanding Small Neutrino Mass In Superstring Theories," Phys. Rev. Lett. **56** (1986) 561.

[17] A. Masiero and J. W. F. Valle, "A Model For Spontaneous R Parity Breaking," Phys. Lett. B **251** (1990) 273.

[18] E. Nikolidakis and C. Smith, "Minimal Flavor Violation, Seesaw, and R-parity," Phys. Rev. D **77**, 015021 (2008) [arXiv:0710.3129 [hep-ph]].

[19] C. Csaki, Y. Grossman and B. Heidenreich, "MFV SUSY: A Natural Theory for R-Parity Violation," Phys. Rev. D **85**, 095009 (2012) [arXiv:1111.1239 [hep-ph]].

[20] P. Fileviez Perez and S. Spinner, "Spontaneous R-Parity Breaking and Left-Right Symmetry," Phys. Lett. B **673** (2009) 251 [arXiv:0811.3424 [hep-ph]].

[21] V. Barger, P. Fileviez Perez and S. Spinner, "Minimal gauged U(1)(B-L) model with spontaneous R-parity violation," Phys. Rev. Lett. **102** (2009) 181802 [arXiv:0812.3661 [hep-ph]].

[22] P. Fileviez Perez and S. Spinner "Spontaneous R-Parity Breaking in SUSY Models," Phys. Rev. D **80**, 01004 (2009) [arXiv:0904.2213 [hep-ph]]

[23] L. L. Everett, P. Fileviez Perez and S. Spinner, "The Right Side of Tev Scale Spontaneous R-Parity Violation," Phys. Rev. D **80** (2009) 055007 [arXiv:0906.4095 [hep-ph]].

[24] M. Evans and B. A. Ovrut, "The World Sheet Supergravity of the Heterotic String," Phys. Lett. B **171**, 177 (1986).

[25] A. Lukas, B. A. Ovrut, K. S. Stelle and D. Waldram, "The Universe as a domain wall," Phys. Rev. D **59**, 086001 (1999) [hep-th/9803235]

[26] V. Braun, Y. -H. He, B. A. Ovrut and T. Pantev, "A Heterotic standard model," Phys. Lett. B **618**, 252 (2005) [hep-th/0501070]

[27] V. Braun, Y. -H. He, B. A. Ovrut and T. Pantev, "The Exact MSSM spectrum from string theory," JHEP **0605**, 043 (2006) [hep-th/0512177]

[28] V. Braun, Y. -H. He and B. A. Ovrut, "Stability of the minimal heterotic standard model bundle," JHEP **0606**, 032 (2006) [hep-th/0602073].

[29] M. Ambroso and B. Ovrut, "The B-L/Electroweak Hierarchy in Heterotic String and M-Theory," JHEP **0910**, 011 (2009) [arXiv:0904.4509 [hep-th]]

[30] P. Fileviez Perez and S. Spinner, "The Minimal Theory for R-parity Violation at the LHC," arXiv:1201.5923 [hep-ph].

[31] P. Fileviez Perez and S. Spinner, "Supersymmetry at the LHC and The Theory of R-parity," Phys. Lett. B **728**, 489 (2014) [arXiv:1308.0524 [hep-ph]].

[32] D. K. Ghosh, G. Senjanovic and Y. Zhang, "Naturally Light Sterile Neutrinos from Theory of R-parity," Phys. Lett. B **698** (2011) 420 [arXiv:1010.3968 [hep-ph]].

[33] V. Barger, P. Fileviez Perez and S. Spinner, "Three Layers of Neutrinos," Phys. Lett. B **696** (2011) 509 [arXiv:1010.4023 [hep-ph]].

[34] P. A. R. Ade *et al.* [Planck Collaboration], "Planck 2013 results. XVI. Cosmological parameters," arXiv:1303.5076 [astro-ph.CO].

[35] S. Borgani, A. Masiero and M. Yamaguchi, "Light gravitinos as mixed dark matter," Phys. Lett. B **386**, 189 (1996) [hep-ph/9605222].

[36] F. Takayama and M. Yamaguchi, "Gravitino dark matter without R-parity," Phys. Lett. B **485**, 388 (2000) [hep-ph/0005214].

[37] W. Buchmuller, L. Covi, K. Hamaguchi, A. Ibarra and T. Yanagida, "Gravitino Dark Matter in R-Parity Breaking Vacua," JHEP **0703**, 037 (2007) [hep-ph/0702184 [hep-ph]].

[38] S. P. Martin, "A Supersymmetry primer," Adv. Ser. Direct. High Energy Phys. **21**, 1 (2010) [hep-ph/9709356].

[39] B. Mukhopadhyaya, S. Roy and F. Vissani, "Correlation between neutrino oscillations and collider signals of supersymmetry in an R-parity violating model," Phys. Lett. B **443**, 191 (1998) [hep-ph/9808265].

[40] E. J. Chun and J. S. Lee, "Implication of Super-Kamiokande data on R-parity violation," Phys. Rev. D **60**, 075006 (1999) [hep-ph/9811201].

[41] E. J. Chun and S. K. Kang, "One loop corrected neutrino masses and mixing in supersymmetric standard model without R-parity," Phys. Rev. D **61**, 075012 (2000) [hep-ph/9909429].

[42] M. Hirsch, M. A. Diaz, W. Porod, J. C. Romao and J. W. F. Valle, "Neutrino masses and mixings from supersymmetry with bilinear R parity violation: A Theory for solar and atmospheric neutrino oscillations," Phys. Rev. D **62**, 113008 (2000) [Erratum-ibid. D **65**, 119901 (2002)] [hep-ph/0004115].

[43] G. Gamberini, G. Ridolfi and F. Zwirner, "On Radiative Gauge Symmetry Breaking in the Minimal Supersymmetric Model," Nucl. Phys. B **331**, 331 (1990).

[44] K. S. Babu, C. F. Kolda and J. March-Russell, "Leptophobic U(1)s and the R(b) - R(c) crisis," Phys. Rev. D **54**, 4635 (1996) [arXiv:hep-ph/9603212].

[45] F. del Aguila, G. D. Coughlan and M. Quiros, "Gauge Coupling Renormalization With Several U(1) Factors," Nucl. Phys. B **307**, 633 (1988) [Erratum-ibid. B **312**, 751 (1989)].

[46] B. Holdom, "Two U(1)'S And Epsilon Charge Shifts," Phys. Lett. B **166**, 196 (1986).

[47] K. R. Dienes, C. F. Kolda and J. March-Russell, “Kinetic mixing and the supersymmetric gauge hierarchy,” Nucl. Phys. B **492**, 104 (1997) [arXiv:hep-ph/9610479].

[48] R. Foot and X. G. He, “Comment On Z Z-Prime Mixing In Extended Gauge Theories,” Phys. Lett. B **267**, 509 (1991).

[49] R. M. Fonseca, M. Malinsky, W. Porod and F. Staub, “Running soft parameters in SUSY models with multiple U(1) gauge factors,” Nucl. Phys. B **854** (2012) 28 [arXiv:1107.2670 [hep-ph]].

[50] K.A. Olive et al. (Particle Data Group), Chin. Phys. C, 38, 090001 (2014).

[51] S. P. Martin and M. T. Vaughn, “Two loop renormalization group equations for soft supersymmetry breaking couplings,” Phys. Rev. D **50**, 2282 (1994) [Erratum-ibid. D **78**, 039903 (2008)] [hep-ph/9311340].

[52] A. Djouadi, “The Anatomy of electro-weak symmetry breaking. I: The Higgs boson in the standard model,” Phys. Rept. **457**, 1 (2008) [hep-ph/0503172].

[53] J. R. Ellis, K. Enqvist, D. V. Nanopoulos and K. Tamvakis, “Gaugino Masses and Grand Unification,” Phys. Lett. B **155**, 381 (1985).

[54] K. Choi, A. Falkowski, H. P. Nilles and M. Olechowski, “Soft supersymmetry breaking in KKLT flux compactification,” Nucl. Phys. B **718**, 113 (2005) [hep-th/0503216].

[55] M. Ambroso and B. A. Ovrut, “The B-L/Electroweak Hierarchy in Smooth Heterotic Compactifications,” Int. J. Mod. Phys. A **25**, 2631 (2010) [arXiv:0910.1129 [hep-th]]

[56] N. Arkani-Hamed and S. Dimopoulos, “Supersymmetric unification without low energy supersymmetry and signatures for fine-tuning at the LHC,” JHEP **0506**, 073 (2005) [hep-th/0405159].

[57] M. E. Cabrera, J. A. Casas and A. Delgado, “Upper Bounds on Superpartner Masses from Upper Bounds on the Higgs Boson Mass,” Phys. Rev. Lett. **108**, 021802 (2012) [arXiv:1108.3867 [hep-ph]].

[58] G. F. Giudice and A. Strumia, “Probing High-Scale and Split Supersymmetry with Higgs Mass Measurements,” Nucl. Phys. B **858**, 63 (2012) [arXiv:1108.6077 [hep-ph]].

[59] LEP2 SUSY Working Group, ALEPH, DELPHI, L3 and OPAL experiments, note LEPSUSYWG/04-01.1, http://lepsusy.web.cern.ch/lepsusy.

[60] LEP2 SUSY Working Group, ALEPH, DELPHI, L3 and OPAL experiments, note LEPSUSYWG/02-09.2, http://lepsusy.web.cern.ch/lepsusy.

[61] LEP2 SUSY Working Group, ALEPH, DELPHI, L3 and OPAL experiments, note LEPSUSYWG/02-10.1, http://lepsusy.web.cern.ch/lepsusy.

[62] LEP2 SUSY Working Group, ALEPH, DELPHI, L3 and OPAL experiments, note LEPSUSYWG/01-03.1, http://lepsusy.web.cern.ch/lepsusy.

[63] LEP2 SUSY Working Group, ALEPH, DELPHI, L3 and OPAL experiments, note LEPSUSYWG/02-04.1, http://lepsusy.web.cern.ch/lepsusy.

[64] CMS Collaboration [CMS Collaboration], “Search for supersymmetry in hadronic final states using MT2 with the CMS detector at sqrt(s) = 8 TeV,” CMS-PAS-SUS-13-019.

[65] G. Aad *et al.* [ATLAS Collaboration], “Search for squarks and gluinos with the ATLAS detector in final states with jets and missing transverse momentum using $\sqrt{s} = 8$ TeV proton–proton collision data,” JHEP **1409**, 176 (2014) [arXiv:1405.7875 [hep-ex]].

[66] [ATLAS Collaboration], “Search for high-mass dilepton resonances in 20 fb^{-1} of pp collisions at $\sqrt{s} = 8$ TeV with the ATLAS experiment,” ATLAS-CONF-2013-017.

[67] CMS Collaboration [CMS Collaboration], “Search for Resonances in the Dilepton Mass Distribution in pp Collisions at sqrt(s) = 8 TeV,” CMS-PAS-EXO-12-061.

[68] G. Aad *et al.* [ATLAS Collaboration], “Measurement of the Higgs boson mass from the $H \to \gamma\gamma$ and $H \to ZZ^* \to 4\ell$ channels with the ATLAS detector using 25 fb^{-1} of pp collision data,” Phys. Rev. D **90**, 052004 (2014) [arXiv:1406.3827 [hep-ex]].

[69] S. Chatrchyan *et al.* [CMS Collaboration], "Observation of a new boson with mass near 125 GeV in pp collisions at $\sqrt{s}$ = 7 and 8 TeV," JHEP **1306**, 081 (2013) [arXiv:1303.4571 [hep-ex]].

[70] J. R. Ellis and D. V. Nanopoulos, "Flavor Changing Neutral Interactions in Broken Supersymmetric Theories," Phys. Lett. B **110**, 44 (1982).

[71] R. Barbieri and R. Gatto, "Conservation Laws for Neutral Currents in Spontaneously Broken Supersymmetric Theories," Phys. Lett. B **110**, 211 (1982).

[72] B. A. Campbell, "Supersymmetry And Neutral Flavor Nonconservation," Phys. Rev. D **28**, 209 (1983).

[73] J. R. Ellis, S. Ferrara and D. V. Nanopoulos, "CP Violation and Supersymmetry," Phys. Lett. B **114**, 231 (1982).

[74] W. Buchmuller and D. Wyler, "CP Violation and R Invariance in Supersymmetric Models of Strong and Electroweak Interactions," Phys. Lett. B **121**, 321 (1983).

[75] J. Polchinski and M. B. Wise, "The Electric Dipole Moment of the Neutron in Low-Energy Supergravity," Phys. Lett. B **125**, 393 (1983).

[76] F. del Aguila, M. B. Gavela, J. A. Grifols and A. Mendez, "Specifically Supersymmetric Contribution to Electric Dipole Moments," Phys. Lett. B **126**, 71 (1983) [Erratum-ibid. B **129**, 473 (1983)].

[77] D. V. Nanopoulos and M. Srednicki, "The Demon of Local SUSY," Phys. Lett. B **128**, 61 (1983).

[78] L. J. Hall, R. Rattazzi and U. Sarid, "The Top quark mass in supersymmetric SO(10) unification," Phys. Rev. D **50**, 7048 (1994) [hep-ph/9306309, hep-ph/9306309].

[79] M. S. Carena, M. Olechowski, S. Pokorski and C. E. M. Wagner, "Electroweak symmetry breaking and bottom - top Yukawa unification," Nucl. Phys. B **426**, 269 (1994) [hep-ph/9402253].

[80] N. Arkani-Hamed, H. C. Cheng and L. J. Hall, "A New supersymmetric framework for fermion masses," Nucl. Phys. B **472**, 95 (1996) [hep-ph/9512302].

[81] C. F. Berger, J. S. Gainer, J. L. Hewett and T. G. Rizzo, “Supersymmetry Without Prejudice,” JHEP **0902**, 023 (2009) [arXiv:0812.0980 [hep-ph]].

[82] J. A. Conley, J. S. Gainer, J. L. Hewett, M. P. Le and T. G. Rizzo, “Supersymmetry Without Prejudice at the LHC,” Eur. Phys. J. C **71**, 1697 (2011) [arXiv:1009.2539 [hep-ph]].

[83] L. E. Ibanez and G. G. Ross, “SU(2)-L x U(1) Symmetry Breaking as a Radiative Effect of Supersymmetry Breaking in Guts,” Phys. Lett. B **110**, 215 (1982).

[84] J. R. Ellis, D. V. Nanopoulos and K. Tamvakis, “Grand Unification in Simple Supergravity,” Phys. Lett. B **121**, 123 (1983).

[85] L. Alvarez-Gaume, J. Polchinski and M. B. Wise, “Minimal Low-Energy Supergravity,” Nucl. Phys. B **221**, 495 (1983).

[86] W. Porod, M. Hirsch, J. Romao and J. W. F. Valle, “Testing neutrino mixing at future collider experiments,” Phys. Rev. D **63**, 115004 (2001) [hep-ph/0011248].

[87] M. Hirsch and W. Porod, “Neutrino properties and the decay of the lightest supersymmetric particle,” Phys. Rev. D **68**, 115007 (2003) [hep-ph/0307364].

[88] P. W. Graham, D. E. Kaplan, S. Rajendran and P. Saraswat, “Displaced Supersymmetry,” JHEP **1207**, 149 (2012) [arXiv:1204.6038 [hep-ph]].

[89] P. W. Graham, S. Rajendran and P. Saraswat, “Supersymmetric crevices: Missing signatures of R -parity violation at the LHC,” Phys. Rev. D **90**, no. 7, 075005 (2014) [arXiv:1403.7197 [hep-ph]].

[90] CMS Collaboration [CMS Collaboration], “Search for Pair-production of First Generation Scalar Leptoquarks in pp Collisions at sqrt s = 8 TeV,” CMS-PAS-EXO-12-041.

[91] E. J. Chun, S. Jung, H. M. Lee and S. C. Park, “Stop and Sbottom LSP with R-parity Violation,” Phys. Rev. D **90**, no. 11, 115023 (2014) [arXiv:1408.4508 [hep-ph]].

[92] F. S. Queiroz, K. Sinha and A. Strumia, “Leptoquarks, Dark Matter, and Anomalous LHC Events,” Phys. Rev. D **91**, no. 3, 035006 (2015) [arXiv:1409.6301 [hep-ph]].

[93] B. Allanach, A. Alves, F. S. Queiroz, K. Sinha and A. Strumia, “Interpreting the CMS $\ell^+\ell^- jj \not{E}_{\rm T}$ Excess with a Leptoquark Model,” arXiv:1501.03494 [hep-ph].

[94] J. A. Evans and Y. Kats, “LHC Coverage of RPV MSSM with Light Stops,” JHEP **1304**, 028 (2013) [arXiv:1209.0764 [hep-ph]].

[95] D. Aristizabal Sierra, M. Hirsch and W. Porod, “R-parity violating sneutrino decays,” JHEP **0509**, 033 (2005) [hep-ph/0409241].

[96] D. Aristizabal Sierra, D. Restrepo and S. Spinner, “LSP sneutrino decays into heavy standard model pairs,” JHEP **1305**, 046 (2013) [arXiv:1212.3310 [hep-ph]].

[97] A. Bartl, M. Hirsch, T. Kernreiter, W. Porod and J. W. F. Valle, “Testing the mechanism of R parity breaking with slepton LSP decays,” JHEP **0311**, 005 (2003) [hep-ph/0306071].

[98] M. A. Luty, “2004 TASI lectures on supersymmetry breaking,” hep-th/0509029.

[99] I. Antoniadis, E. M. Babalic and D. M. Ghilencea, “Naturalness in low-scale SUSY models and ”non-linear” MSSM,” Eur. Phys. J. C **74**, no. 9, 3050 (2014) [arXiv:1405.4314 [hep-ph]].

[100] P. Ciafaloni and A. Strumia, “Naturalness upper bounds on gauge mediated soft terms,” Nucl. Phys. B **494**, 41 (1997) [hep-ph/9611204].

[101] B. de Carlos and J. A. Casas, “One loop analysis of the electroweak breaking in supersymmetric models and the fine tuning problem,” Phys. Lett. B **309**, 320 (1993) [hep-ph/9303291].

[102] J. A. Casas, J. R. Espinosa and I. Hidalgo, “The MSSM fine tuning problem: A Way out,” JHEP **0401**, 008 (2004) [hep-ph/0310137].

[103] J. R. Ellis, K. Enqvist, D. V. Nanopoulos and F. Zwirner, “Observables in Low-Energy Superstring Models,” Mod. Phys. Lett. A **1**, 57 (1986).

[104] R. Barbieri and G. F. Giudice, "Upper Bounds on Supersymmetric Particle Masses," Nucl. Phys. B **306**, 63 (1988).

[105] G. W. Anderson and D. J. Castano, "Measures of fine tuning," Phys. Lett. B **347**, 300 (1995) [hep-ph/9409419].

[106] The ATLAS collaboration, ATLAS-CONF-2015-015, ATLAS-COM-CONF-2015-017.

[107] R. Barbier, C. Berat, M. Besancon, M. Chemtob, A. Deandrea, E. Dudas, P. Fayet and S. Lavignac *et al.*, "R-parity violating supersymmetry," Phys. Rept. **420**, 1 (2005) [hep-ph/0406039].

[108] M. Kusakabe, T. Kajino, T. Yoshida and G. J. Mathews, "Effect of Long-lived Strongly Interacting Relic Particles on Big Bang Nucleosynthesis," Phys. Rev. D **80**, 103501 (2009) [arXiv:0906.3516 [hep-ph]].

[109] S. Raby, "Gauge mediated SUSY breaking at an intermediate scale," Phys. Rev. D **56**, 2852 (1997) [hep-ph/9702299].

[110] E. L. Berger and Z. Sullivan, "Lower limits on R parity violating couplings in supersymmetry," Phys. Rev. Lett. **92**, 201801 (2004) [hep-ph/0310001].

[111] M. R. Buckley, B. Echenard, D. Kahawala and L. Randall, "Stable Colored Particles R-SUSY Relics or Not?," JHEP **1101**, 013 (2011) [arXiv:1008.2756 [hep-ph]].

[112] G. Aad *et al.* [ATLAS Collaboration], "Search for stable hadronising squarks and gluinos with the ATLAS experiment at the LHC," Phys. Lett. B **701**, 1 (2011) [arXiv:1103.1984 [hep-ex]].

[113] G. Aad *et al.* [ATLAS Collaboration], "Search for decays of stopped, long-lived particles from 7 TeV pp collisions with the ATLAS detector," Eur. Phys. J. C **72**, 1965 (2012) [arXiv:1201.5595 [hep-ex]].

[114] G. Aad *et al.* [ATLAS Collaboration], "Searches for heavy long-lived sleptons and R-Hadrons with the ATLAS detector in pp collisions at $\sqrt{s} = 7$ TeV," Phys. Lett. B **720**, 277 (2013) [arXiv:1211.1597 [hep-ex]].

[115] G. Aad *et al.* [ATLAS Collaboration], "Search for displaced vertices arising from decays of new heavy particles in 7 TeV pp collisions at ATLAS," Phys. Lett. B **707**, 478 (2012) [arXiv:1109.2242 [hep-ex]].

[116] G. Aad *et al.* [ATLAS Collaboration], "Search for long-lived, heavy particles in final states with a muon and multi-track displaced vertex in proton-proton collisions at $\sqrt{s} = 7$ TeV with the ATLAS detector," Phys. Lett. B **719**, 280 (2013) [arXiv:1210.7451 [hep-ex]].

[117] S. Chatrchyan *et al.* [CMS Collaboration], "Search for long-lived particles decaying to photons and missing energy in proton-proton collisions at $\sqrt{s} =$ 7 TeV," Phys. Lett. B **722**, 273 (2013) [arXiv:1212.1838 [hep-ex]].

[118] P. Minkowski, "mu $\to$ e gamma at a Rate of One Out of 1-Billion Muon Decays?," Phys. Lett. B **67**, 421 (1977).

[119] T. Yanagida, in *Proceedings of the Workshop on the Unified Theory and the Baryon Number in the Universe*, eds. O. Sawada et al., p. 95, KEK Report 79-18, Tsukuba (1979).

[120] M. Gell-Mann, P. Ramond and R. Slansky, "Complex Spinors and Unified Theories," Conf. Proc. C **790927**, 315 (1979) [arXiv:1306.4669 [hep-th]].

[121] R. N. Mohapatra and G. Senjanovic, "Neutrino Mass and Spontaneous Parity Violation," Phys. Rev. Lett. **44**, 912 (1980).

[122] A. de Gouvea, W. -C. Huang and J. Jenkins, "Pseudo-Dirac Neutrinos in the New Standard Model," Phys. Rev. D **80**, 073007 (2009) [arXiv:0906.1611 [hep-ph]].

[123] MAntonello, BBaibussinov, PBenetti, ECalligarich, NCanci, SCentro, ACesana and KCieslik *et al.*, "Experimental search for the LSND anomaly with the ICARUS detector in the CNGS neutrino beam," Eur. Phys. J. C **73**, 2345 (2013) [arXiv:1209.0122 [hep-ex]].

[124] D. V. Forero, M. Tortola and J. W. F. Valle, "Global status of neutrino oscillation parameters after Neutrino-2012," Phys. Rev. D **86**, 073012 (2012) [arXiv:1205.4018 [hep-ph]].

[125] M. C. Gonzalez-Garcia, M. Maltoni, J. Salvado and T. Schwetz, "Global fit to three neutrino mixing: critical look at present precision," JHEP **1212**, 123 (2012) [arXiv:1209.3023 [hep-ph]].

[126] G. L. Fogli, E. Lisi, A. Marrone, D. Montanino, A. Palazzo and A. M. Rotunno, "Global analysis of neutrino masses, mixings and phases: entering

the era of leptonic CP violation searches," Phys. Rev. D **86**, 013012 (2012) [arXiv:1205.5254 [hep-ph]].

[127] NuFit webpage, www.nu-fit.org.

[128] R. N. Cahn, D. A. Dwyer, S. J. Freedman, W. C. Haxton, R. W. Kadel, Y. .G. Kolomensky, K. B. Luk and P. McDonald *et al.*, "White Paper: Measuring the Neutrino Mass Hierarchy," arXiv:1307.5487 [hep-ex].

[129] S. Dawson, E. Eichten and C. Quigg, "Search for Supersymmetric Particles in Hadron - Hadron Collisions," Phys. Rev. D **31**, 1581 (1985).

[130] M. Kramer, A. Kulesza, R. van der Leeuw, M. Mangano, S. Padhi, T. Plehn and X. Portell, "Supersymmetry production cross sections in pp collisions at $\sqrt{s} = 7$ TeV," arXiv:1206.2892 [hep-ph].

[131] LHC SUSY Cross Section Working Group webpage, http://twiki.cern.ch/twiki/bin/view/LHCPhysics/SUSYCrossSections.

[132] J. Beringer *et al.* [Particle Data Group Collaboration], "Review of Particle Physics (RPP)," Phys. Rev. D **86**, 010001 (2012).

[133] G. Aad *et al.* [ATLAS Collaboration], "Search for third generation scalar leptoquarks in pp collisions at $\sqrt{s}$ = 7 TeV with the ATLAS detector," JHEP **1306**, 033 (2013) [arXiv:1303.0526 [hep-ex]].

[134] G. Aad *et al.* [ATLAS Collaboration], "Search for first generation scalar leptoquarks in pp collisions at $\sqrt{s} = 7$ TeV with the ATLAS detector," Phys. Lett. B **709**, 158 (2012) [Erratum-ibid. **711**, 442 (2012)] [arXiv:1112.4828 [hep-ex]].

[135] G. Aad *et al.* [ATLAS Collaboration], "Search for second generation scalar leptoquarks in pp collisions at $\sqrt{s} = 7$ TeV with the ATLAS detector," Eur. Phys. J. C **72**, 2151 (2012) [arXiv:1203.3172 [hep-ex]].

[136] S. Chatrchyan *et al.* [CMS Collaboration], "Search for pair production of first- and second-generation scalar leptoquarks in pp collisions at $\sqrt{s} = 7$ TeV," Phys. Rev. D **86**, 052013 (2012) [arXiv:1207.5406 [hep-ex]].

[137] S. Chatrchyan *et al.* [CMS Collaboration], "Search for third-generation leptoquarks and scalar bottom quarks in pp collisions at $\sqrt{s} = 7$ TeV," JHEP **1212**, 055 (2012) [arXiv:1210.5627 [hep-ex]].

[138] S. Chatrchyan *et al.* [CMS Collaboration], "Search for pair production of third-generation leptoquarks and top squarks in pp collisions at $\sqrt{s} = 7$ TeV," Phys. Rev. Lett. **110**, 081801 (2013) [arXiv:1210.5629 [hep-ex]].

[139] [ATLAS Collaboration], "Search for direct top squark pair production in final states with one isolated lepton, jets, and missing transverse momentum in $sqrts = 8$,TeV pp collisions using 21 fb^{-1} of ATLAS data," ATLAS-CONF-2013-037.

[140] [ATLAS Collaboration], "Search for direct production of the top squark in the all-hadronic ttbar + etmiss final state in 21 fb-1 of p-pcollisions at sqrt(s)=8 TeV with the ATLAS detector," ATLAS-CONF-2013-024.

[141] CMS Collaboration [CMS Collaboration], "Search for supersymmetry using razor variables in events with b-jets in pp collisions at 8 TeV," CMS-PAS-SUS-13-004.

[142] [CMS Collaboration], "Search for Pair-production of Second generation Leptoquarks in 8 TeV proton-proton collisions.," CMS-PAS-EXO-12-042.

[143] G. Aad *et al.* [ATLAS Collaboration], "Search for direct third-generation squark pair production in final states with missing transverse momentum and two b-jets in $\sqrt{s} = 8$ TeV pp collisions with the ATLAS detector," JHEP **1310**, 189 (2013) [arXiv:1308.2631 [hep-ex]].

[144] [CMS Collaboration], "Search for supersymmetry in final states with missing transverse energy and 0, 1, 2, 3, or at least 4 b-quark jets in 8 TeV pp collisions using the variable AlphaT," CMS-PAS-SUS-12-028.

[145] M. E. Machacek and M. T. Vaughn, "Two Loop Renormalization Group Equations in a General Quantum Field Theory. 2. Yukawa Couplings," Nucl. Phys. B **236**, 221 (1984).